THREE WAY CATALYTIC CONVERTER REACTIONS ON PALLADIUM SURFACES

A THESIS SUBMITTED TO THE

UNIVERSITY OF PUNE

FOR THE DEGREE OF

DOCTOR OF PHILOSOPHY

IN CHEMISTRY

BY

S. NAGARAJAN

(RESEARCH GUIDE)

Dr. CHINNAKONDA S. GOPINATH

CATALYSIS DIVISION

NATIONAL CHEMICAL LABORATORY

PUNE 411 008

INDIA

MARCH 2011

DECLARATION BY RESEARCH SCHOLAR

I hereby declare that the thesis "**Three Way Catalytic Converter Reactions on Palladium Surfaces**" submitted for the degree of **Doctor of Philosophy** to the University of Pune has been carried out by me at the Catalysis and Inorganic Chemistry Division, National Chemical Laboratory, Pune - 411 008, under the supervision of **Dr. C. S. Gopinath**. Such material as has been obtained by other sources has been duly acknowledged in this thesis. I declare that the present work or any part thereof has not been submitted to any other University for the award of any other degree or diploma.

Date: 25/03/11

S. NAGARAJAN
Catalysis Division,
National Chemical Laboratory,
Pune 411 008
Maharashtra
India

राष्ट्रीय रासायनिक प्रयोगशाला
(वैज्ञानिक तथा औद्योगिक अनुसंधान परिषद)
डॉ. होमी भाभा मार्ग, पुणे - 411 008. भारत
NATIONAL CHEMICAL LABORATORY
(Council of Scientific & Industrial Research)
Dr. Homi Bhabha Road, Pune - 411 008. India.

हीरक जयन्ती वर्ष 2009-10

CERTIFICATE BY RESEARCH GUIDE

This is to certify that the work incorporated in the thesis, entitled **"Three Way Catalytic Converter Reactions on Palladium Surfaces"** submitted by **Mr. S. Nagarajan,** for the Degree of **Doctor of Philosophy,** was carried out by the candidate under my supervision in the Catalysis Division, National Chemical Laboratory, Pune – 411 008, India. Such material as has been obtained from other sources has been duly acknowledged in the thesis. To the best of my knowledge, the present work or any part thereof has not been submitted to any other University for the award of any other degree or diploma.

C. S. Gopinath

Date: 25/03/11

Dr. C. S. Gopinath
(Research Supervisor)
Catalysis Division,
National Chemical Laboratory,
Pune 411 008
Maharashtra
India

Communication Channels
NCL Level DID : 2590
NCL Board No. : +91-20-25902000
EPABX : +91-20-25893300
+91-20-25893400
FAX
Director's Office : +91-20-25902601
COA's Office : +91-20-25902660
COS&P's Office : +91-20-25902664
WEBSITE
www.ncl-india.org


தாத்தா, பாட்டி, பெற்றோர்,
உறவினர்கள் மற்றும்
ஆசிரியர்கள்
அனைவருக்கும்
அர்ப்பணம்!!!!!!!!!!!!!!
.....Dedicated to
my Grandparents, Parents,
Relatives, and all my
Chemistry teachers!!!!!!!!

Acknowledgements

It gives me immense pleasure to extend my cordial gratitude and sincere thanks to all those who helped me in pursuing my doctoral work.

First of all, I would like to take this opportunity to thank my research supervisor, ***Dr. C. S. Gopinath*** *for his ideas, enthusiasm, encouragement, and support throughout my PhD work. I really admired the way he handle the scientific and nonscientific things with perfection and sincerity.*

I am very much grateful to ***Dr. S. D. Prasad*** *for in-depth and detailed discussions. I am thankful to* ***Dr. C. P. Vinod*** *for his valuable suggestions and his effort to teach so many scientific things.*

I am, very grateful to Dr. D. Srinivas, Dr. C. V. V. Satyanarayana, Dr. T. Raja, Dr. Joy, Dr. Nandhini, and Dr. C. V. Rode for their valuable helps. I thank Mr. Deo and Mr. Suriyavanshi for their help. I would like to thank the present and erstwhile heads of the division, Dr A. P. Singh, and Dr. Rajivkumar, for providing me all the divisional facilities required for my research work. I am grateful to Dr. S. Sivaram, and Dr. Sourav Pal, erstwhile and current Directors, NCL, for allowing me to carry out the research work in a prestigious and well-equipped laboratory. CSIR, New Delhi is gratefully acknowledged for the research fellowship.

I am grateful to ***Prof. Mike Bowker****, Cardiff University, UK, for the collaboration through Royal Society and British Council. I am very thankful to Dr. Balu and his family for care and affection when I was in Cardiff, UK. I am thankful to Sivaram, Upendra Dr. Jonathan Counsell, Kareem, Lee, for their company during my visit to Cardiff. I thank* ***Prof. Sir, David A King****, University of Cambridge for helpful discussions during my visit. I thank Dr. Iyngaran for giving me accommodation in Cambridge during my visit.*

I am thankful to the American College former Principal Dr. Samuel Sudhananda, and our Chemistry Department staffs. ***Dr. P. M. Sundaram****, Dr. N. Rajaram, Dr. Monica, Dr. John, Dr. Sheela, Dr. Mathew John, Dr. T. K. Ganesan. I am very grateful to my chemistry teacher (Std XI and XII)* ***Mr. Alagappan****.*

I thank my school friends ***Vijay****,* ***Padmanabhan****,* ***Sridhar****,* ***Muthu****,* ***Saravana****,* ***Rajagopal****,* ***Sarguru****,* ***Velraj****,* ***Selva****,****Vinod****,* ***John****,* ***Charls*** *etc.*

I am very much thank full to my UG and PG classmates in the American College, especially ***Durai***, ***Judu***, ***Uma***, ***Suriya***, ***Parthiban*** *etc*

Seniors are always great and roll model in my life. I had wonderful seniors during my college days as well as in research life. My deepest thanks to my college seniors ***Dr. Sankar***, ***Dr. Selvakannan***, ***Dr. Devaraj***, ***Dr. Suresh***, ***Dr. David***, ***Dr. Selva***, ***Dr. John***, ***Dr. Velayudham***, ***Dr. Vijayanand***, ***Mr. Loganathan***, ***Mr. Sethu***, ***Dr. Abbas***, ***Dr. Vengadesh***, ***Dr. Sivanesan***, ***Dr. Subbu***, ***Dr. Thirumurugan***, ***Dr. Annalakshmi***, *Dr.* ***Murugaboopathi Raja***, *Dr. Thayumanavan, Dr. Thiru, Dr. Senthilkumar, Dr. Arlin, Dr. Uma, Dr. Tamil, Dr. Karthikayan, Dr. Velkannan, Dr, Vivek etc*

NCL seniors ***Dr. Vijayaraj***, ***Dr. Thirunavukkarasu***, ***Dr. Maitri***, ***Dr. Murugan***, ***Dr. Neelam***, ***Mr. Marimuthu***, ***Dr. Malli***, ***Dr. Rama***, ***Dr. Easwar***, ***Dr. Pradeep***, *Dr. Suresh(bio), Dr. Suresh(org), Dr, Meera, Dr. Marivel, Dr. Elangovan, Mr. Muthurajan, Dr. Pratap, Dr. Ramesh, Dr. victor, Dr. Ramya, Dr. Subashini, Dr. Vijay, Dr. Selva, Mr. Khaja, Dr. Venkatesh, Dr. Bala, Dr. Nitin, are kindly acknowledged. I am very much thankful to Army suresh,* ***Balaji anna,*** *and* ***his family***, ***Kannan and anni*** *for their homely environment during my stay in NCL.*

I am thankful to ***all my divisional friends*** *and Ankush, Anand, Rao, Dubey, Sandeep, Malvi, Dillu, Javix, Prinson, Kamu, Tanpreet, Prasanna, Sathish, Naren, Ketan, Anuj, Maneesh, Muthu, Venki, T.M.S, Dharma, Nagesh, Remya, Kuttan, Kanak,* ***Shabab*** *&* ***Subhadeep*** *(room partners).*

My deepest acknowledgement goes to ***Amma***, ***Appa***, ***Thambi***, *and all my relatives and friends for their love, support and encouragements throughout my life.*

Last but not least, my deepest acknowledgement to, my dear fiancée Ms. ***Thushara K. S****,(Kutty) for everything in my life, her love and affection towards me make a wonderful life, she makes me perfect in all aspect of my life. I felt very proud for her caring and affection towards me and providing variety of wonderful foods from her magic hands.*

S. NAGARAJAN

List of Abbreviations

AES	Auger Electron Spectroscopy
AT	Ambient Temperature
BE	Binding Energy
HC	Hydrocarbon
HPXPS	High Pressure X-ray Photoelectron Spectroscopy
HREELS	High Resolution Electron Energy Loss Spectroscopy
ICE	Internal Combustion Engine
IRAS	Infrared Reflection Absorption Spectroscopy
ISS	Ion Scattering Spectroscopy
L	Langmuir
LEED	Low Energy Electron Diffraction
MBI	Molecular Beam Instrument
ML	Mono Layer
PGM	Platinum Group Metals
QMS	Quadrupole Mass Spectrometer
RDS	Rate Determining Step
SIMS	Secondary Ion Mass Spectrometry
SM	Surface Modified
SS	Steady State
STM	Scanning Tunneling Microscopy
SXRD	Surface X-ray Diffraction
TPD	Temperature Programmed Desorption
TS	Transient State
TWC	Three Way Catalytic
UHV	Ultra High Vacuum
UVPES	Ultra Violet Photo Electron Spectroscopy
VOC	Volatile Organic Compounds
XPS	X-ray Photoelectron Spectroscopy

List of Symbols

E_a	Activation energy
F_{CO}	CO flux
F_{O_2}	O_2 flux
F_{CO+O_2}	CO + O_2 mixed beam flux
$F_{NO+CO+O_2}$	NO + CO + O_2 mixed beam flux
$F_{ethanol+NO}$	Ethanol + NO mixed beam flux
$F_{ethanol+O_2}$	Ethanol + O_2 mixed beam flux
Γ	Delay in CO adsorption or CO_2 Production (sec)
$Pd^{\delta+}$	Mildly oxidized Palladium
θ_{CO}	CO coverage
θ_o	Coverage
$\theta_{o_{sub}}$	Subsurface oxygen
rs	Reactive sticking coefficient
rs_{CO}	Reactive sticking coefficient of CO
rs_{O_2}	Reactive sticking coefficient of O_2
S	Sticking coefficient
S_{CO}	CO sticking coefficient
S_{O_2}	O_2 sticking coefficient
S^0	Initial sticking coefficient
S_{CO}^0	Initial sticking coefficient of CO
$S_{O_2}^0$	Initial sticking coefficient of O_2

Table of Contents

Abstract of the thesis

The present generation automobile internal combustion (IC) engines are working in the high air to fuel ratio than the stoichiometric value (14.7), to an almost complete combustion of fuel. As a consequence, automotive exhaust contains more oxygen and it is ideal for oxidation, but not for reduction. For many years the classical Pt/Rh catalyst dominated the automotive three way catalytic (TWC) market; in Europe the Pt/Rh was used in a ratio of about 5:1 and in the US a Pt/Rh ratio of about 10:1 was common. One of the first changes in technology was the substitution of Rh by Pd. Pt/Pd catalysts were mainly used in the 1980s. At the beginning of 1990, platinum was increasingly replaced by palladium giving the Pt/Pd/Rh (with Pt:Pd:Rh ratios from 1:14:1 to 1:28:1) and finally the Pd/Rh- and Pd-only catalysts. Out of noble metals, Pd is widely used and replaces the Rh and Pt to a large extent.

According to United States geological survey, the overall production of palladium was 222 metric tons in 2006 and out of which most of the palladium is utilized in TWC in automobile industry and this underscores the importance of palladium. **Chapter 1** deals with brief introduction of the concept of oxygen migration to the subsurface layers of Pd at various reaction conditions. Oxygen dissolution on Pd systems is a well known phenomenon; the conditions for oxygen migration to the subsurface of palladium are simple; at temperatures above 500 K and at high oxygen partial pressure, oxygen subsurface diffusion begins, and different oxygen species, including chemisorbed oxygen, metastable oxide to bulk oxides, have been observed. However, how the different species influences the catalysis is not known. Present thesis addresses the influence of oxygen in subsurfaces towards oxidation catalysis.

Chapter 2 focuses the description of Molecular Beam Instrument (MBI) to study the fundamental kinetic aspects under isothermal conditions. Details about the calculation of important parameters like sticking coefficients (*s*), surface coverages, from experimental kinetic data mechanistic details like, whether the reaction is Langmuir-Hinshelwood or Eley-Rideal, qualitative idea on surface composition, transient and steady state rate of the reactions, etc are described.

The concept of oxygen subsurface diffusion has been observed on Pd system and the same aspect was explored to oxidation catalysis in **Chapter 3**. CO + O_2 on Pd(111) and polycrystalline palladium surfaces have been carried out in a wide range of temperature and CO:O_2 beam compositions. It is observed that there is a diffusion of significant coverage of oxygen into the subsurfaces of Pd, especially ≥ 600 K. Interesting information derived from the above studies is the necessity to fill up the subsurface layers with oxygen atoms to threshold coverage ($\theta_{o_{sub}}$), above which the reactive CO adsorption occurs on the surface and subsequent CO_2 production. $\theta_{o_{sub}}$ was determined to be 0.4 monolayer (ML) at 900 K with pure O_2-beam. These underscores a change in the electronic state of Pd-surfaces towards mildly oxidized (or $Pd^{\delta+}$) state and likely an electronic decoupling occurs between bulk and top few surface atomic layers. Similar observation with polycrystalline Pd-surfaces suggests the defects sites are the likely channels for oxygen diffusion into subsurfaces. In another set of experiments, O_2 has been dosed systematically from 5 to 110 minutes at 900 K for surface modification (SM) of Pd(111) by populating oxygen atoms in the subsurfaces, prior to CO + O_2 reactions. The CO + O_2 composition has been varied from (7:1) CO-rich to (1:11) O_2-rich compositions and the temperature varied from 273 and 525 K. Ambient temperature (AT) CO oxidation has been observed with SM Pd(111) surfaces. Sustainable CO_2 production has been observed for an hour in O_2-rich conditions without any decrease in the rate of CO_2 production underscores the importance of SM Pd(111) surfaces.

Our study, presented in **Chapter 4**, explores the influence of oxygen on NO:CO reaction on Pd(111) surfaces with wide range of temperatures between 400 and 800 K and beam compositions. Maximum reactivity was found between 500 and 600 K for all beam composition ranges. Surface oxygen decreases the net NO adsorption and dissociation above 550 K and maintains the CO-oxidation rates. The overall reaction is largely controlled by the N+N recombination between 500 and 600 K and NO-dissociation also contribute to the rate determining step with increasing temperature and oxygen content in the beam. The rate of formation of CO_2, and N_2 does not vary much with CO flux. Pd(111) surface show reversible nature with respect to oxygen-rich and oxygen-lean conditions. Large NO-dissociation occurs on relatively oxygen-free Pd-

surfaces (oxygen lean) or only in transient kinetics on oxygen rich conditions, which is observed through fast beam switching for better de-NO_x management.

In **Chapter 5**, NO reduction with ethanol has been studied on Pd(111) surfaces under oxygen rich and lean conditions using a molecular beam approach to study the effect of ethanol blended gasolines. Significant nitrogen production and ethanol oxidation was observed with EtOH + NO (and O_2) beams at temperatures above ~ 500 K, even though ethanol sticking coefficient was immeasurably low ≤400 K on clean and oxygen covered Pd(111) surfaces. Generally, oxygen favours the complete ethanol oxidation on Pd(111) surfaces, and CO_2 production increases with increasing oxygen content. Fast beam switching experiments were performed in order to show NO-reduction management under net oxidizing environments.

Chapter 6 deals with conclusions and future scope of the work. In general, oxygen in the subsurface layers of Pd facilitates high temperature (>700 K) as well as low temperature (273 K) CO oxidation. This proof of concept has to be extended to real world powder catalysts not only with oxygen, but as well with carbon and hydrogen. Using the concept of oxygen subsurface diffusion, industrially important reactions like partial oxidation of methane, methanol oxidations needs to be studied in wide range of temperature and pressures. Possible NO_x management under net oxidizing environment has been suggested. However, this aspect needs to be tested with real-world TWC system and suitably implemented.

Chapter 1

Introduction

1.1. Introduction to catalysis

Catalyst is a substance that accelerates a chemical reaction without itself being affected, and the process is called Catalysis. In general, a catalyst accelerates the chemical reaction by decreasing the activation energy. Promoters are the substances, in general, increase the activity of the catalyst, and the catalytic poisons are the substances in general, deactivate the catalysts. The catalyst has a remarkable role in petrochemicals, environmental pollution control, fuels, lubricants, dyes, polymer, fine chemicals, and pharmaceuticals etc. It contributes great part in the processes of converting solar energy to various forms of energies, for example (photosynthesis of the plants). Catalysts have a key role in maintaining the living nature on the mother earth. The approximate annual sale of the whole catalysts would be few billion dollars. Almost 90% of the chemical industry has a catalysis related process and it contributes 5% of the total investment of the chemical process.

Catalysis can form complex with reactants or products and it can control the rate of elementary steps in the process; few points illustrates the above aspect, (i) the reaction activation energy is altered, (ii) the intermediate formed are different from those formed during non-catalyze reaction and (iii) the rate of the reactions are altered. It is a highly multidisciplinary area and nowadays considered as a big business. In general, catalysts can be broadly classified into two types, homogeneous and heterogeneous, based on the *phase* of the reactants and the catalysts.

1.2. Heterogeneous catalysis

Heterogeneous catalysis has attracted Nobel prizes for Fritz Haber in 1918 and Carl Bosch in 1931, Irving Langmuir in 1932, and Gerhard Ertl in 2007. Heterogeneous

catalysis generally occurs at the surface-interface of the solid catalysts. Surface atoms in the heterogeneous catalyst always lack in co-ordination which results in adsorption of the reactant molecules or atoms on the surfaces. Depending on the strength of the interaction, it can be classified as physisorption (a weak bond or vander waals interaction) or chemisorption (strong bond). Generally physisorbed moiety will be desorbed when the catalyst temperature is raised, whereas chemisorbed species may dissociate or diffuse into the subsurface layers of the catalyst or it can convert into another species and subsequently they desorbs as products. Right now more than 80% of the industrial catalysis practiced is heterogeneous and all of the reactions studied in this thesis also is on heterogeneous catalysis.

1.3. Air pollution and environmental catalysis

There were about 806 million cars and light trucks on the road in 2007 around the world, and about 250 million vehicles are in use in the USA, consuming over 260 billion gallons of gasoline and diesel fuel annually [1]. According to the environmental science engineering program at the Harvard School of Public Health, about 4% of deaths in the United States can be attributed to air pollution. The primary pollutants are CO, NO_x, SO_x, volatile organic compounds (VOC), and particulate matter and this mainly due to "stationary sources" like power plants and other industrial exhausts, and "mobile sources" like motor vehicles, marine vessels and aircraft from all over the world. India is at 4^{th} position for highest CO_2 emission, and it emitted 1,510 $x10^6$ tons in 2006 and it contributes 5.3% of total CO_2 emission in the world. In addition to that India occupies 2^{nd} position in particulate matter emission which was 150 $\mu g/m^3$ in 2004. New York people's faces 25% increase risk of lungs related diseases, because of dense smog in this city viewed from world trade centre (Figure 1.1) in 1988 [1]. Another important form of air pollution is VOC refers to organic chemical compounds which can directly affect environment and human health. Respiratory problems, allergic, or immune effects in infants or children are associated with man-made VOCs and other indoor or outdoor air pollutants [2]. Some VOCs, such as styrene and limonene, can react with nitrogen oxides or with ozone to produce new oxidation products and secondary aerosols, which can cause sensory irritation symptoms [2].

Figure 1.1 Smog in New York City as viewed from the World Trade Center in 1988. A 2009 report indicates that, despite the City's air being close to the EPA's short-term ozone standard, that New Yorkers still face a 25 per-cent increased risk of dying from lung disease.

Unspecified VOCs are important in the creation of smog [2]. Figure 1.2 describes the various sources of VOC emissions in the year 2005. In order to control these, there are various air pollution control technologies has been suggested.

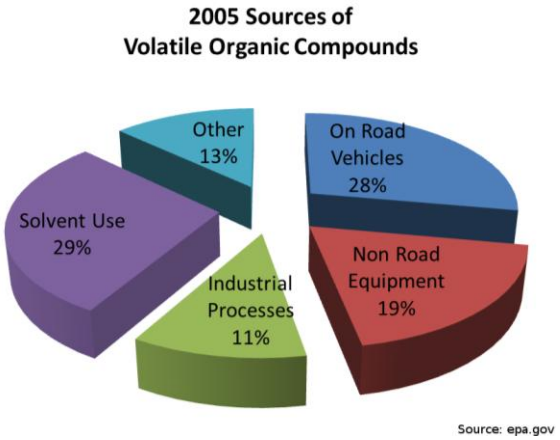

Figure 1.2 Various sources of VOC emissions. Note that non road equipment is mostly gasoline and diesel stations [2].

There is a special care has been taken to control the mobile sources motor vehicles, marine vessels etc like increase in fuel efficiency and cleaner fuels (such as bio ethanol, bio diesel and moving towards electric vehicles etc). Emissions standards have been designed to control the pollutants that are released into the environment. Many

emission standards focus on regulating pollutants released by automobiles (motor cars) and other powered vehicles and also regulate emissions from industry, power plants, small equipment such as diesel generators. Figure 1.3 measures the CO pollution in troposphere (March 2010). The average level of CO throughout the world was 100-150 ppbv (parts per billion by volume) and the maximum observed was 300 ppbv in countries like western part of US, California, Europe, central Africa, India, western China, Japan etc.

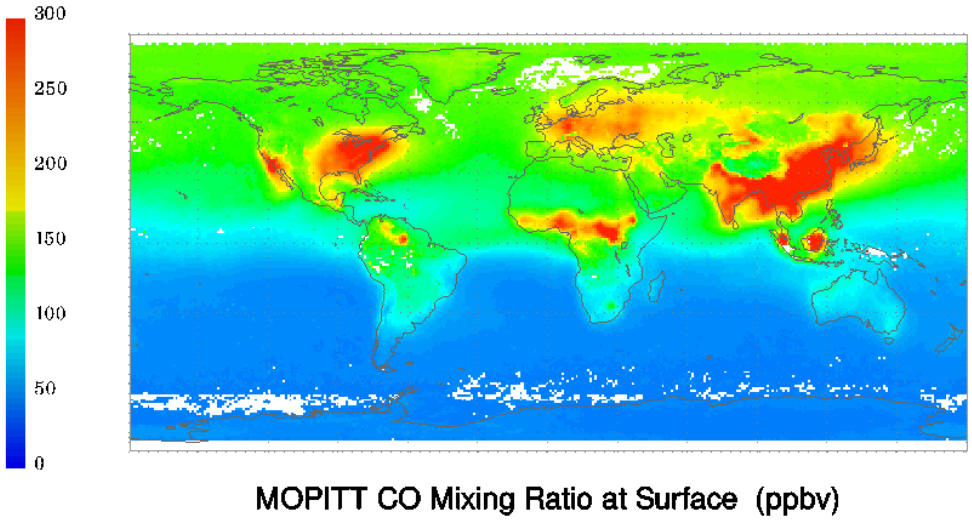

Figure 1.3 Measurements of Pollution in the Troposphere (MOPITT) satellite computer image of carbon monoxide (March 2010).

1.4. Role of catalytic converters

Catalytic converter is a device used to reduce the toxicity of emissions from an internal combustion engine (ICE). A catalytic converter works by using a catalyst to stimulate a chemical reaction in which toxic by-products of combustion are converted to ubiquitous or less-toxic substances [3]. In automobiles, this typically results in 90% conversion of carbon monoxide (CO), hydrocarbons (HC), and nitrogen oxides (NO_x) into less harmful gases. For over 35 years, catalytic converters based on Platinum Metal Groups (PGM) have been used for pollution abatement. It collectively refers to six metallic elements clustered together in the periodic table namely Ruthenium, Rhodium, Palladium, Osmium, Iridium, and Platinum. These elements are all transition metals, lying in the d-

block elements. They were first introduced in the USA and since 1981 all cars and light duty trucks sold in the US have included catalytic converters as standard equipment. Today, over 95% of new cars sold worldwide are fitted with catalytic converters. In fact, the average family car in the US would emit 15 tons of toxic and harmful polluting gases (CO, HC and NO_x), over a 10-year life, if catalytic converters were not fitted to all new cars to remove up to 98% of pollution as required by current regulations [3, 4].

1.4.1. Functioning of catalytic converters

In general, conventional petrol/gasoline engine catalyst contains an oxide support on which more than two precious metals (Pd, Pt and Rh etc) are dispersed in very low concentrations (0.1- 0.3 wt % of the monolith). A catalytic converter works by using a ceramic or metal honeycomb structure of thousands of channels coated with a combination PGM of platinum, rhodium and/or palladium. This exposes the maximum surface - a combined area about the size of a football pitch - of a catalyst to the exhaust stream, while also minimizing the amount of catalyst required [3]. The monolith (*honeycomb*-type) is typically made of cordierite and the composition ($2MgO{\cdot}2A1_2O_3{\cdot}5SiO_2$) and washcoat contains 10-30 wt% of corderiete, γ-$A1_2O_3$ and various proprietary base metals, to provide a high surface area film on which the catalytic component (PGM) is highly dispersed [4-6]. The main properties required for the washcoat are the ability to be impregnated by the noble metal particles and to exhibit chemical inertia to reaction medium. Most of these requirements are fulfilled by using γ-$A1_2O_3$ in excess of about 90% and a mixture of rare-earth metals and/or alkaline earth metals, and other metal oxides are CeO_2, La_2O_3, ZrO_2, BaO, TiO, Y_2O_3, NiO,WO_3, etc are used. The exact catalyst composition is generally protected proprietary item. Nowadays, combined metal oxides of three elements are being utilized as promoters of the precious metal activity in the newer generation of commercial catalysts [7]. As exhaust passes through this device, the catalytic converter changes HC, CO and NO_x into water (H_2O), nitrogen (N_2) and carbon dioxide (CO_2).

1.4.2. Effectiveness of catalytic converters

By most estimates, catalytic converters fitted inside the exhaust pipe of a gasoline-operated car converts over 90% of HC, CO and NO_x from the engine into less harmful CO_2, N_2 and H_2O. Diesel engines, in addition to the above, emit particulates. The use of a particulate filter, in conjunction with a catalyst, can reduce their mass by 90% and reduce the number of ultra-fine particles by 99% [7]. With the spread of automotive catalysts and the development of environmental legislation (e.g. EURO phase I-V, US-Environmental Protection Agency Tier 1-2 or California Low Emission Vehicle I-II emission standards) the annual total demand of PGE for automotive catalysts increased continuously from 35 tons in the year 1980 to 235 tons in the year 2000.

The present three-way catalytic (TWC) converters technology meets the requirements of oxidation of CO as the exhaust contains more air. NO_x reduction is a real challenge task in these oxygen rich environments. For NO_x reduction, there were few new technologies [8-9] introduced in the past decade, like NO_x storage or zeolites based catalysts, which provided different insights into the NO reduction. However, regarding long-term stability, low and high-temperature NO reduction is still a challenge [10]. The above points clearly indicate that there is an urgent need to develop catalysts for NO_x reduction under net oxidizing conditions. In this respect, obtaining molecular-level insights into underlying catalysis aspects of NO reduction is a major challenge for current research programmes. There are considerable amount of reports available on the NO reduction over Pd-based catalysts on different faces of single crystals and a variety of supported powder catalyst systems [11-27] in the recent past. However, there is a lack of fundamental understanding of NO reduction on the Pd surfaces. Infrared reflection absorption spectroscopy (IRAS) and high-resolution electron energy loss spectroscopy (HREELS) have been employed to study NO adsorption and its co-adsorption with CO on Pd(100) and Pd(111) single crystals [28, 29].

Goodman and coworkers found that the closely packed Pd(111) facet was significantly more active than the relatively more open Pd(100) facet for the NO + CO reaction, [28, 29] in spite of the fact that Pd(100) has a higher NO dissociation activity.

This effect was attributed to the strong bonding of a fraction of the N_{ads} on Pd(100), leading to partial poisoning of the surface [28]. Also, the N_2/N_2O product ratio was found to depend on the crystallographic orientation, the Pd(100) face is more active for NO dissociation and atomic N stabilization than the close packed (111) plane [28]. In more recent work, high N_2O/N_2 product ratios were observed on the Pd(111) surface at elevated pressures [29]. Some differences between the TPD results reported by Goodman et al [29] on Pd(111) and Pd(100) and those reported by other groups, [13, 14, 16, 18] remain unresolved in particular, to N_2 desorption above 550 K.

1.4.3. Role of (PGM) as a catalyst for catalytic converters

The PGMs have outstanding catalytic properties, especially this group metals are the best catalyst for the catalytic converter reactions. It was estimated that 1,300 tonnes of PGM are used in the vehicles as a catalyst. For many years the classical Pt/Rh catalyst dominated the automotive TWC market; in Europe the Pt/Rh was used in a ratio of about 5:1 and in the US a Pt/Rh ratio of about 10:1 was common [30]. The continuing price rise of noble metals, shrinking Rh supply, and technical improvements in ICE stimulated an increasing substitution of Pt and Rh by Pd. One of the first changes in technology was the substitution of Rh by Pd. Pt/Pd catalysts were mainly used in the 1980s. At the beginning of 1990, platinum was replaced by palladium giving the Pt/Pd/Rh (with Pt:Pd:Rh ratios from 1:14:1 to 1:28:1) and finally the Pd/Rh- and Pd-only catalysts [31]. Out of noble metal particles Pd is widely used and replaces the Rh and Pt to a large extent. Although Rh is very active for NO reduction under fuel-rich conditions, this is not the case under net oxidizing conditions, since the excess oxygen inhibits the NO reduction as well as CO oxidation activity of Rh by oxidizing it to Rh_2O_3 [32-34]. Platinum catalysts are reported to be very good for CO oxidation, but the formation of irreversible oxide leads to make platinum to be replaced.

1.4.4. Role of ethanol as a fuel and its NO_x reduction capacity

Ethanol is most often used as a motor fuel, mainly as a biofuel additive for gasoline. World ethanol production for transport fuel tripled between 2000 and 2007 from 17 billion to more than 52 billion liters. From 2007 to 2008, the share of ethanol in global

gasoline type fuel use increased from 3.7% to 5.4% [35]. In 2009 worldwide ethanol fuel production reached 19.5 billion gallons (73.9 billion liters). Ethanol is widely used in Brazil and in the United States, and together both countries were responsible for 86 percent of the world's ethanol fuel production in 2009 [36]. Most cars on the road today in the U.S. can run on blends of up to 10% ethanol [37], and the use of 10% ethanol gasoline is mandated in some U.S. states and cities. Since 1976 the Brazilian government has made it mandatory to blend ethanol with gasoline, and since 2007 the legal blend is around 25% ethanol and 75% gasoline (E25) [38]. In addition, by December 2010 Brazil had a fleet of 12 million flex-fuel automobiles and light trucks and over 500 thousand flex-fuel motorcycles regularly using neat ethanol fuel (known as E100) [39-42]. As a fuel, ethanol has advantages and disadvantages over fuels such as petrol (gasoline) and diesel. In spark ignition engines, ethanol can run at a much higher exhaust gas recirculation rates and with higher compression ratios. Ethanol have a high octane rating, 109 RON (Research Octane Number), 90 MON (Motor Octane Number), (which equates to 99.5 AKI) [43]. Note that AKI refers to 'Anti-Knock Index' which averages the RON and MON ratings (RON+MON)/2, and is used on U.S. gas station pumps. Regular European petrol is typically 95 RON, 85 MON, equal to 90 AKI. As a compression ignition engine fuel, ethanol creates very little particulates, but their low cetane number means that an ignition improver like glycol must be mixed into the fuel with approx. 5%. When used in spark ignition engines alcohols have the potential to reduce NO_x, CO, HC and particulates. A test with E85 fueled Chevrolet Luminas showed that NMHC [44] went down by 20-22%, NO_x by 25-32% and CO by 12-24% compared to reformulated gasoline [45].

By adding ethanol to the gasoline air pollution might be controlled better, since ethanol is highly combustible. Addition of ethanol reduces the emission of olefins, aromatics, complex hydrocarbons benzene, 1, 3 Butadiene and SO_x [46]. However, there are few problems associated with ethanol and it leads to the emission of small amounts of aldehydes (acetaldehyde in particular) and/or even some amount of unburned ethanol into the environment [47]. It would be ideal if NO reduction can be managed directly with unburned ethanol or aldehydes. Dong et al [48] reported that a high NO_x conversion up to 90% was achieved with ethanol using a three component catalyst system, namely,

Ag/Al_2O_3 + Pt/TiO_2 + Cu/TiO_2, between 350 and 450°C. They reported that NO_x conversion efficiency increases with increase in the ethanol dosage, but it cause CO emission also. Dzwigaj et al [49] studied the effect of zeolites with isolated Co^{II} and Fe^{III} species for selective catalytic reduction of NO with ethanol. De Mello et al [50] studied NO reduction with ethanol using MoO_3/Al_2O_3 and CeO_2-ZrO_2 supported Pd catalysts. Temperature programmed desorption (TPD) analysis of adsorbed NO and ethanol showed that the Pd/CeO_2-ZrO_2 catalyst has a higher ability for the dissociation of NO to N_2 and for the oxidation of ethanol to CO_2. A comparison on the catalytic behavior of Pd/Al_2O_3 and Pd-Mo/Al_2O_3 showed former to be more active for NO conversion. Velu et al [51] studied the oxidative steam reforming of ethanol with CuNiZnAl mixed oxide, and observed 100% ethanol conversion at 300^o C to CH_3CHO and H_2. It is important to mention that ethanol as a fuel in modern internal combustion engines increases the oxygen content in the exhaust, and NO reduction under net oxidizing conditions becomes increasingly difficult.

Bowker et al [52] studied methanol oxidation on iron molybdate, and ethanol oxidation and acetic acid decomposition on Pd(110) surfaces [52, 53]. It was demonstrated that several pathways exist for ethanol decomposition and oxidation, including decarbonylation to produce methane and CO and via acetate as an intermediate species to combustion [52, 54]. These pathways were confirmed by use of high resolution X-ray photoelectron spectroscopy (XPS) [54]. Literature reports show that there is very limited molecular level understanding of NO reduction using ethanol, especially under net oxidizing conditions. (**Chapter 4**) describes the importance of understanding of NO reduction with ethanol on Pd-surfaces, and the possibility of managing NO-reduction under oxidizing conditions. Molecular beam methods were utilized to explore the optimum conditions for maximum NO reduction. Fast oscillation between fuel-lean and fuel rich compositions (NO + Ethanol + O_2) ensures the surface is not poisoned, particularly with oxygen; this is the key aspect towards the management of NO reduction under net-oxidizing conditions.

1.5. Advantages of Palladium as a catalyst for TWC

According to United States geological survey, the overall production of palladium was 222 metric tons in 2006 and out of which most of the palladium is utilized in TWC in automobile industry and this underscores the importance of palladium [30, 31]. Present generation IC engines which are working at high air/fuel ratio necessitates the need to study the effect of oxygen on Pd-surfaces under various oxygen rich conditions. Palladium has been suggested as an alternative active element for NO reduction due to significant NO dissociation capacity and its stability at high temperature and under oxidizing conditions, as well as for CO and HC oxidation. Palladium based catalysts are more suitable for current automotive catalysts, which does not undergo irreversible oxidation even at high air/fuel ratio and the cost is relatively lower than other noble metals. This factor underscores the importance of Pd in TWC converters.

1.6. Surface science aspect of the catalyst

"Most finely divided catalysts must have structures of great complexity, and it is probable that the atoms are attached to each other in the form of branching chains so that there are hardly any groups of as little as three or four atoms which are as closely packed as they would be in the crystalline solid. In order to simplify our theoretical consideration of reactions on surfaces, let us confine our attention mainly to reactions on plane surfaces. If the principles in this case are well understood, it should then be possible to extend the theory to the case of porous bodies"[55].

- Langmuir, I. *Trans. Faraday. Soc.* 17, **1922**, 607

Ultra high vacuum (UHV) is required for all the surface science experiments for two important reasons: (i) to enable preparation of atomically clean surfaces, and (ii) such surfaces to be maintained in a contamination-free state for the duration of the experiment and to use the electron/ion/photon-based *in-situ* experimental techniques without undue interference from gas phase scattering. Most spectroscopic techniques are capable of detecting molecules in the gas phase; in these cases it is preferable that the number of species present on the surface substantially exceeds those present in the gas phase

immediately above the surface - to achieve a surface/gas phase discrimination of better than 10:1.

In order to begin experiments with a reproducibly clean surface and to ensure that significant contamination by background gases does not occur during an experiment, the background pressure must be kept very low (high vacuum) in such a way that the time required for contaminant build-up is substantially greater, i.e. it should be in hours than that required to conduct an experiment. The implication with regard to the required pressure depends upon the nature of the surface, but for the more reactive surfaces this necessitates the use of UHV (10^{-9} Torr).

1.6.1. Model studies using metal single crystals

Surface science explores the elementary reaction steps involved in the reaction with various reaction dynamics on the *'metal single crystal surfaces'* representing a real industrial catalyst to understand a given chemical process. These surface science experiments are called model experiments, and in these studies, a well- defined, single crystal plane is used to model a site or set of sites expected to exist on a real-world high surface-area catalysts [56]. Though a clean surface of a practical catalyst may be prepared with less contamination, it usually contains large surface defects, kinks etc. The catalytic processes occurring in those models are still complicated to understand even with the advantage of simplicity in their structure compared to the real-world catalysts. Some of the chemical processes are found to be sensitive to the structure of the plane of the catalyst surface and the same can be understood with the help of model experiments [57]. In fact, Boudart [58] first mentioned the phrase called 'surface-sensitive or demanding reactions/surface-insensitive reactions or facile reactions' for this effect on catalyst surfaces by using 0.5 weight % of Pt or Pd on γ-alumina, η-alumina, silica-alumina gels and crystalline alumino-silicates (Zeolites). The degree of '*dispersion'* of the metal defined as the ratio of surface metal atoms to the total number of metal atoms is extremely high, frequently approaching unity, so that the ultimate goal of '*atomic dispersion'* has even been claimed in certain instances. It was only natural that such novel and interesting catalysts be exploited in fundamental research.

In general, model studies using metal single crystals provide important information like reaction mechanism, Rate determining step (RDS), nature of the adsorbed species, etc. One more advantage of using metal single crystals as model catalysts should be mentioned here. In the study of CO oxidation on Ru surfaces, Ertl et al, [59, 60] found that excitation with femtosecond infrared laser pulses in the pre-adsorbed CO and oxygen species on Ru(0001) single crystal surface enables the formation of CO_2; but mere conventional heating of the same Ru surface leads exclusively to the desorption of CO. In contrast, the desorption is caused by coupling of the adsorbate to the phonon bath of the Ru substrate, whereas the oxidation reaction is initiated by hot substrate electrons, as evidenced by the observed sub-picosecond reaction dynamics, which can only be observed as metal single crystals as model catalyst. Further activity/selectivity information obtained at UHV conditions may not be extended or correlated to that at high pressure, due to very high surface coverage including weakly bound species. Goodman et al [61] found that, sensitive techniques like Low energy electron diffraction (LEED), XPS, Auger-electron spectroscopy (AES), HREELS, Secondary-ion mass spectrometry (SIMS) and Ion scattering spectroscopy (ISS) etc provides information to the understanding of basic information's like reaction rate and its mechanisms and it provides direct relationship between structure and its activity and compositions.

1.7. Oxygen diffusion on Palladium surfaces

1.7.1. General aspects

Palladium - a silvery white metal belonging to the d-block element having atomic number 46 and occupying 10^{th} group in the periodic table. It belongs to the fm-3m space group with space group number - 225 and having cubic-close packing (CCP) structure. It has a unique property of oxygen and hydrogen dissolution. There are significant number of studies carried out on Pd interaction with oxygen in wide temperature and pressure range which results in the formation of oxide on surface, subsurface, metastable oxides (Pd_xO_y) and bulk oxide formation [62-78]. In 1969 Sandler et al [71] observed the bulk oxide formation on Pd powder when exposed to oxygen for a long time. The total surface area of palladium powder increased when 400 monolayer (ML) oxygen was deposited. The

total surface area of the powder, measured by the BET method with krypton, was 5100 cm^2 for the degassed palladium and 6600 cm^2 after depositing 400 ML of oxygen. Hoffman et al [72] observed that oxygen dissociatively adsorb on Pd above 200 K and it forms p(2x2) LEED pattern at room temperature, which corresponds to 0.25 ML oxygen coverage, with oxygen atom occupying the three fold hollow sites. In general at an oxygen coverage (θ_o) of 0.25 ML on Pd(111) formation of (2x2) structure has been observed by LEED, and Scanning tunneling microscopy (STM) by many groups [72, 76]. In the presence of oxygen between 10^{-7} and 6 x 10^{-5} mbar and the temperature between 573 and 683 K, there is a two dimensional metastable Pd_5O_4 oxide was observed by many research groups [63, 64].

Gopinath et al [73, 74] studied NO adsorption and decomposition on Pd(111) through molecular beam technique. It has been observed that at above 475 K, NO dissociation was observed followed by oxygen diffusion into the subsurface. θ_o measured through CO-titration demonstrates a decreasing θ_o above 450 K in spite of significant NO dissociation. Indeed what is noticeable in that the oxygen adatom (O_{ad}) formed, due to NO dissociation, disappears from the Pd(111) surfaces ≥475 K. which is in agreement with the oxygen subsurface diffusion model. Kinetic oscillation has been observed in the rate of formation of CO_2 from CO + O_2 reactions and subsurface diffusion of oxygen on Pd(110) surfaces [75]. It has been demonstrated that the presence of subsurface oxygen decreases the work function beyond θ_o = 0.5 ML as oxygen atoms located beneath the topmost layer will be associated with dipole pointing inwards with respect to surface plane [76]. Conrad et al [77, 78] studied the interaction of NO and O_2 on Pd(111) surfaces using LEED, TPD, and Ultraviolet-photoelectron spectroscopy (UVPES).

Titkov et al [62] observed the oxygen diffusion into the subsurface of Pd(110) at ≥400 K and the O_2 partial pressure between $2x10^{-8}$ to $7.5x10^{-2}$ Torr. Results obtained by TPD and XPS indicate that oxygen penetrates into the subsurface layers of palladium (≥ 15–20 Å) and is distributed in a low concentration. Growth and decomposition of the metastable surface Pd_5O_4 oxide [64, 65] on Pd(111) was studied at temperatures between 573 and 683 K and O_2 pressures between 10^{-7} and $6x10^{-5}$ mbar. Klötzer et al [64] and Leisenberger et al [66] studied the adsorption and desorption of oxygen on Pd(111)

surfaces using molecular beam adsorption, LEED, TPD, and STM, between 300 and 623 K and up to 1 ML using high flux molecular beam of oxygen. It is shown that the formation and decay of p(2x2) surface structure involves a massive rearrangement of surface Pd atoms and change in the surface geometry. Figure 1.4 shows the thermal desorption spectral results observed from Pd(111) upon dosage of 4000 ML of oxygen at temperature 623 K. Before that, the Pd(111) was heated to 1273 K. The maximum desorption of chemisorbed oxygen occurred in a single peak at 750 K and there is no oxygen desorption above 900 K; no additional peaks appeared at higher temperatures in Figure 1.4a. Figure 1.4b was obtained after an oxygen pre-dose of 8000 ML at 973 K, followed by 4000 ML of oxygen at 623 K [87]. This pretreatment was carried out to populate the oxygen into the subsurface levels of palladium, which produces an additional desorption peak at 1142 K. It has been claimed that at least five times higher exposure was necessary to populate the subsurface layers as well as to measure the small thermal desorption feature that occur around 1140 K; it is because of very low defect density in the single crystal, especially with (111) facets.

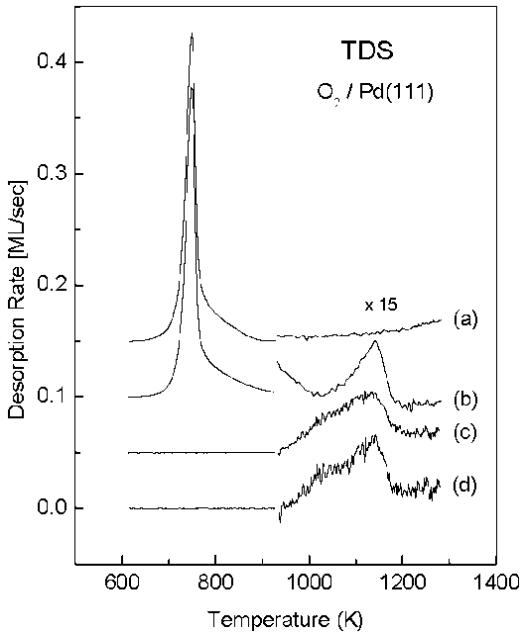

Figure 1.4 Thermal desorption spectra of oxygen from Pd(111): (a) after heating to 1273 K and 4000 ML oxygen at 623 K; (b) after exposure to 8000 ML at 973 K and 4000 ML at 623 K; (c) after preparation (b), but desorption to 923 K and cooling to 300 K; (d) after preparation (b) followed by reaction with 300 ML CO at 523 K.(Adapted from [66])

The chemisorbed oxygen can easily be removed thermally by heating up to 923 K (Figure 1.4c) or by CO titration at 523 K (Figure 1.4d) without markedly affecting the desorption feature at 1142 K [66]. This also indicates that the subsurface oxygen cannot be removed by CO titration. The supply of oxygen to the near surface is relatively easier than oxygen migration to the bulk. Figure 1.5 shows the phase diagram of Pd-O system in a wide temperature and pressure regime. Pd(111) structure was slowly converted to PdO with increase in the O_2 partial pressure from 10^{-5} Torr to 1 Torr using high pressure X-ray photoelectron spectroscopy (HPXPS) [67].

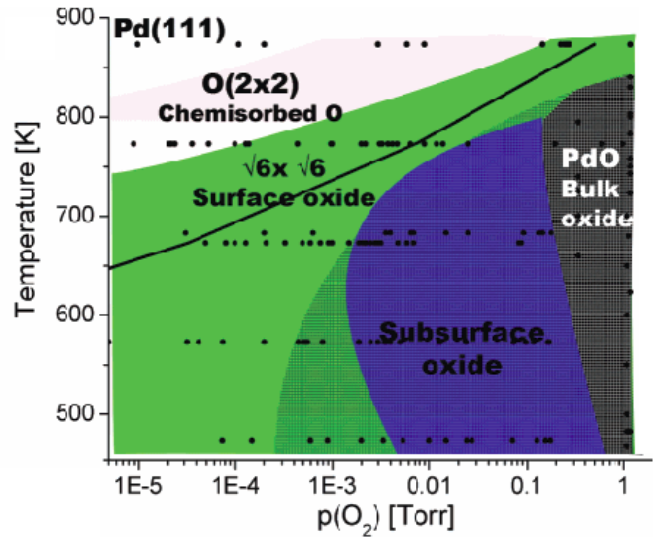

Figure 1.5 Phase diagram showing the stability regions of the different palladium oxide structures as a function of oxygen partial pressure and temperature. The points mark the conditions under which XPS data were acquired while increasing the oxygen pressure at fixed temperature (oxidizing conditions). At these points, no change was observed in the spectra over several minutes. The solid line indicates the phase transition of bulk Pd to bulk PdO. The hatched region shows the PdO bulk oxide stability region when the pressure is reduced from 1 Torr at fixed temperature. (Adapted from [67])

Surface and subsurface structures formed during the oxidation of Pd(111) has been explored. Initially (2x2) structure forms above 800 K with O_2 partial pressure between 10^{-5} and 10^{-3} Torr. The surface oxide formation with √6x√6 structure has been observed between 650 and 750 K. No "subsurface oxide" is observed during diffusion-controlled reduction. It has been proposed that an epitaxial "subsurface oxide" forms as a metastable intermediate in the bulk oxidation, and that the low activation energy for this

process kinetically stabilizes the "subsurface oxide". Bulk PdO forms around 1 Torr between 500 and 800 K.

1.7.2. Structure aspects

Leisenberger et al [66] observed the surface and subsurface oxygen on Pd(111) between 300 and 1000 K using several methods including HREELS. Figure 1.6 shows HREEL spectra taken in 5^o off-specular geometry from (a) Pd(111)-O_I and (b) Pd(111)-O_{II} surfaces before and after a 5 Langmuir (L) CO dose at room temperature, followed by heating to 423 K.

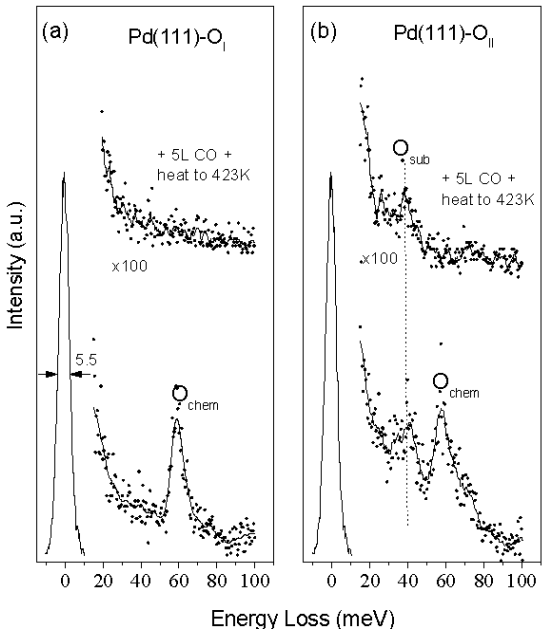

Figure 1.6 HREELS spectra in 5° off-specular geometry before and after removal of the chemisorbed oxygen by dosing (a)Pd(111)-O_I and (b) Pd(111)-O_{II} surfaces with 5 L of CO followed by a heating to 423 K. (Adapted from [66]).

In the specular mode, there is a loss peak observed at 58.9 meV, mentioned as O_{chem}, due to chemisorbed oxygen on Pd(111) at 300 K . This peak is also present in the HREELS spectrum recorded from the 523 K oxygen dosed Pd surface (lower curve in Figure 1.6b). Here, however, there is an additional weaker peak, at loss structure ~ 40 meV is also observed. It is suggested to be the vibrational modes of oxygen which is present in the subsurface region, and mentioned as O_{sub}.

Dosing the Pd(111)-O_{II} surface with 5 L CO and subsequently heating to 423 K removes the O_{chem} peak completely, but leaves the O_{sub} loss peak virtually unaffected (Figure 1.6, upper curves). Further, the O_{sub} structure could be removed from the HREEL spectra only after prolonged (about 1 h) sputtering and annealing treatments (up to 1000 K), again suggesting its subsurface nature. Hence, the loss feature at 40 meV is assigned to vibrations of O located in the subsurface region of the Pd(111) surface. The slow removal of O_{sub} can be further explained by Ar^+ ion sputtering and annealing treatments. After 40 L dosing of O_2 at two different temperatures (300 K and 523 K), LEED patterns were measured. The spots corresponds to 300 K looks sharp and intense half orders, whereas the half-order reflections are weak and diffuse for 523 K, due to decrease in the concentration of oxygen result in subsurface migration [66]. Conrad et al [77, 78] studied by exposing 3 L of O_2 on clean Pd(111) surface at 300 K. The appearance of diffuse half order spots in the LEED pattern which becomes sharper with further increase of the O_2 exposure. After about 8 L exposure a (2x2) and $(\sqrt{3}x\sqrt{3})/R30^o$ structures were identified. This structure also is quite resistant to the attack of hydrogen, a reaction which on the other hand very effectively removes adsorbed oxygen. Apparently, this structure originating from the high temperature treatment is not due to adsorbed oxygen but must be associated with a more tightly bound species in the form of a "surface oxide" which is also a precursor to PdO.

Voogt et al [79] studied the oxygen interaction on Pd(111) and polycrystalline palladium with TPD, LEED, XPS, AES, etc. It gave an indication for the formation of surface oxide at higher temperatures (> 470 K) and at O_2 partial pressure of ~ $7.5x\ 10^{-7}$ Torr. XPS showed that almost 0.5 ML PdO on the surface. Whereas any amount of oxygen could be observed by AES, as its electron beam easily removed adsorbed oxygen. This is more pronounced in Pd(111) than polycrystalline Pd which suggests that oxygen is bound tightly to the defect sites. Lattice parameters calculated from the complex LEED patterns, neither matched with Pd(111) nor PdO, and the structure was more close to speculated PdO(010). The desorption energy calculated from the TPD results were 140 ± 17 kJ/mol and this value is close to the heat of formation of PdO, 112.8 kJ/mo1.

Lundgren et al [80, 81] observed the formation of surface oxide on Pd(111) through STM, and Surface X-ray diffraction (SXRD). Structure of surface oxide on Pd(111) was found to be a coplanar Pd_5O_4 overlayer, forming a two-dimensional oxide on the close-packed Pd(111) substrate. Above study revealed that the two-dimensional Pd_5O_4 oxides showing no resemblance to bulk oxides. As per both structure and energetics, the two-dimensional oxide is an intermediate phase between oxygen over layer and a bulk oxide.

Lundgren et al [82] observed the oxidation of Pd(100) surfaces in a wide range of oxygen pressure (10^{-6} to 10^{3} Torr) and temperature (up to 1000 K) by in-situ SXRD. Using atomistic thermodynamics calculations, bulk oxide growth was identified even at 675 K. Using SXRD the presence of (√5x√5) R27° surface oxide was confirmed, and bulk oxide film was formed predominantly with PdO(001). The observed diffraction changed significantly as the oxygen pressure and temperature is increased to $7.5x10^{2}$ Torr and 675 K respectively, the (√5x√5) R27° surface oxide has completely disappeared from the surface, i.e., the initially formed PdO(101) plane does not continue to grow but instead restructures. It has been shown that there are totally six different states of oxygen on Pd(100), including the first stage of dissociative O_2 chemisorption [83-85]. A p(2x2) chemisorbed layer was formed up to θ_o = 0.25 ML coverage. Above 0.25 ML both c(2x2) and p(2x2) was observed. Above 400 K a PdO(001)-like (√5x√5)R27° reconstruction which is further confirmed by STM and at the last stage surface roughening happenes corresponds to bulk PdO. It has been concluded that chemisorbed oxygen is far more reactive toward CO than the PdO(001)-like reconstructed surface which in turn is more reactive than bulk PdO. Markovits et al [86] studied oxygen diffusion on Pd(111) surface from a 3-3 hollow site, the most stable adsorption mode, to a 3-1 hollow site through a bridge site using first-principle quantum mechanics calculations and slab models. The mobility of the surface induces a large restructuring and avoiding the cleavage of the strong (Pd-O) bonds associated with the adsorption was predicted. The surface atoms remain attached to the adsorbate during diffusion was found. An altogether different conclusion derived from above theoretical simulation is that oxygen covered Pd layer slips into the subsurfaces and the metallic Pd layer moves to the surface and this avoids

the energetically expensive breaking and making of Pd-O bonds. Although an energetically viable method for oxygen diffusion was suggested by the above calculation [86], none of the experimental observation indicates the above mechanism.

1.7.3. Spectroscopy aspects

Titkov et al [62] studied the O_2 interaction on Pd(110) at 400 K using XPS. O 1s peak was observed at 529.3 eV, and with higher exposure (10^8 L) the intensity of the peak remained constant which indicates the invariability of chemical state and coverage of oxygen on Pd(110). The XPS analyzer located at 55° with respect to the sample surface provided the analysis depth about 15–20 Å. The presence of oxygen in the subsurfaces of palladium within 15–20 Å was confirmed. Leisenberger et al [66] studied the interaction between oxygen and Pd(111), and subsurface oxygen (BE= 529.7 eV) could be distinguished from surface oxygen (BE= 529.2 eV) by both XPS and off-specular HREELS by CO titration.

Bondzie et al [75] observed the migration of oxygen into Pd(110) subsurfaces and the same has been attributed to be responsible for oscillations in the kinetics of catalytic oxidation of CO. The oxide layer decomposes upon heating in vacuum and results in a much stronger than normal subsurface oxygen desorption event in TPD spectra. Figure 1.7 describes the importance of in-situ spectroscopy technique to probe the presence of subsurface oxygen. In-situ high pressure XPS has been utilized for Pd(111) at oxygen partial pressure of 0.06 mbar at 573 K [87, 88].

Pd $3d_{5/2}$ core level peak contains contributions from bulk Pd (335.0 eV) and two additional components at BEs. of 335.6 and 336.3 eV. The Pd $3d_{5/2}$ peak with Binding energy (BE) = 335.6 eV and was 336.3 eV peak is likely due to adsorbed oxygen (O_{ad}) and PdO. On turning-off O_2 supply, all the high BE features, > 335 eV, disappears demonstrating the highly metastable nature of surface oxide species. This metastable oxide phase is considered to be the precursor state before the oxygen diffusion into subsurface begins. The above point illustrates that, in-situ techniques are more important to measure the observation of metastable oxide formation on any surface [87, 88].

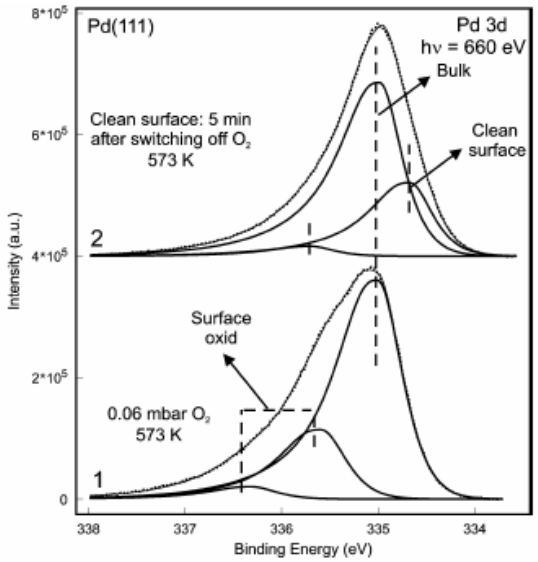

Figure 1.7 Pd $3d_{5/2}$ region of Pd(111) single crystal (1) in the presence of 0.06 mbar O_2 at 573 K (2) and right after switching off O_2. Incident photon energy, *hv* = 660 eV. Dashed line: measured data, full line: fits. (Adapted from [88])

Gabasch et al [89] observed the formation of 2D oxide phase on Pd(111), which is Pd_5O_4 and supersaturated with O_{ads} layer. The surface was completely covered with 2D oxide between 600 K and 655 K and it decomposes completely above 717 K due to diffusion of oxygen into the palladium bulk. During cooling from high temperature and at $2.25x10^{-3}$ Torr O_2, the oxidized Pd^{2+} species appeared at 788 K; whereas the similar species decomposed at 717 K during heating is to be noted. The surface oxidized states exhibited an inverse hysteresis. The oxidized palladium observed during cooling was assigned to a new oxide phase, probably the $(\sqrt{67}x\sqrt{67})$ R12.2^o structure. The structural changes and the formation of palladium oxide (Pd_xO_y) are highly dependent on temperature and oxygen pressure.

Kim et al [90] studied the palladium-oxygen interaction using ESCA. Both oxygen-chemisorbed palladium atoms (PdO_{ad}) and PdO species has been observed on metal substrates exposed to air at 873 to 1173 K. By examining the peak areas of the Pd and the oxygen spectra, the presence of excess oxygen in the form of different species including, hydrated PdO_2, PdO_2, and $Pd(OH)_2$ or $Pd(OH)_4$ were clearly indicated. According to Weissman et al [91, 92], high oxygen exposures of about 10 to 20 L at sample temperatures of around 1000 K are the most effective way to populate the

subsurface oxygen. Corro et al [93] showed a direct relation between Pd activity for CH_4 oxidation and the degree of oxidation of Pd species. Nakai et al [94] studied CO oxidation on O-covered Pd(111) surface with fast XPS. The oxygen overlayer is compressed upon CO co-adsorption from a p(2x2) structure into a $(\sqrt{3}x\sqrt{3})R30°$ structure and then into a p(2x1) structure with increasing CO coverage at 300 K. These three O phases exhibit distinctly different reactivity with p(2x2) phase reacting with CO unless the surface temperature is sufficiently high (>290 K).

1.7.4. CO oxidation on Pd-surfaces containing subsurface oxygen

Thirunavukkarasu et al [74] carried out CO titration on NO dissociated at different temperatures on Pd(111) surface and decrease in the CO_2 production was observed when the NO dissociation temperature increased from 450 K to 525 K; this is attributed to subsurface diffusion of oxygen above 475 K. Bondzie et al [75] investigated the kinetics of oxide formation and its reduction by CO on Pd(110) surfaces. The rate of oxide reduction measured was found to be $r = 2.38x10^5\ p_{CO}\ e^{0.37/RT}$ at 350 K (1.34 ML/s) and at 400 K (14.1 ML/s) agree approximately with the value determined by Ertl et al ($r = 9x10^8\ e^{-14/RT}$) at 350 K (1.6 ML/s) and at 400 K (19.9 ML/s). This is also in agreement with several other reports [95-98], for chemisorbed oxygen, indicating that the oxide species is weakly bound or unstable.

Very recently CO-oxidation on Pd(111) surfaces has been reinvestigated and the effect of subsurface oxygen on CO-oxidation was addressed in detail, by molecular beam techniques [99-103]. CO oxidation has been measured with various ratios of CO and O_2 to demonstrate that the initial oxygen (from the CO + O_2 beam) adsorbed on Pd(111) surface diffuses into the subsurface levels of palladium, and after attaining the threshold subsurface coverage the actual oxidation reaction begins on the surface. Indeed no significant CO adsorption was observed, especially at high temperatures (>600 K), till the threshold ($\theta_{O_{Sub}}$) occurs. The amount of oxygen that is present in the subsurface levels of Pd(111) surfaces increase with increase in temperature up to a threshold value under UHV conditions; however no further oxygen uptake occurs above the threshold coverage ($\theta_{O_{Sub}}$). In this process, the top few layer of metallic Pd is converted to a mildly oxidized

form ($Pd^{\delta+}$), and hence the metallic bulk Pd is decoupled from the surface due to this process.

The concept of oxygen in the subsurface and oxidation of Pd towards oxidation reactions has been observed in the powder catalysts also. Roy et al [104, 105] used solution combustion method to synthesis $Ti_{1-x}Pd_xO_{2-\delta}$ for the first time, a new photo catalyst for CO oxidation, NO reduction and C_xH_y oxidation purpose. The photo catalytic activity was investigated by varying Pd content and 1 atom % of Pd ion is found to exhibit high activity. High rates of photo oxidation of CO with O_2 over $Ti_{1-x}Pd_xO_{2-\delta}$ are observed at room temperature. It was shown that enhanced CO oxidation at Pd^{2+} ion site and O_2 or NO photo dissociation at oxide ion vacancy is responsible for the enhanced catalytic activity. Baidya et al [106] synthesized $Ce_{1-x}Sn_xO_2$ (x= 0.1-0.5) solid solution and its Pd substituted analogue by a single step solution combustion method. Oxygen storage capacity of $Ce_{1-x}Sn_xO_2$ was found to be much higher than that of $Ce_{1-x}Zr_xO_2$ due to accessible Ce^{4+}/Ce^{3+} and Sn^{4+}/Sn^{2+} redox couples between 473 and 673 K. Pd^{2+} ions in $Ce_{0.78}Sn_{0.2}Pd_{0.02}O_{2-\delta}$ are highly ionic, and the lattice oxygen of this catalyst is highly labile, leading to low temperature CO to CO_2 conversion. The rate of CO oxidation was 2 μmol/g s at 323 K. Thus, Pd^{2+} ion substituted $Ce_{1-x}Sn_xO_2$ was suggested to be a superior catalyst compared to Pd^{2+} ions in CeO_2, $Ce_{1-x}Zr_xO_2$, and $Ce_{1-x}Ti_xO_2$ for low temperature exhaust applications due to the involvement of the Sn^{2+}/Sn^{4+} redox couple along with Pd^{2+}/Pd^0 and Ce^{4+}/Ce^{3+} couples.

Oxygen storage with nano palladium clusters on ordered Fe_3O_4 film has been reported [107]. Pd particle size has been varied between 2 to 100 nm. For low metal loading and small particles, oxidation is highly efficient, but the total oxygen-storage capacity is limited by the small amount of Pd available per catalyst surface area. Formation of Pd oxide becomes kinetically hindered for high metal loading and large particles. The maximum oxygen uptake is observed at intermediate Pd loading at a particle size 7 nm. Here, the particles are large enough to allow substantial amounts of interface oxide to be formed (between Pd particles and support) but are yet small enough to avoid strong kinetic hindrance to oxide formation. It is to be noted that the oxide

formed is at the metal-support interface and there is no metal oxide on the surface is reported.

1.8. TWC converter reactions on Palladium surfaces - structure of the thesis

Pd was found to be a versatile catalyst for three way catalytic converter reactions. Especially towards CO oxidation and the influence of oxygen on the subsurfaces of Pd, NO reduction using various reductant like CO, ethanol, etc. **Chapter 1** briefly introduces the concept of air pollution and environmental catalysis, the role of catalytic converters in the vehicular exhausts. Catalytic converter reactions like CO oxidation, VOC oxidation, and NO_x reduction reactions on Pd surfaces have been described. Further, in this chapter surface science aspects and the model single crystals studies for oxygen diffusion on Pd surfaces has been described with structure and spectroscopy aspects.

Chapter 2 focuses the description of Molecular Beam Instrument (MBI) to study the fundamental kinetic aspects under isothermal conditions developed in our laboratory. Details about the calculation of important parameters like sticking coefficients (*s*), surface coverages, etc, from experimental kinetic data are described

In **Chapter 3**, CO oxidation with O_2 on Pd(111) and polycrystalline palladium surfaces have been carried out in a wide range of temperature and CO:O_2 beam compositions. It is identified that there is a diffusion of significant coverage of oxygen into the subsurfaces of Pd, especially ≥600 K. A revisit to CO oxidation on Pd(111) surfaces was to explore the influence of subsurface oxygen on overall kinetics, and particularly transient state kinetics. Interesting information derived from the above studies is the necessity to fill up the subsurface layers with oxygen atoms to threshold coverage ($\theta_{o_{sub}}$), above which the reactive CO adsorption occurs on the surface and subsequent CO_2 production. Variety of experiments has been carried out to confirm the above conclusion. $\theta_{o_{sub}}$ was determined to be 0.3 ML between 500 and 850 K before the onset of CO adsorption under reaction conditions; however, $\theta_{o_{sub}}$ increases from insignificant value <500 K to 0.4 ML at 900 K with pure O_2-beam. Onset of CO adsorption with significant s_{CO} (up to 0.25) on the Pd-surfaces, that is covered with significant subsurface oxygen, underscores a change in the electronic state of Pd-surfaces

towards mildly oxidized (or $Pd^{\delta+}$) state and likely an electronic decoupling occurs between bulk and top few surface atomic layers. Similar observation with polycrystalline Pd-surfaces suggests the defects sites are the likely channels for oxygen diffusion into subsurfaces. In another set of experiments, oxygen has been dosed systematically from 5 to 110 minutes at 900 K (surface modified (SM) Pd(111)) to populate the oxygen in the subsurfaces of Pd(111), prior to CO + O_2 reactions. The CO + O_2 composition has been varied from (7:1) CO-rich to (1:11) O_2-rich compositions and the temperature varied from 273 and 525 K. Ambient temperature (AT) CO oxidation has been observed with surface modified (SM) Pd(111) surfaces. Sustainable CO_2 production has been observed for an hour in O_2-rich conditions without any decrease in the rate of CO_2 production underscores the importance of SM Pd(111) surfaces. It is also important to understand the detailed nature of surface/interface changes under oxidizing conditions with spectroscopic and structural tools.

Our study, presented in **Chapter 4**, explores the influence of oxygen on NO:CO reaction on Pd(111) surfaces with wide range of temperatures between 400 and 800 K and beam compositions. The beam compositions varied from stoichiometric to CO, NO rich beams with respect to NO, CO and O_2. Maximum reactivity were found between 500 and 600 K for all beam composition ranges. The kinetic data are presented to understand the role of oxygen and the main effect of the oxygen addition to the NO:CO mixture is to inhibit the NO-dissociation rates and clearly enhance the rate of CO_2 production under most circumstances. Surface oxygen decreases the net NO adsorption and dissociation above 550 K and maintains the CO-oxidation rates. The overall reaction is largely controlled by the N+N recombination between 500 and 600 K and NO-dissociation also contribute to the rate determining step with increasing temperature and oxygen content in the beam. The rate of formation of CO_2, and N_2 does not vary much with CO flux. Pd(111) surface show reversible nature with respect to oxygen-rich and oxygen-lean conditions. Large NO-dissociation occurs on relatively oxygen-free Pd-surfaces (oxygen lean) or only in TS on oxygen rich conditions, which is observed through fast beam switching for better de-NO_x management.

In **Chapter 5**, nitric oxide (NO) reduction with ethanol has been studied on Pd(111) surfaces under oxygen rich and lean conditions using a molecular beam approach to study the effect of ethanol blended gasolines. Significant nitrogen production and ethanol oxidation was observed with the Ethanol + NO (and O_2) beams at temperatures above ~ 500 K, even though ethanol sticking coefficient was immeasurably low ≤400 K on clean and oxygen covered Pd(111) surfaces. Generally, oxygen favors the complete ethanol oxidation on Pd(111) surfaces, and CO_2 production increases with increasing oxygen content. Fast beam switching experiments were performed in order to show NO-reduction management under net oxidizing environments.

Chapter 6 deals with conclusions and future scope of the work. In general, oxygen in the subsurface layers of Pd facilitates high temperature (>700 K) as well as low temperature (273 K) CO oxidation. With this, new concept CO oxidation regime broadens at low and high temperatures **(Chapter 3)**. Systematic addition of CO to the beam effectively utilizes the chemisorbed O atoms, and makes Pd surface free for NO adsorption **(Chapter 4)**. Addition of ethanol effectively utilizes NO reduction even in the oxidizing environment. Further, beam switching experiments between O_2-rich and O_2-lean underscores net NO reduction in oxidizing environment **(Chapter 5)**. Addition of oxygen to the beam always ends up in lesser NO reduction. Systematic addition of CO to the beam effectively utilizes the chemisorbed O atoms, and makes Pd surface free for NO adsorption. Fast beam switching experiments between O_2-rich and O_2-lean underscores the possibility of managing NO reduction under net-oxidizing environment.

1.9. References

1. (a)http://www.plunkettresearch.com/Industries/AutomobilesTrucks/AutomobileTrends/tabid/89/Default.aspx Retrieved 2010-09-09.
   (b)http://www.worldometers.info/cars/
   (c)http://www.sasi.group.shef.ac.uk/worldmapper/display.php?selected=31
2. (a) http://www.epa.gov/air/emissions/voc.htm. (b) Mendell, M. J. *Indoor Air*, **2007**, *17*, 259. (c) Wolkoff, P.; Wilkins, C. K.; Clausen, P. A.; Nielsen, G. D. *Indoor Air*, **2006**, *16*, 7. (d) Bernstein, J. A.; Alexis, N.; Bacchus, H.; Bernstein, I.

L.; Fritz, P.; Horner, E.; Li,. N.; Mason, S *et al*. *Journal of Allergy and Clinical Immunology* **2008**, *121*, 585.

3. http://www.ipa-news.com/en/89-0-Catalytic+Converters.html
4. Taylor, K. C. *Catal. Rev. Sci. Eng.* **1993**, *3*, 457.
5. Shelef, M.; Graham, G. W. *Catal. Rev. Sci. Eng.* **1994**, *36*, 433.
6. Kreuzer, T.; Lox, S. E.; Lindner, D.; Leyrer, J. *Catal. Today.* **1996**, *29*, 17.
7. http://www.aecc.eu/
8. Berndt, H.; Schutze, F. W.; Richter, M.; Sowade, T.; Grunert, W. *Appl. Catal. B* **2003**, *40*, 51.
9. Olsson, L.; Persson, H.; Fridell, E.; Skoglundh, M. *J. Phys. Chem. B* **2001**, *105*, 6895.
10. Jobson, E. *Top. Catal.* **2004**, *28*, 191.
11. Schmick, H.-D.; Wassmuth, H.-W. *Surf. Sci.* **1982**, *123*, 471.
12. Conrad, H.; Ertl, G.; Küppers, J.; Latta, E. E. *Surf. Sci.* **1977**, *65*, 235.
13. Bertolo, M.; Jacobi, K.; Nettesheim, S.; Wolf, M.; Hasselbrink, E. *Vacuum* **1990**, *41*, 76.
14. Bertolo, M.; Jacobi, K. *Surf. Sci.* **1990**, *226*, 207.
15. Ramsier, R. D.; Gao, Q.; Waltenburg, N.H.; Lee, K.-W.; Nooij, O. W.; Leerts, L.; Yates, Jr., J. T. *Surf. Sci.* **1994**, *320*, 209.
16. Ramsier, R. D.; Gao, Q.; Neergaard Waltenburg, H.; Yates, Jr., J. T. *J. Chem. Phys.* **1994**, *100*, 6837.
17. Sugai, S.; Watanabe, H.; Kioka, T.; Miki, H.; Kawasaki, K. *Surf. Sci.* **1991**, *259*, 109.
18. Nakamura, I.; Fujitani, T.; Hamada, H. *Surf. Sci.* **2002**, *514*, 409.
19. Sharpe, R. G.; Bowker, M. *Surf. Sci.* **1996**, *360*, 21.
20. de Wolf, C. A.; Nieuwenhuys, B. E. *Surf. Sci.* **2000**, *469*, 196.
21. Piccolo, L.; Henry, C. R. *Appl. Surf. Sci.* **2000**, *162-163*, 670.
22. Piccolo, L.; Henry, C. R. *Surf. Sci.* **2000**, *452*, 198.
23. Prèvot, G.; Henry, C. R. *J. Phys. Chem. B* **2002**, *106*, 12191.
24. Seldmair, C.; Seshan, K.; Jentys, A.; Lercher, J. A. *J. Catal.* **2003**, *214*, 308.
25. Hirsimaki, M.; Valden, M. *J. Chem. Phys.* **2001**, *114*, 2345.

26. Johánek, V.; Schauermann, S.; Laurin, M.; Libuda, J.; Freund, H.-J. *Angew. Chem. Int. Ed.* **2003**, *42*, 3035.
27. Johánek, V.; Schauermann, S.; Laurin, M.; Gopinath, C. S.; Libuda. J.; Freund, H.-J. *J. Phys. Chem. B* **2004**, *108*, 14244.
28. Rainer, D. R.; Vesecky, S. M.; Koranne, M.; Oh, W. S.; Goodman, D. W. *J. Catal.* **1997**, *167*, 234.
29. Ozensoy, E.; Hess, C.; Goodman, D. W. *J. Am. Chem. Soc.* **2002**, *124*, 8524.
30. (a) Reinhard, B. *Palladium Emissions in the Environment, Automotive Catalysts, Springer Berlin Heidelberg* (Book Chapter). (b) Kielhorn, J.; Melber, C.; Keller, D.; Mangelsdorf, I. *Int. J. Hyg. Environ. Health* **2002**, *205*, 417
31. Kielhorn, J.; Melber, C.; Keller, D.; Mangelsdorf, I. *Int. J. Hyg. Environ. Health* **2002**, *205*, 417.
32. Gopinath, C. S.; Zaera, F., *J. Catal.* **1999**, *186*, 387.
33. Tagliaferri, S.; Köppel, R. A.; Baiker, A. *Stud. Surf. Sci. Catal.* **1998**, *116*, 61.
34. Johánek, V.; Schauermann, S.; Laurin, M.; Gopinath, C. S.; Libuda, J.; Freund, H-J. *J. Phys. Chem. B* **2004**, *108*, 14244.
35. http://www.unep.fr/scp/rpanel/pdf/Assessing_Biofuels_Full_Report.pdf. Retrieved 2009-10-24.
36. http://www.ethanolrfa.org/page/-/objects/pdf/outlook/RFAoutlook2010_fin.pdf?nocdn=1. Retrieved 2011-02-12.
37. Worldwatch Institute and Center for American Progress (2006). *American energy: The renewable path to energy security*
38. http://extranet.agricultura.gov.br/sislegis-consulta/consultarLegislacao.do?operacao=visualizar&id=17886. Retrieved 2008-10-05.
39. http://www.anfavea.com.br/tabelas/autoveiculos/tabela10_producao.pdf. Retrieved 2011-02-05. *Production up to December 2010*
40. http://anfavea2010.virapagina.com.br/anfavea2010/. Retrieved 2011-02-05.
41. http://www.abraciclo.com.br/images/stories/dados_setor/motocicletas/producao/2010%20produo-dezcorreto.pdf. Retrieved 2011-02-15.

42. http://unica.com.br/noticias/show.asp?nwsCode=4771CECF-FDB8-43B5-9CF9-E342B99F5C23. Retrieved 2010-02-10.
43. Owen, K., Coley., C.S. Weaver, "Automotive Fuels Reference Book", SAE International, ISBN 978-1-56091-589-8
44. http://www.atmosphere.mpg.de/enid/EN__Compounds/NMHC_5rg.html
45. Kelly, K.J., Bailey, B.K., Coburn, T.C., Clark, W., Lissiuk, P. "Federal Test Procedure Emissions Test Results from Ethanol Variable-Fuel Vehicle Chevrolet Luminas", SAE Technical Paper 961092
46. (a) Miyadera, T., *Appl. Catal. B* **1997**, *13*, 157. (b) Karina, T.; Maria, A. S., *Catal. Lett*. **2008**, *124*, 59. (c) Moreira, J.R.; Goldemberg, J., *Energy Policy*, **1999**, *27*, 229.
47. (a) Shelef, M., *Catal. Rev. Sci. Eng*. **1975**, *11*, 1; (b) Shelef, M., *Chem. Rev*. **1995**, *95*, 209. (c) Belton, D. N.; Taylor, K. C., *Curr. Opin. Solid State Mater Sci*. **1999**, *4*, 97.
48. Dong, H.; Shuai, S.; Li, R.; Wang, J.; Shi, X.; He, H., *Chem. Engn. J*. **2008**, *135*, 195.
49. Dzwigaj, S.; Janas, J.; Machej, T.; Che, M., *Catal. Today* **2007**, *119*, 133.
50. (a) De Mello, L. F.; Auxiliadora, M.; Baldanza, S.; Noronha, F. B.; Schmal, M., *Catal. Today*, **2003**, *385*, 3. (b) De Mello, L.F.; Noronha, F.B.; Schmal, M., *J. Catal*. **2003**, *220*, 358.
51. (a) Velu, S.; Satoh, N.; Gopinath, C. S.; Suzuki, K., *Catal. Lett*. **2002**, *82*, 145. (b) Velu, S.; Suzuki, K.; Vijayaraj, M.; Barman, S.; Gopinath, C. S., *Appl. Catal. B.* **2005**, *55*, 287. (c) Velu, S.; Suzuki, K.; Gopinath, C. S.; Hattori, T.; Yoshida, H., *Phys. Chem. Chem. Phys.* **2002**, *4*, 1990.
52. Bowker, M.; Holroyd, R.P.; Sharpe, R.G.; Corneille, J.S.; Francis, S.M., *Surf. Sci*. **1997**, *370*, 113.
53. (a) Bowker, M.; Morgan, C.; Couves, J., *Surf. Sci.* **2004**, *555*, 145. (b) Bowker, M.; Hollroyd, R.; Elliott, A.; Morrall, P.; Alouche, A.; Entwistle, C.; Toerncroma, A., *Catal. Lett*. **2002**, *83*, 165.

54. Holroyd, R. P.; Bennett, R. A.; Jones, I. Z. ; Bowker, M., *J. Chem. Phys*. **1999**, *110*, 8703.
55. Langmuir, I. *Trans. Faraday. Soc.* **1922**, *17*, 607
56. Goodman, D. W. *Ann. Rev. Phys. Chem.* **1986**, *37*, 425.
57. Goodman, D. W. *Surf. Sci*, **1994**, *299/300*, 837.
58. Boudart, M. *Adv. Catal.* **1969**, *20*, 153.
59. Bonn, M.; Funk, S.; Hess, Ch.; Denzler, D. N.; Stampfl, C.; Scheffler, M.; Wolf, M.; Ertl, G. *Science* **1999**, *285*, 1042.
60. Ertl, G. *Chem. Rec.* **2001**, *1*, 33.
61. Goodman, D. W. *Acc. Chem. Res.* **1984**, *17*, 194.
62. Titkov, A. I.; Salanov, A. N.; Segrey, V.; Boronin, K.; A. I. *React. Kinet. Catal. Lett.* **2005**, *86*, 371.
63. (a) Han, J.; Zemlyanov, D. Y.; Ribeiro, F. H. *Surf. Sci.* **2006**, *600*, 2730. (b) Han, J.; Zemlyanov, D. Y.; Ribeiro, F. H. *Surf. Sci.* **2006**, *600*, 2752.
64. Klötzer, B.; Hayek, K.; Konvicka, C.; Lundgren, E.; Varga, P. *Surf. Sci.* **2001**, *482*, 237.
65. Gabasch, H.; Unterberger, W.; Hayek, K.; Klötzer, B.; Kresse, G.; Klein, C.; Schmid, M.; Varga, P. *Surf. Sci.* **2006**, *600*, 205.
66. Leisenberger,; F, P.; Koller, G.; Sock, M.; Surnev, S.; Ramsey, M. G.; Netzer, F. P.; Klötzer, B.; Hayek, K. *Surf. Sci.* **2000**, *445*, 380.
67. Ketteler, G.; Ogletree, F.; Bluhm, H.; Liu, H.; Eleonore, L. D.; Hebenstreit.; Salmeron, M. *J. Am. Chem. Soc.* **2005**, *127*, 18269.
68. Kan, H. H.; Shumbera, R. B.; Weaver, J. F. *Surf. Sci.* **2008**, *602*, 1337.
69. Wickam, D. T.; Banse, B. A.; Koel, B. *Surf. Sci.* **1991**, *243*, 83.
70. Banse, B.A.; Koel, B.E. *Surf. Sci.* **1990**, *232*, 275.
71. Sandler, Y. L.; Durigon, D. D. *Journal of Physical Chemistry*, **1969**, *73*, 2392.
72. Hoffman, A.; Guo, X. C.; Yates, J.T. Jr. *J. Chem. Phys.* **1989**, *90*, 5787.
73. Thirunavukkarasu, K.; Thirumoorthy, K.; Libuda, J.; Gopinath, C. S. *J. Phys. Chem. B* **2005**, *109*, 13283.
74. Thirunavukkarasu, K.; Thirumoorthy, K.; Libuda, J.; Gopinath, C. S. *J. Phys. Chem. B* **2005**, *109*, 13272.

75. Bondzie, V. A.; Kleban, P.; Dwyer, D. J. *Surf. Sci.* **1996**, *347*, 319.
76. Ladas, S.; Imbhil, R.; Ertl, G. *Surf. Sci.* **1989**, *219*, 88.
77. Conrad, H.; Ertl, G.; Kuppers, J.; Latta, E. E. *Surf. sci.* **1977**, *65*, 235.
78. Conrad, H.; Ertl, G.; Kuppers, J.; Latta, E. E. *Surf. sci.* **1977**, *65*, 245.
79. Voogt, E. H.; Mens, A. J. M.; Gijzeman, O. L. J.; Geus, J. W. *Surf. Sci.* **1997**, *373*, 210.
80. Lundgren, E.; Kresse, G.; Klein, C.; Borg, M.; Andersen, J. N.; Santis, M. D.; Gauthier, Y.; Konvicka, C.; Schmid, M.; Varga, P. *Phys. Rev. Lett.* **2002**, *88*, 246103.
81. Westerström, R.; Weststrate, C. J.; Gustafson, J.; Mikkelsen, A.; Schnadt, J.; Andersen, J. N.; Lundgren, E.; Seriani, N.; Mittendorfer, F.; Kresse, G. *Phys. Rev. B* **2009**, *80*, 125431.
82. Lundgren, E.; Gustafson, J.; Mikkelsen, A.; Andersen, J. N.; Stierle, A.; Dosch, H.; Todorova, M.; Rogal, J.; Reuter, K.; Scheffler, M. *Phys. Rev. Lett.* **2004**, *92*, 046101.
83. Zheng, G.; Altman, E. I. *Surf. Sci.* **2000**, *462*, 151.
84. Zheng, G.; Altman, E. I. *Surf. Sci.* **2002**, *504*, 253.
85. Zheng, G.; Altmann, E. I. *J. Phys. Chem. B* **2002**, *106*, 1048.
86. Markovits, A.; Minot. C. *Chem. Phys. Lett.*, **2008**, *458*, 92.
87. Zemlyanov, D.; Kiss, B. A.; Kleimenov, E.; Teschner, D.; Zafeiratos, S.; Hävecker, M.; Knop-Gericke, A.; Schlogl, R.; Gabasch, H.; Unterberger, W.; Hayek, K.; Klotzer, B. *Surf. Sci.* **2006**, *600*, 983.
88. Teschner, D.; Pestryakov, A.; Kleimenov, E.; Haevecker, M.; Bluhm, H.; Sauer, H.; Knop-Gericke, A.; Schlogl, R. *J. Catal.* **2005**, *230*, 186.
89. Gabasch, H.; Unterberger, W.; Hayek, K.; Klötzer, B.; Kleimenov, E.; Teschner, D.; Zafeiratos, S.; Haevecker, M.; Gericke, A. K.; Schlögl, R.; Han, J.; Ribeiro, F. H.; Kiss, B. A.; Curtin, T.; Zemlyanov, D *Surf. Sci*. **2006**, *600*, 2980.
90. Kim, K. S.; Gossmann, A. F.; Winograd, N. *Anal. Chem.* **1974**, *46*, 197.
91. Weissman, D.L.; Shek, M. L.; Stefan, P. M.; Spicer, W. E. *Surf, Sci.* **1980**, *92*, L59.

92. Weissman, D.L.; Shek, M. L.; Stefan, P. M.; Lindau, I.; Spicer, W. E. *Surf. Sci.* **1983**, *127*, 513.
93. Corro, G.; Văzquez-Cuchillo, O.; Banuelos, F.; Fierro, J. L.G.; Azomoza, M. *Catal. Commun*, **2007**, *8*, 1977.
94. Nakai, I.; Kondoh, H.; Shimada, T.; Resta, A.; Andersen, J. N.; Ohta, T. *J. Chem. Phys.* **2006**, *124*, 224712.
95. Engel, T.; Ertl, G. *J. Chem. Phys.* **1978**, *69*, 1267.
96. Engel, T. *J. Chem. Phys.* **1978**, *69*, 373.
97. Engel, T.; Ertl, G. *Adv.Catal.* **1979**, *28*, 1.
98. Salo, P.; Honkala, K.; Alatalo, M.; Laasonen, K. *Surf. Sci.* **2002**, *516*, 247.
99. Gopinath, C. S.; Thirunavukkarasu, K.; Nagarajan, S. *Chem. Asia J.* **2009**, *4*, 74.
100. Nagarajan, S.; Thirunavukkarasu, K.; Gopinath, C. S. *J. Phys Chem. C.* **2009**, *113*, 7385.
101. Thirunavukkarasu, K.; Nagarajan, S.; Gopinath, C. S. *Appl. Surf. Sci.* **2009**, *256*, 443.
102. Nagarajan, S.; Thirunavukkarasu.; K.; Gopinath, C. S. Jonathan Counsell, J.; Gilbert, L.; Bowker, M. *J. Phys. Chem. C.* **2009**, *113*, 9814.
103. Nagarajan, S.; Gopinath, C. S. *J. Ind. Inst. Sci.*, **2010**, *90*, 245.
104. Roy, S.; Hegde, M. S.; Ravishankar, N.; Madras, G. *J. Phys. Chem. C* **2007**, *111*, 8153.
105. Roy, S.; Marimuthu, A.; Hegde, M. S.; Madras, G. *Appl. Cata B: Environmental*, **2007**, *73*, 300.
106. Baidya, T.; Gupta, A.; Deshpandey, P. A.; Madras, G.; Hegde, M. S. *J. Phys. Chem. C* **2009**, *113*, 4059.
107. Schalow, T.; Brandt, B.; Starr, D. E.; Laurin, M.; Shaikhutdinov, S. K.; Schauermann, S.; Libuda, J.; Freund, H-J *Angew. Chem. Int. Ed.* **2006**, *45*, 3693.

Chapter 2

Molecular Beam Instrument (MBI): A Versatile Surface Science Tool

2.1. Introduction

There are many techniques available for the surface scientists which have been developed progressively over the past five decades with the help of advancement in vacuum science. No technique by itself can completely characterise a surface's structure and its reactivity. However, if many techniques are combined, some of the elementary and useful information on surface, adsorbate structure and its activity, electronic nature and physical properties, oxidation states and chemical nature can be explored in detail. Among all techniques to understand the properties of surface, molecular beam is one of the versatile techniques to study the kinetics of vapour phase reactions on metal substrates in detail, and molecular level understanding of surface-adsorbate interactions. This chapter deals an overview of the functioning of molecular beam instrument and its importance towards the three way catalytic converter reactions on flat metal surfaces. Molecular beam instrument was fabricated in our laboratory, to study the gas or vapor phase reactions on metal surfaces under ultra high vacuum conditions [1].

2.1.1. Introduction to molecular beams

A molecular beam is produced by allowing a gas at higher pressure to expand through a small orifice into a chamber at lower pressure to form a beam of particles (atoms, free radicals, molecules or ions) moving at approximately equal velocities, with very few collisions between the particles.There are many advantages when the molecular beam techniques are used, one can find the sticking coefficient of any molecules on metal surfaces, coverage calculations, mechanistic details like, whether the reaction is

Langmuir-Hinshelwood or Eley-Rideal, qualitative idea on surface composition, transient and steady state rate of the reactions, and competitive adsorption of two species in a mixed molecular beam interactions, are the few advantages of molecular beam methods.

As a form of surface science experimentation, it is significant because it probes surfaces indirectly as part of the surface phenomenon itself. Molecular beam instrument (MBI) method is capable of determining microscopic features of surface reactions [2-4]. Molecular beams may be defined as unidirectional beams of atoms or molecules with uniform velocity aimed at a solid surface (target). In ultra-high vacuum (UHV) conditions, the molecules in the beam can propagate without interacting with each other [5]. Figure 2.1 Illustrates the relationship between pressure, molecular density, monolayer formation time and mean free path. The importance of UHV on flat metal surfaces is also represented here. When the pressure is in UHV range (10^{-10} mbar), the molecular density is reduced by 10 orders of magnitude, which makes monolayer formation to 10^4 sec and the mean free path is 10^4 m. Molecular beam experiments are exactly working in this region with beam flux concentrated entirely on the target surfaces.

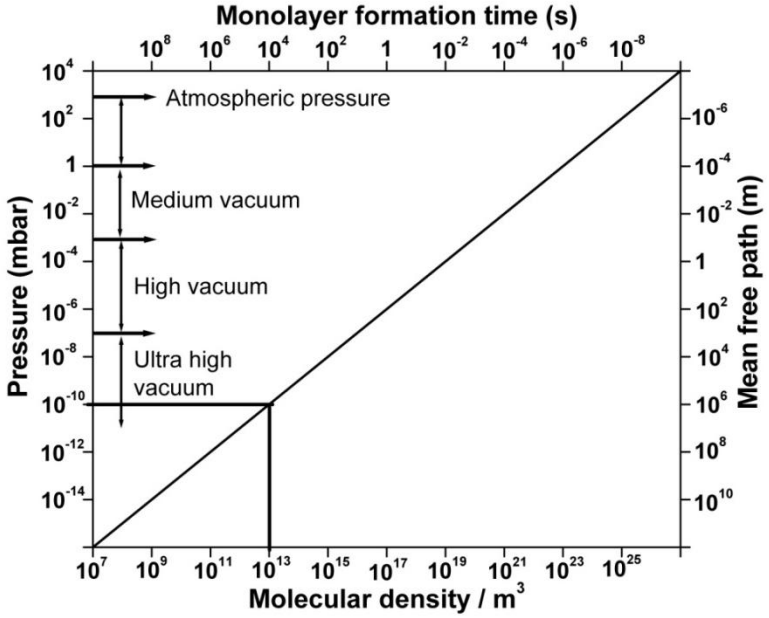

Figure 2.1 Values of molecular density, mean free path and time to form a monolayer as a function of pressure for air at 298 K.

The quantum (translational, rotational and vibrational) states of molecules (in the MB) colliding with a surface will affect the nature of adsorption and surface reaction. Thus molecular beams are used to investigate surface reaction kinetics including sticking probabilities and activation energies of adsorption. Changing the direction of molecular beams can be difficult. Like surface sensitive techniques, molecular beams interact with the outermost surface layer only: they are thus very surface specific and are usually used on very well prepared surfaces. Compared to direct dosing for temperature programmed desorption, beams allow more control over dosing with respect to collision rate and spatial distribution [6]. Hence more accurate adsorption and reaction data can be obtained, even at temperatures higher than normal molecular desorption. Table illustrates, various sources of vacuum, and its corresponding vacuum in Torr, mean free path of the molecules and its density.

Table 2.1 Various sources of vacuum, corresponding vacuum in Torr, mean free path and molecular density.

	Pressure (Torr)	Mean free path	Molecules / cm^3
Vacuum cleaner	600	70 nm	10^{19}
Liquid ring vacuum pump	24	1.75 μm	-
Freeze drying	10^{0}-10^{-1}	100 μm to 1 mm	10^{16} to 10^{15}
Rotary vane pump	10^{0} to 10^{-2}	100 μm to 10 cm	10^{16} to 10^{13}
Incandescent light bulb	10^{-1} to 10^{-2}	1 mm to 1 cm	10^{15} to 10^{14}
Thermos bottle	10^{-2} to 10^{-4}	1 cm to 1 m	10^{14} to 10^{12}
Earth thermosphere	10^{-2} to 10^{-9}	1 cm to 100 km	10^{14} to 10^{7}
Vacuum tube	10^{-7} to 10^{-10}	1 to 1,000 km	-
Cryo pumped MBE chamber and MBI system	10^{-9} to 10^{-11}	100 to 10,000 km	10^{7} to 10^{5}
Pressure on the moon	10^{-11}	10,000 km	-

The molecular beams are classified into two types namely (a) effusive and (b) nozzle sources. With effusive beams, gas effuses from an oven at the gas source. The source pressure (usually of the order of 0.1 atm) is changed to give a Knudsen number K > 1 so that the gas' mean free path is greater than the source aperture width (usually of the order of 0.1 mm) [6]. For simple 'thermal' beams, Knudsen conditions are fulfilled [7], and there is no mass transport in the direction of propagation, and these molecules have well defined Maxwell and Boltzmann distributions, which correspond to velocities and internal energies respectively. In this case the molecular flow is 'free' and beam properties are only dependent on the source pressure and container temperature.

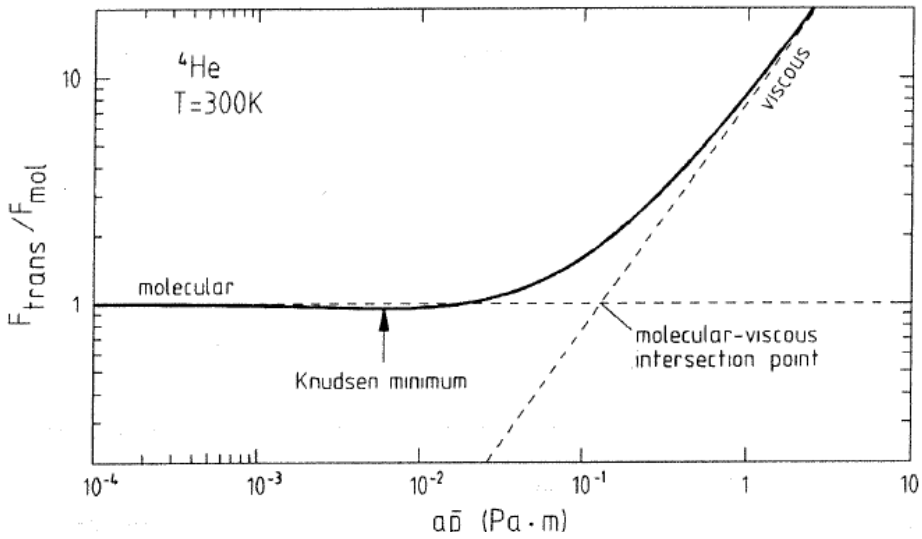

Figure 2.2 Normalized conductance for ^{4}He as a function of pressure showing the transition from molecular to the viscous flow.

Thus both the intensity and the monochromaticity of the beam can be affected conveniently at the same time. 'Thermal' beams have the same temperature as the nozzle or orifice, and typically have fluxes of the order of 10^{18} molecules m^{-2} s^{-1} = 0.01 to 0.1 ML/s [8]. 'Supersonic' beams can also be produced using nozzle sources, where the source pressure is several atmospheres and the orifice is only 100 μm wide, resulting in a molecular velocity greater than the speed of sound. These beams fix all quantum modes into their ground states, so the contribution of each mode to surface kinetics can be investigated [7, 8]. They are often called 'cold' beams as their Maxwell-Boltzmann

velocity distributions are very sharp and occur at a low temperature due to cooling on gas expansion, as shown in Figure 2.2 (indicate the regime in Figure 2.2). 'Supersonic' beam fluxes are several orders of magnitude higher than those of 'thermal' beams. However, only 'thermal' nozzle beams were used during the course of the experiments described in the following chapters.

2.2. Fabrication of molecular beam instrument

A 12 L capacity stainless steel UHV chamber evacuated to the base pressure of about $2x10^{-10}$ Torr with a 210 L/s turbo-molecular drag pump (Pfeiffer, TMU261 MBI is equipped with a molecular beam doser setup, and a sputter ion gun (AG5000, VG Scientific) placed exactly opposite to each other at 180^{o} apart (Figures 2.3 and 2.4) [1]. There are four more cylindrical ports at 45^{o} angle to the central horizontal axis going through Pd(111) sample and turbo pump of MBI; a view-port and an alternate gas leaking source are attached (not seen in Figure 2.4).

An xyz-manipulator with a rotary platform for mounting the Pd(111) sample on a power-thermocouple feed-through (Caburn, 30 A-DC and 5 KV) is placed perpendicular to the doser and sputter ion set-up so that the sample can be moved in all three direction and rotated 360^{o}. The above feed-through is connected to liquid nitrogen well. Thus the crystal can be cooled to about 100 K with liquid nitrogen or resistively heated to 1373 K by a temperature controller capable of maintaining any temperature within ± 2K [1]. A stationary quadrupole mass spectrometer (Pfeiffer, Prisma Quadrupole mass spectrometer (QMS) 200M3), which can detect gas phase species, up to 300 amu and a cold cathode ion gauge (Pfeiffer, IKR270) for measuring the chamber pressure are connected opposite to each other and away from the beam doser.

A five-way valve was connected to the gas manifold system to have fast beam switching experiments, which is reported elsewhere [38]. In beam switching experiments where the gas composition of the beam needed to be changed rapidly, the valve was flipped twice (two 90^{0} turns) within a second, first to one of the pumping positions, and then to a gas reservoir.

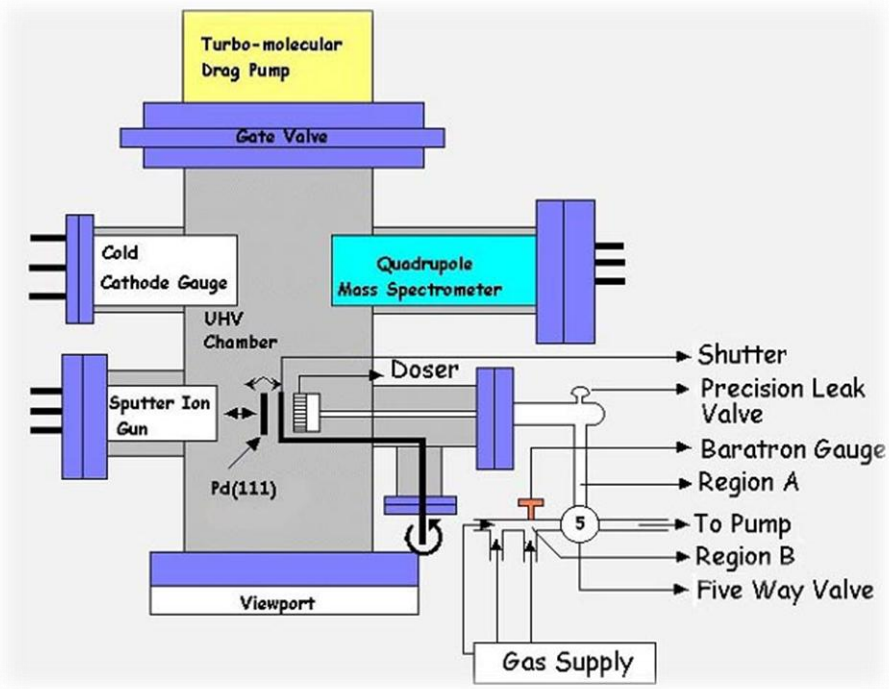

Figure 2.3 Schematic representation of the Molecular Beam Instrument.

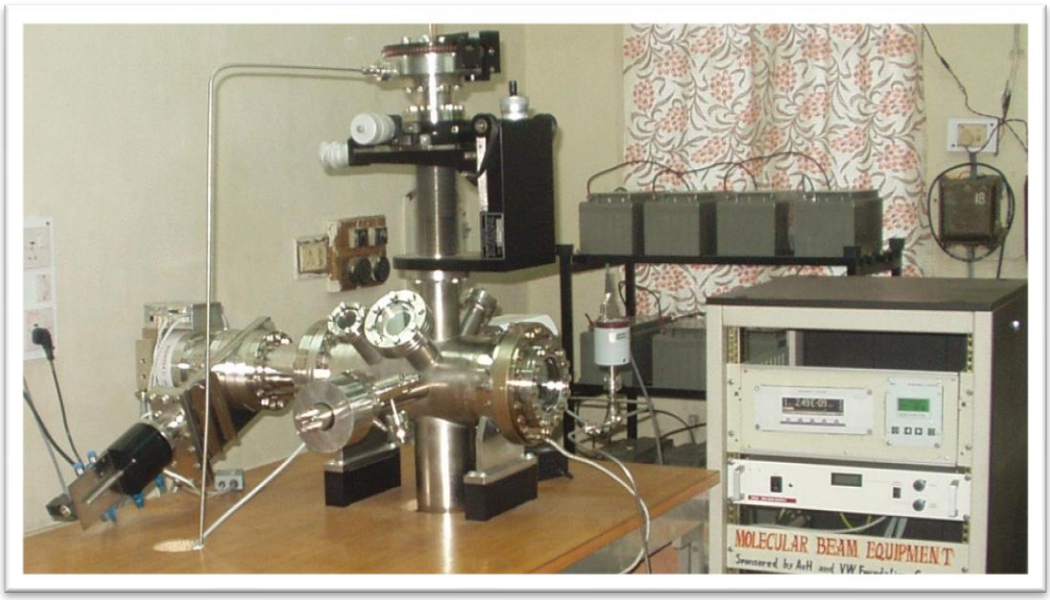

Figure 2.4 Photograph of Molecular Beam Instrument.

The mass spectrometer is kept out of the line-of-sight of the Pd(111) sample to avoid any angular desorption effects. Thus both the QMS and cold cathode ion gauge

were kept at the same distance from turbo pump to minimize the difference between the total pressure readings. The Pd(111) single crystal sample was mounted by spot-welding a 0.5 mm thick tantalum wire on the backside of the crystal and connected to a pair of copper rods, which in turn were connected to the above power-thermocouple feedthrough. A K-type thermocouple was welded on the top of the crystal and to the thermocouple leads of the feed-through. The present set-up is based on the extension of the King and Well's method [9].

2.3. Design considerations of the doser assembly

Clausing's classic work on 1932 [10] introduced the details of molecular flow in a capillary tube. Low energy molecular beams can be created by an array of these microcapillary tubes [11]. Collimated gas beams are the main part of many important experimental techniques in molecular physics, mechanism of chemical reactions, many spectroscopic techniques, surface science and epitaxial growth of crystals [11]. Particularly molecular beams are extensively used in surface science studies [12-25].

Molecular beam doser consists of a multichannel array of capillary disk with open segment of disk diameter to the sample (10 mm) is larger than that of the sample diameter (8 mm). An important concept in describing the quality of a doser, the enhancement factor (E), which is the ratio between the true flux at the sample and the gas flux at pressure P, is calculated by the following expression.[26]

$$E = 1 + [\frac{fS}{k_B T(1 - fs)v_c A}] \quad (2.1)$$

where, v_c is the velocity of the gas molecules, $v_c = (2\pi m k_B T)^{\frac{1}{2}}$, f is the fraction of beam intercepted by the sample, S is the pumping speed, k_B Boltzmann constant, T is the temperature of the gas molecules, *s* is the sticking probability of the molecules, A is the surface area of the sample, and m is the mass of the gas molecules. Aspect ratio calculation of microcapillaries, which is capillary length (L) to diameter (a) ratio, decides the beam profiles. For microcapillary beam doser with an aspect ratio >40, there would

be no considerable beam profile changes except a reduction in conductance with increasing ratio. In the present case we have employed an aspect ratio of 100. In fact, Zaera et al [27] showed that the flattening of the beam profile was widely spread for a microcapillary with a = 10 μm than that of a larger diameter (a=50 μm) with same lengths of capillary (L = 2 mm) but a reduction in conductance was observed with a = 10 μm capillary array and beam quality was good. Indeed the present design provides uniform flux on the overall surface of the metal substrate of 8 mm diameter.

The molecular beam doser, which is connected at present, consists of a 13 mm disk multichannel array made up of microcapillary glass tubes of 1 mm in length and 10 μm in diameter each (Collimated Holes Inc.USA). The doser is attached through a threaded cap and head with teflon O-rings. It is to be mentioned that the open portion of the above microcapillary is only 10 mm, due to the above design in holding the capillary.

A quarter inch tube (OD) of 15 cm in length with baffles (shown in Figure 2.5) to avoid the gas acquiring the shape of the tube is attached with the beam-doser head. Thus a minimum dead volume and a minimum gas load can be maintained in the present set-up compared to a recently reported beam doser [28]. A laterally movable stainless steel shutter, which is manually operated, is placed between the microcapillary doser and the Pd(111) crystal in order to interrupt the beam at will (Figure 2.5 inset).

Hence we could maintain a minimum of 5 mm doser to sample distance in our present setup, which gives an enhancement factor (E) of ~12 [26] and ~45 % fraction of the beam (f) impinges on the surface. Cyclohexane condensation was performed at 125 K (not shown) for the calculation of f value from 2.1. The fraction of the beam intercepted by Pd(111), which is also an important factor for calculating the adsorbate coverage at time, t. [26]

$$\theta(t) = \frac{N(t)}{A} = \frac{1}{A}\int_0^t [\alpha \Delta P(\tau) + \beta s(\tau) P(\tau)] dt \qquad (2.2)$$

where N(t) is the number of adsorbate molecules, A is the surface atom density of the Pd(111) sample (surface atom density of Pd = 1.53×10^{15} cm^{-2}), α, β are constants and it isindependent of beam flux, sample-to-surface distance and surface temperature.

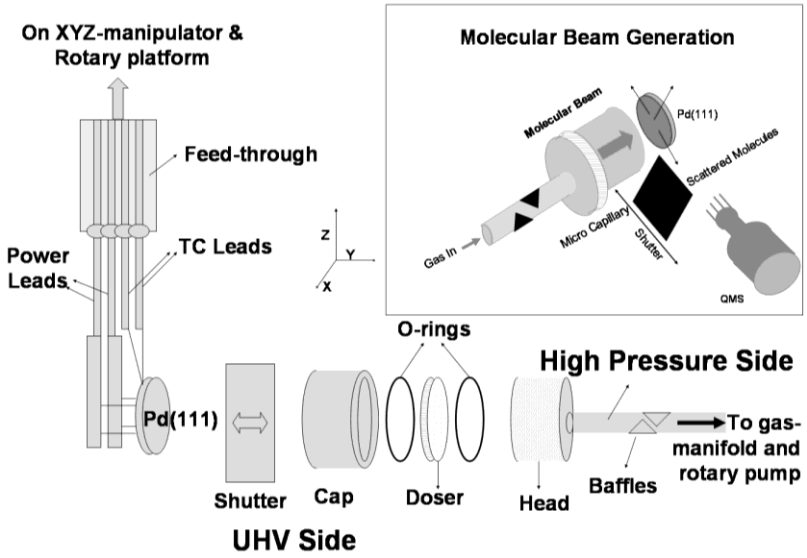

Figure 2.5 Schematics of doser assembly of MBI and the inset show the generation of molecular beam.

Calculated values for α and β are 2.99×10^6 molecules/g and 1.76×10^5 molecules/g respectively for our present set-up. The pumping rate is determined by means of the following equation. [29]

$$P = P_o \exp\left[-\left(\frac{\Lambda RT}{V}\right)t\right] \tag{2.3}$$

where P, P_o, Λ and V here represent the pumping rate, pumping coefficient, pumping constant and volume of the chamber, respectively.

The gas-flux in the molecular beam is determined and controlled by the precision leak-valve opening and the backing gas pressure in the gas-manifold. The gas flux is set by setting both the precision leak valve, and the backing gas pressure in volume B, which is measured by a MKS Baratron pressure gauge initially calibrated against the equilibrium vapor pressure of water at different temperatures. For flux dependent measurements, normally the backing pressure varied and the precision leak valve-opening kept at a predetermined position. The metal substrate, an 8 mm diameter Pd single crystal cut in the (111) direction was used as supplied (Metal Crystals and Oxides Ltd., Cambridge), and mounted by the method described below. Before each experiment,

the crystal is cleaned *in-situ* by a combination of argon ion sputter-anneal cycles at 1000 K in oxygen atmosphere and oxygen treatments at 1000 K followed by flashing to 1200 K as described by Ramsier et al. [30, 31]. The cleanliness of the sample was verified by recording standard temperature programmed desorption (TPD) measurements after adsorption of NO or CO and reproducible CO oxidation kinetics. The cleanliness of the Pd(111) surface was further checked by AES and XPS in another UHV chamber. There were no Si, S and P impurities detected on Pd(111).

2.4. Quadrupole Mass Spectrometry (QMS)

Mass Spectroscopy is an analytical technique for the identification of ions by way of measuring their mass-to-charge ratios. While, in optical spectroscopy frequency and intensity are the most important parameters, in mass spectrometry there are four parameters namely, mass, charge, velocity, and intensity. However, fundamentally, any mass spectrometer determines only the m/e ratio.

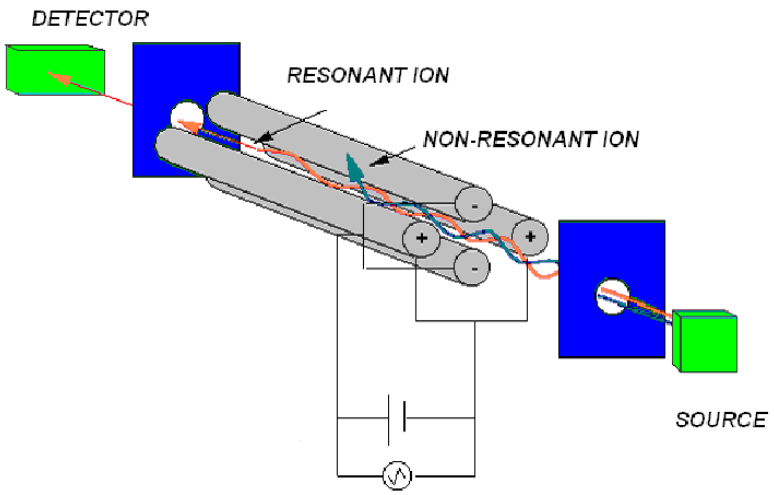

Figure 2.6 A QMS analyser setup.

Mass spectrometers manipulate ionised gases with different masses and electric charges through specific spatial trajectories [23]. This is achieved in many ways, for instance, quadrupole mass spectrometry (QMS) uses an alternating E-field to separate

ions by mass. QMS is a convenient method of mass spectrometry in UHV, and is especially convenient for RGA due to low cost and power requirements and ease of analysis. A QMS analyser is shown in Figure 2.6 Quadrupole mass spectrometers consist of an ion source, ion optics to accelerate and focus the ions through an aperture into the quadrupole filter, the quadrupole filter itself with control voltage supplies, an exit aperture, an ion detector, detection electronics, and a high-vacuum system.

A quadrupole mass filter consists of four parallel metal rods arranged as in the figure below. Two opposite rods have an applied potential of (U+Vcos(wt)) and the other two rods have a potential of -(U+Vcos(wt)), where U is a dc voltage and Vcos(wt) is an ac voltage. The applied voltages affect the trajectory of ions traveling down the flight path centered between the four rods. For given dc and ac voltages, only ions of a certain mass-to-charge ratio pass through the quadrupole filter and all other ions are thrown out of their original path. A mass spectrum is obtained by monitoring the ions passing through the quadrupole filter as the voltages on the rods are varied. There are two methods: varying w and holding U and V constant, or varying U and V for a constant w. The quadrupole analyzer is a relatively low resolution mass filter compared to magnetic sector mass spectrometers, but is more suitable for RGA in UHV.

2.5. Materials and methods

2.5.1. Sample

The Pd(111) sample is spot welded on the back side of the crystal using 0.5 mm thick tantalum wire and connected to the copper rods and K-type thermocouple is welded on the periphery of the crystal.

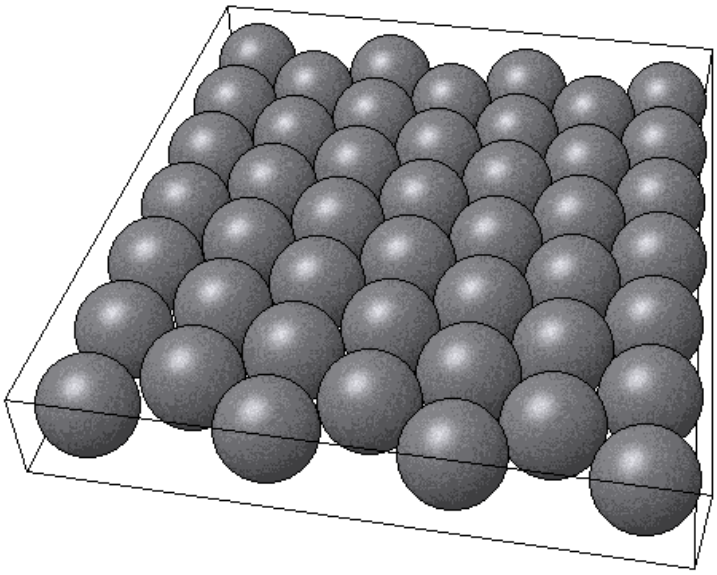

Figure 2.7 Model of Pd(111) surfaces, generated by surface explorer.

The Pd(111) was supplied by Metal Crystals & Oxides Ltd. UK and the surface was cleaned by cycles of (Argon + Oxygen = $1.5x10^{-6}$ Torr) for an hour at 1000 K, and annealing ($1x10^{-7}$ mbar O_2, 1000 K, 30 min) and flashing (1200 K, 2 min) as documented elsewhere [29]. The major elemental impurities on Pd(111) was carbon, and the same was removed during the sputtering cycles. As an alternative, O_2 dosing, followed by TPD was used to check for the presence of CO and CO_2 in the desorption trace [27, 28].

2.5.2. Reactant preparation

Gas handling manifold is made of SS tube (quarter inch thickness) which is pumped by rotary pump to the base vacuum of ~ $5x10^{-3}$ Torr and the gas lines are flushed 2-3 times by the reactant gases before introducing into the manifold. The liquid reactant (ethanol) was purified by freeze pump thawing before filling the gas manifold. The reactants with desired compositions has been taken in this gas manifolds using baratran guage with the pressure of 6 millibar (in all the reactions). The gaseous chemicals used in experiments: Ar, O_2, ^{12}CO, ^{13}CO, ^{14}NO, ^{15}NO, H_2 and D_2 were used in lecture bottles provided by Inox and Sigma-Aldrich Ltd, with purities of more than 99.5% respectively. Before any

experiment, liquid samples (ethanol in our case) were subjected to rotary pumping and freeze-pump-thaw cycles to remove dissolved gaseous and high vapour pressure contaminants such as oxygen. Samples were checked regularly by mass spectrometry for air leaks and isomerised contaminants (Table 2.2.).

Table 2.2. A list of the main fragments of interest during the studies of this thesis. The main fragments are listed, and several have to be monitored simultaneously to prevent confusion between molecules with the same amu, to avoid this, isotopic labeled molecules were used.

Name	**Symbol**	**Mass Pattern (amu)**
Argon	Ar	40, 38, 36, 20
Oxygen	O_2	32, 16
Carbon monoxide (C-12)	^{12}CO	28, 16, 12
Carbon monoxide (C-13)	^{13}CO	29, 16, 13
Nitric oxide (N-14)	^{14}NO	30, 16, 14
Nitric oxide (N-15)	^{15}NO	31, 16, 15
Ethanol	C_2H_5OH	46, 45, 43, 31
Hydrogen	H_2	2, 1
Deuterium	D_2	4, 2

2.6. Typical experimental data

For all experiments, the clean Pd(111) metal surface was kept at constant temperature and exposed to an effusive NO molecular beam. All the relevant gas-phase species formed during the reaction are detected by a quadrupole mass spectrometer as a function of time. A typical experiment is explained here with NO adsorption on Pd(111) surfaces. First, the NO molecular beam was allowed to enter the UHV chamber with the shutter in a closed position to block the surface, so as to avoid the direct interaction of NO molecules and Pd(111) surface. Typical experimental details are available in earlier sections 2.2, 2.3 and

2.4 and also in [29]. Still, a small amount of NO adsorption from the background cannot be prevented. After a few seconds, at t = 14 s, the shutter was removed to allow the beam to directly impinge on the Pd(111) surface. An instantaneous decrease in the partial pressure of NO for the next few seconds can be noticed in the mass signal as a result of NO adsorption on Pd(111) surface from the beam (see Figure 2.8 (a) This adsorption in the transient state continues until the surface is saturated with NO.

Figure 2.8 (a) represents a typical gas phase temporal profile for the NO adsorption. Notice the sudden dip in the partial pressure, once the shutter is opened, signaling the onset of rapid adsorption. The gas phase concentration further shows almost 'a constant value', implying an almost constant rate of adsorption, viz. a constant sticking coefficient, especially in the initial part of adsorption. Further, the well depth and breadth of adsorption decreases with increasing temperature, as it should, as the competing desorption increases substantially with temperature from 375 K and above. At t = 75 s the doser is switched off, and the molecular beam flux is stopped.

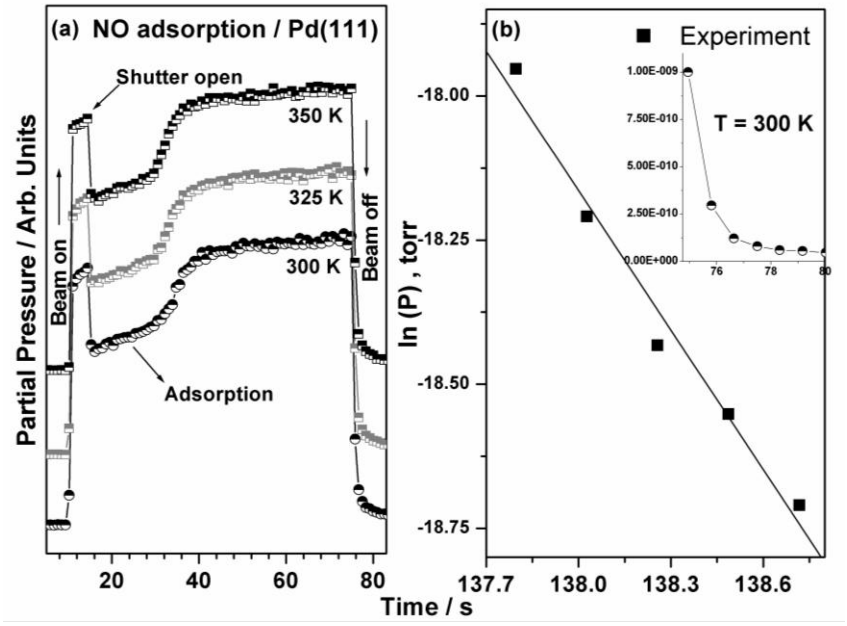

Figure 2.8 (a) A typical gas phase profile Vs time for NO adsorption. Note the shallow basin like structure, especially at low temperatures, suggesting the Precursor State Model (PSM). (b) Graph illustrating the log plot of chamber pressure Vs time for pumping speed (mass flow rate) calculation (adapted from [29a]).

Figure 2.8 (b) indeed shows that the above relationship is valid, and directly leads us to the pumping speed in a straightforward least squares procedure using a simple logarithmic transformation. As is shown in the inset in Figure 2.8 (b), some tailing of the gas phase concentration is evident at higher times, due to desorption from the walls, but this can be corrected by a Least Squares fitting of the back ground to a linear relationship. However, the exponential fall means that the experimental pressure values immediately after the closing of the shutter of the doser is important in evaluating the pumping speeds, and rightly gives us this quantity.

2.7. Summary

A simple and home-built molecular beam instrument (MBI) is described. Using the above setup, three way catalytic converters reactions like CO oxidation, NO_x reduction using various reductants like CO and ethanol has been carried out in the presence and absence of oxygen on Pd(111) surfaces. Results presented in the next chapters for the above reactions, indeed, demonstrates the effectiveness of MBI for catalysis research.

2.8. References

1. Thirunavukkarasu, K.; Gopinath, C. S. *Catal. Lett.* **2007**, *119*, 50.
2. Stuckless, J. T.; Al-Sarraf, N.; Wartnaby, C.; King, D. A. *J. Chem. Phys*., **1993**, *99*, 2202.
3. Bowker, M.; Guo, Q.; Li, Y.; Joyner, R. W. *Surf. Sci*., **1991**, *257*, 33.
4. Poelsema, B.; de Zwart, S. T.; Comsa, G. *Phys. Rev. Lett*., **1982**, *49*, 578.
5. Comsa, G. *Surf. Sci*., **1994**, *299*, 77.
6. Bowker, M. *Appl. Catal. A: General* **1997**, *160*, 89.
7. Zhu, G.; Han, J.; Zemlyanov, D. Y.; Ribeiro, F. H. *J. Am. Chem. Soc.* **2004**, *126*, 9896.
8. Campbell, C. T.; Goodman, D. W. *Surf. Sci.* **1982**, *123*, 413.
9. King, D. A.; Wells, M. G. *Surf. Sci.* **1972,** *29*, 454.
10. Clausing, P. *J. Vac. Sci. Tech.* **1932,** *8*, 636.

11. (a) Pauly, H. in: Scoles, G. (Ed.) **1988** Atomic and Molecular Beam Methods, *1* (Oxford University Press) 99. (b) Scoles, G. in: Scoles, G. (Ed.), *Atomic and Molecular Beam Methods, Vol. 1* (Oxford University Press) **1988,** 1.
12. Freund, H-J.; Bäumer, M.; Libuda, J.; Risse, T.; Rupprechter, G.; Shaikhutdinov, S. *J. Catal.* **2003,** *216*, 223.
13. Hoffmann, J.; Meusel, I.; Hartmann, J.; Libuda, J.; Freund, H-J. *J. Catal.* **2001,** *204*, 378.
14. Bertarione, S.; Scarano, D.; Zecchina, A.; Johánek, V.; Hoffmann, J.; Schauermann, S.; Frank, M. M.; Libuda, J.; Rupprechter, G.; Freund, H-J. *J. Phys. Chem. B* **2004**, *108*, 3603.
15. Bowker, M.; Holroyd, R. P.; Sharpe, R. G.; Corneille, J. S. Francis, S. M.; Goodman, D. W. *Surf. Sci.* **1997,** *370*, 113.
16. King, D. A.; Wells, M. G. *Surf. Sci.* **1972,** *29*, 454.
17. Libuda, J.; Freund, H-J. *J. Phys. Chem. B* **2002,** *106*, 4901 and references therein.
18. Zaera, F. *Prog. Surf. Sci.* **2001**, *69*, 1 and references therein.
19. Kleyn, A. W. *Chem. Soc. Rev.* **2003**, *32*, 87 and references therein.
20. Zaera, F. *Int. Rev. Phys. Chem.* **2002,** *21*, 433 and references therein.
21. Piccolo, L.; Henry, C. R. *Appl. Surf. Sci.* **2000**, *162-163*, 670.
22. Piccolo, L.; Henry, C. R. *Surf. Sci.* **2000**, *452*, 198.
23. Prèvot, G.; Henry, C. R. *J. Phys. Chem. B* **2002**, *106*, 12191.
24. Piccolo, L.; Henry, C.R. *J. Mol. Catal. A: Chemical* **2001,** *167*, 181,
25. Judai, K.; Abbet, S.; Wőrz, A.S.; Heiz, U.; Henry, C.R. *J. Am. Chem. Soc.* **2004,** *126*, 2732.
26. (a) Campbell, C. T.; Valone, S. M. *J. Vac. Sci. Technol. A* **1985,** *3*, 408. (b) Liu, J.; Xu, M.; Nordmeyer, T.; Zaera, F. *J. Phys. Chem.* **1995,** *99*, 6167.
27. Guevremont, J. M.; Sheldon, S.; Zaera, F. *Rev. Sci. Instrum.* **2000,** *71*, 3869.
28. Fisher, G.L.; Meserole, C.A. *J. Vac. Sci. Technol. A*, **2005,** *23*, 722.
29. (a) Thirunavukkarasu, K.; Nagarajan. S.; Gopinath. C. S.; Prasad, S.D. (Submitted *J. Phys. Chem. C* **2011**) (b) Nagarajan. S.; Gopinath. C. S.; Thirunavukkarasu, K. *J. Phys.Chem. C.* **2009**, *113*, 7385. (c) Thirunavukkarasu, K.; Nagarajan. S.;

Gopinath. C. S. Appl. Surf. Sci. **2009**, *256*, 443. (d) Nagarajan. S.; Gopinath. C. S. *J. Indi. Inst. Sci.* **2010**, *90*, 245.

30. Ramsier, R. D.; Gao, Q.; Waltenburg, N.H.; Lee, K.-W.; Nooij, O. W.; Leerts, L.; Yates, Jr., J. T. *Surf. Sci.* **1994**, *320*, 209.
31. Ramsier, R. D.; Gao, Q.; Neergaard Waltenburg, H.; Yates, Jr., J. T. *J. Chem. Phys.* **1994**, *100*, 6837.
32. Ramsier, R. D.; Gao, Q.; Waltenburg, N.H.; Lee, K.-W.; Nooij, O. W.; Leerts, L.; Yates, Jr., J. T. *Surf. Sci.* **1994**, *320*, 209.
33. Ramsier, R. D.; Gao, Q.; Neergaard Waltenburg, H.; Yates, Jr., J. T. *J. Chem. Phys.* **1994**, *100*, 6837.
34. Zhu, G.; Han, J.; Zemlyanov, D. Y.; Ribeiro, F. H. *J. Am. Chem. Soc.* **2004**, *126*, 9896.
35. Campbell, C. T.; Goodman, D. W. *Surf. Sci.* **1982**, *123*, 413.

Chapter 3

$CO + O_2$ Reactions on Pd(111) Surfaces

3.1. Introduction

Carbon monoxide (CO) is a colourless, odourless and tasteless gas, which is lighter than air but lethal. It is generally produced from the partial oxidation of carbon containing compounds. Worldwide, the largest source of carbon monoxide is natural; it is due to photochemical reactions in the troposphere which generate about 5×10^{12} kilograms per year. Other natural sources of CO include volcanoes, forest fires, and other forms of combustion. Typical concentrations in parts per million (ppm) and the source of emission are given in table 3.1[1].

Table 3.1 Typical concentration of CO in parts per million (ppm) and its effects on human

Concentration	Source
0.1 ppm	Natural atmosphere level
0.5 to 5 ppm	Average level in homes
5 to 15 ppm	Near properly adjusted gas stoves in homes, modern vehicle exhaust emissions
100 to 200 ppm	Exhaust from automobiles in the Mexico City central area (Slight headache within two to three hours; loss of judgment)
5,000 ppm	Exhaust from a home wood fire
7,000 ppm	Undiluted warm car exhaust without a catalytic converter (Headache and dizziness in one to two minutes. Convulsions, respiratory arrest, and death in less than 20 minutes).

Carbon monoxide is toxic to all aerobic forms of life. It is easily absorbed through the lungs and difficult for humans to detect. Inhaling even relatively small amounts of the gas can lead to hypoxic injury, neurological damage, and even death. Different people

and populations may have a different carbon monoxide tolerance level. On average, exposures at 100 ppm or greater is dangerous to human health [2]. The acute effects produced by carbon monoxide in relation to ambient concentration increases severely with increasing CO-content, especially above 100 ppm. The other main form of CO emission is from automobile engines from all over the world. Every year the number of vehicles on the earth is increasing exponentially due to advancement in technology. As a consequence, CO emissions also increased. The noble metals like (Pd, Pt, Rh) [3] supported on various metal oxides like Al_2O_3, CeO_2, ZrO_2, La_2O_3 etc are together present in vehicles as a catalytic converters which is converting 90% of the CO, NO_x, and VOC to harmless (CO_2, N_2 and H_2O) gases. Among noble metals, Pd attracted the automobile industries and technologists due to various reasons already described in (**Chapter 1**).

Detailed work on CO and O_2 adsorption and CO + O_2 reaction on Pd(111) surfaces has been reported by Engel et al [4] To understand the molecular level mechanism of CO oxidation and NO reduction on the well-defined surfaces. Many interesting phenomena were observed, such as the oscillatory nature of CO oxidation with a high O_2:CO ratio [5]. The surface chemistry of oxygen interaction with Pd-surfaces seems to be complicated, mainly due to diffusion of oxygen into subsurfaces and/or bulk, and metastable Pd_xO_y formation depending on the experimental conditions [6-19]. Up to an oxygen coverage (θ_o) of 0.25 ML and below 500 K, a (2x2) structure was observed on Pd(111) surfaces by LEED and STM [6-8, 16]. At temperatures above 500 K, and either at high O_2 pressure or with stronger oxidants (NO_2), oxygen subsurface diffusion begins and different surface structures were observed. For example, two-dimensional metastable surface oxide (Pd_5O_4) formation was observed and confirmed by in-situ XPS, when the partial pressure of oxygen was 10^{-3} mbar on Pd(111) or on prolonged exposure at 10^{-6} mbar between 500-600 K [12, 14]. Zheng and Altmann [8] identified that oxygen desorption occurs at two temperature regimes, 750-850 K and ~1150 K due to surface and subsurface oxygen from TPD studies. Further subsurface oxygen does not produce any CO_2 up on CO titration. HREEL spectra distinguish the surface oxygen loss peak at 59 meV and subsurface oxygen at 40 meV [8]. After CO titration, surface oxygen peak vanishes at 59 meV; however, 40 meV remains after CO

titration, confirms the difference between surface and subsurface oxygen. Stable surface oxides also have been observed at high pressures and temperatures and characterized [12, 14, 19]. Nevertheless, it is not known how the subsurface oxygen influences any reactions on Pd-surfaces.

In order to understand the molecular level mechanism of CO oxidation and NO reduction on the catalytic converter, well ordered single crystals of Pd, other noble metals and powder catalysts has been studied extensively under relevant reactions [20-33]. Although CO-oxidation steady-state kinetics is practically independent of surface orientation [20], practical catalysts and metal deposited catalysts display preferential 111 orientation than other facets [22, 32]. Many other interesting phenomena like observation of oxidized Pd species after methane oxidation on Pd/Al_2O_3 [30-32]. There is controversy exist in deciding the nature of active species to be Pd or Pd^{x+} on Pd-catalyzed oxidation reactions [8, 12, 13, 30-32]. Nonetheless, there is an increasing convergence towards the conclusion that oxidized Pd does have some influence in oxidation reactions. Few groups independently studied $Pd/\gamma\text{-}Al_2O_3$ for methane oxidation [30-32]. XPS evidence shows the presence of Pd^{2+} species and the same might be responsible for oxidation of methane, which suggests the oxidation of Pd to PdO. Above results indicate that the oxidation state of Pd surface could play a major role in the catalytic behavior, especially at high temperatures. Many $CO + O_2$ reaction studies have been carried out on different facets of Pd surfaces [20-33]. Detailed work on CO and O_2 adsorption and $CO + O_2$ reaction on Pd(111) surfaces by Ertl et al [20] and confirmed the Langmuir-Hinshelwood mechanism for the reaction. Goodman et al [22] studied CO oxidation on Pd single crystals and compared with Pd deposited silica thin films. A strong metal–support interaction, manifested as encapsulation, inter-diffusion, and alloying, was found to alter the catalytic property significantly. A direct CO-adsorption with relatively high reactive sticking coefficient (rs_{CO}) observed at high temperatures on Pd(111) surfaces that contains significant amount of subsurface oxygen suggested the likelihood of oxidized Pd-surface might be responsible for catalytic activity [34]. Markovits et al [35] reported energy calculations on oxygen diffusion into Pd(111) subsurfaces. It is suggested that there might be a slipping movement of entire layer covered with oxygen to the metallic layer

beneath for oxygen diffusion, instead of breaking and making Pd-O bonds which is energy intensive. The interaction of O_2 with Pd(110) has been studied by TPD and XPS indicate that oxygen penetrates deep into the subsurface layers of palladium (15-20 Å) and is distributed in its bulk in a low concentration [13]. Although there have already been reports on the steady-state behaviour of CO + O_2 reaction on Pd-surfaces [20-33], there have not been, to the best of our knowledge, any careful studies on the transient state (TS) aspects of the above reaction, especially at high temperatures with technically relevant conditions like high temperatures and wide range of CO:O_2 ratios. The present chapter addresses above.

3.2. Experimental section

Isothermal experiments with CO + O_2 reaction on Pd-surfaces were conducted in a MBI between 273 and 900 K and CO:O_2 ratios between 7:1 and 1:11. More Details about the MBI used for the experiments is available in (Chapter 2 section 2.2, 2.3 and 2.4) and also in [18, 37].

3.3. High temperature CO oxidation results

3.3.1. General considerations-raw kinetic data

A typical raw isothermal kinetic data of the reaction of CO + O_2 with a beam composition of (1:2) at 490 K is presented in Figure 3.1. (1) At t = 10 s a molecular beam of a mixture of reactants (CO + O_2 = 1:2, F_{CO+O_2} = 0.32 ML/s) was turned on. At this point reactant molecules (CO and O_2) are scattered in the UHV chamber. An immediate increase in the partial pressures of CO and O_2 could be clearly seen and their partial pressure values reaches to a new steady-state value. It is to be noted that the partial pressure of CO_2 does increase marginally at this point due to the reaction between the background reactants on Pd(111) surface; however the extent of above contribution from the background is <5% [36, 37], which is not included in our calculations. (2) Around t = 15 s the shutter was opened, till then blocking the beam from impinging the Pd(111) surface directly, to allow for the direct adsorption of reactants on the surface kept at 400 K. A sudden decrease in

the partial pressure of the reactants was observed, along with a gradual increase in the CO_2 partial pressure. This stage is termed as the TS and will be discussed in detail later.

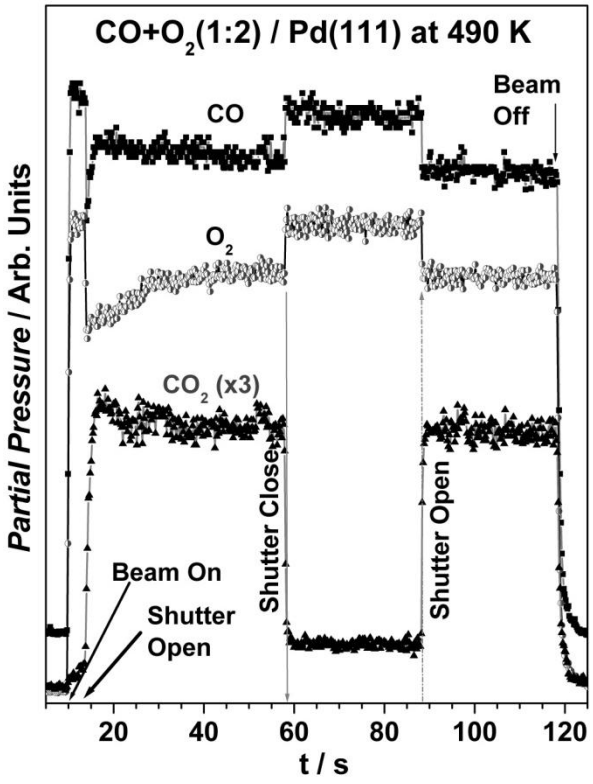

Figure 3.1 A typical raw kinetic data measured under isothermal condition. An effusive 1:2 CO:O_2 molecular beam was directed onto Pd(111) surface kept at 490 K were followed as a function of time. The beam was deliberately blocked between 60 and 90 s (solid and dotted arrows) in the steady state to measure the rate of the reaction respectively.

(3) The CO + O_2/Pd(111) system is allowed to evolve until a steady state (SS) is reached, which normally occurs within a minute after shutter removal; in the present example (Figure 3.1) SS reaches around t = 25 s (10 s after shutter opening). (4) In the SS the molecular beam was deliberately blocked at t = 60 s and unblocked at 90 s to measure the SS rate of the reaction. There is a clear increase in the partial pressure of CO and O_2 and a drop in CO_2 partial pressure was observed. The changes measured in the partial pressure of CO, O_2, and CO_2 allow to directly determining the SS reaction rate, of course after calibration of relevant species. At the point of shutter closing (reopening), an increase (a decrease) in CO pressure momentarily above (below) the normal SS partial pressure level observed underlines the high CO-coverage under SS reaction conditions.

However, no such observation was made with oxygen suggests a highly competing CO for adsorption sites, in spite of lower CO content than oxygen. Such observations noticed in experiments were discussed at relevant places in this chapter. (5) The beam was turned off at 120 s to stop the reaction.

3.3.2. O_2 and CO adsorption on Pd(111) surfaces

Independent CO adsorption, O_2 adsorption (and CO titration) experiments were carried out to demonstrate that indeed there is oxygen diffusion into Pd-subsurfaces occurs as well to show significantly large oxygen sticking coefficient (S_{O_2}) on clean Pd(111) surface. Figure 3.2a shows CO adsorption on Pd(111) surfaces between 350 and 600 K. Upon shutter opening a decrease in the partial pressure of CO indicates its uptake on the surface (hatched area in Figure 3.2a for 350 K data) and it continues till the surface is saturated and no further adsorption occurs. Note the direct measurable CO adsorption decreases with increasing temperature due to increasing rate of desorption and decreasing CO sticking coefficient S_{CO} hence no net CO adsorption is observed above 550 K on clean Pd(111). It is in good agreement with the literature reports [20, 22].

O_2 adsorption on Pd(111) surfaces measured between 500 and 900 K is shown in Figure 3.2b. O_2 adsorption rate on clean Pd(111) surfaces remains high at all temperatures studied. Unlike a systematic decrease in the extent of direct CO adsorption from 350 to 550 K, direct O_2 adsorption continues above the oxygen desorption maximum (750-850 K) [6, 8] at a comparable rate to that of at low temperatures. Note the small amount of surface oxygen desorption from the O-saturated surfaces at the time of shutter closing (denoted as C in Figure 3.2b), and again oxygen adsorption at shutter opening at ≥800 K at latter time (denoted as O). Indeed the above O_2-adsorption measurement at 900 K is in excellent agreement to that of the measurement made by Leisenberger et al [6] under similar conditions and it is attributed to the subsurface diffusion.

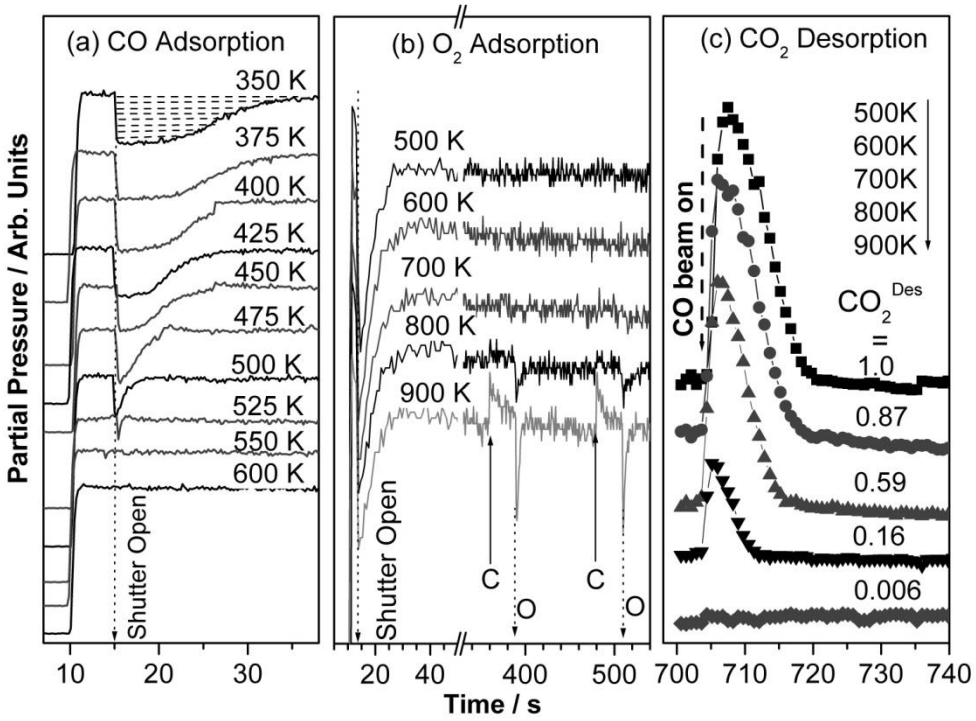

Figure 3.2 a) CO adsorption, and b) O_2 adsorption on Pd(111) surfaces at different temperatures. c) CO titration carried out on the surface prepared in (b) to measure the surface O. Hatched area in panel a indicates the extent of CO-adsorption.

This clearly suggests that there is subsurface diffusion of oxygen on Pd(111) surfaces. Further the rate of oxygen desorption seems to be significantly lower compared to rate of oxygen diffusion into subsurfaces at ≥800 K. Oxygen saturated Pd(111) surfaces, prepared by oxygen dosing for 650 s at different temperatures (Figure 3.2b), were titrated with CO at 500 K to measure the surface θ_o through CO_2 desorption. CO_2 estimated in the above titration decrease with increasing O_2 adsorption temperature, and suggests surface θ_o decreases linearly. Above decrease in CO_2 yield at high temperatures is attributed to an increasing oxygen subsurface diffusion. The above observations also suggest the oxygen saturated surfaces does not prevent CO-adsorption and subsequent CO_2 production below ≤800 K; however the CO_2 production depends on the θ_o available on the surface, which decreases with increasing temperature.

3.3.3. Subsurface oxygen $(\theta_{o_{sub}})$

Extent of $\theta_{o_{sub}}$ diffusing into the subsurfaces during the experiment is calculated directly from the O_2 adsorption studies. Figure 3.3 shows the $\theta_{o_{sub}}$ at different temperatures calculated from the direct oxygen uptake for 750 s on Pd(111) surfaces at different temperatures with same oxygen beam flux. Surface θ_o measured from CO titration was excluded in the above calculation. $\theta_{o_{sub}}$ begins to appear from 500 K, and increases linearly up to 900 K. Rate of migration of oxygen into subsurfaces increases with increasing temperature.

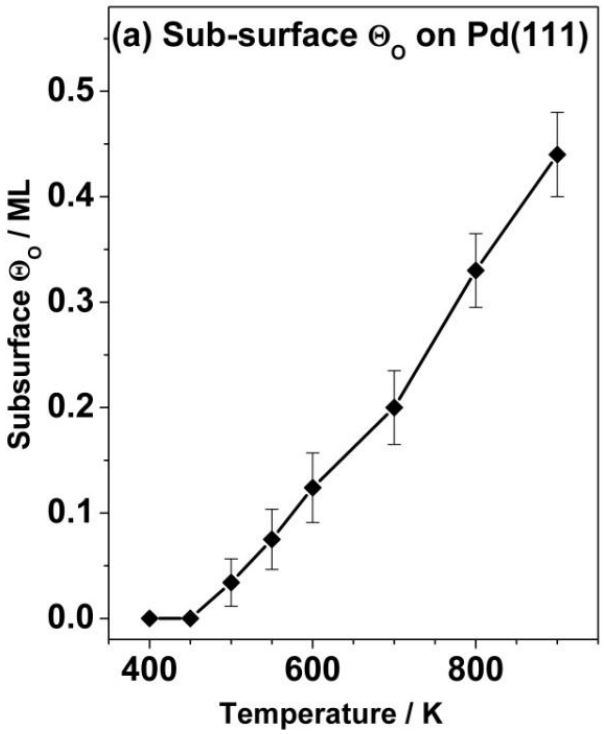

Figure 3.3 Subsurface oxygen coverage calculated directly from the oxygen uptake on Pd(111) exposed for 750 s.

Above findings in combination with our results of up to $\theta_{o_{sub}}$ = 0.4 ML suggests the nature of surface Pd atoms are likely to change significantly, especially electronically, in the presence of oxygen atoms. A simple flashing the Pd(111) to 1150 K in vacuum, desorbs any subsurface oxygen [12].

This scenario may be viewed as a precursor to metastable oxide phase, and likely the surface layers is decoupled electronically from the bulk and responsible for high temperature activity reported herewith. Metastable oxide formation observed by Zemlyanov et al [12] through in-situ XPS on Pd(111) surfaces at oxygen pressure above 10^{-3} mbar supports the above discussion. Figure 3.4a shows oxygen adsorption on clean Pd(111) surface at 900 K. A decrease in O_2 partial pressure at the time of shutter removal demonstrates an unambiguous adsorption. It is to be underscored that direct O_2 adsorption continues above the oxygen desorption range (~750-850 K) [6, 8, 20, 22] at a significant rate. Intermittent beam modulation was carried out to observe the trend in adsorption with time.

Note some amount of surface oxygen desorption from the O-saturated surfaces at the time of shutter closing (Figure 3.4a), and again oxygen adsorption observed on shutter opening at a latter time. Continuous oxygen adsorption for longer time is evident from the relatively lower partial pressure value at high temperatures (≥700 K). A gradual decrease in oxygen adsorption at higher times is to be noted and above t = 500 s, no significant oxygen adsorption indicating a saturation of subsurface layers with oxygen atoms. This directly demonstrates the diffusion of oxygen into subsurface layers. In view of this oxygen adsorption was carried out for 75 and 750 s without any beam oscillation at different temperatures to measure subsurface coverage quantitatively and to know more about oxygen diffusion. CO titration experiments were carried out to measure the surface θ_o after oxygen adsorption at different temperatures through CO_2 production. Figure 3.4b shows θ_o (or CO_2 produced) from the O_2 saturated surfaces for 75 and 750 s and the difference between them. Amount of CO_2 desorbed decreases with increase in the oxygen adsorption temperature in both cases. Notably, there is no CO_2 production at 900 K, even though there was direct oxygen adsorption for several minutes. An important point to be noted here is the difference in θ_o observed for 75 and 750 s, especially at high temperatures (>500 K). It was expected to show same θ_o at a given temperature, provided there is no oxygen disappearance from the surface due to diffusion into subsurfaces or any other processes.

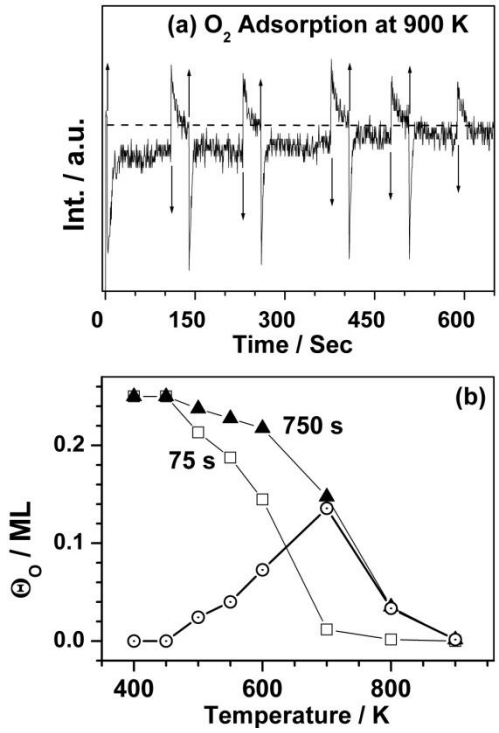

Figure 3.4 (a) Oxygen adsorption on Pd(111) surface at 900 K for extended period. The dotted line corresponds to the base pressure level without adsorption or desorption. Note a continuous oxygen adsorption at a slow rate of adsorption for about 500 s before it reaches a state without any further adsorption. Intermittent beam oscillation performed to show the desorption of adsorbed oxygen exclusively from the surface and quickly reaches the background pressure. Upward and downward arrows indicate the open and closed position of the shutter, respectively. (b) Surface oxygen coverage (θ_o) measured through CO titration after oxygen exposure at different temperatures for 75 and 750 s continuously. Difference between the two set of values plotted (circles) indicates the disappearance of oxygen coverage from the first set of experiments due to migration into subsurfaces.

However, significant difference observed above demonstrates that under the present experimental conditions, oxygen diffuses into the subsurface above 500 K. It is expected that the subsurface levels are filled in the latter experiments (750 s dosing) in addition to surface saturation, and hence there may not be any disappearance of surface oxygen due to diffusion into subsurface. However in the former case for 75 s oxygen dosing, some oxygen disappearance from the surface is expected due to diffusion. The difference between them is plotted and this is the quantity of oxygen migrated into the

subsurface $\theta_{o_{sub}}$. It shows a maximum value at 700 K. Temperatures above 700 K show lower $\theta_{o_{sub}}$ value due to oxygen loss in desorption.

Extent of $\theta_{o_{sub}}$ diffusing into the Pd(111) subsurfaces was calculated directly from oxygen adsorption studies for 750 s at different temperatures and shown in Figure 3.3. Surface θ_o measured from CO titration was excluded in the above calculation. $\theta_{o_{sub}}$ begins to appear from 500 K, and increases linearly up to 0.4 ML at 900 K. Rate of migration of oxygen into subsurfaces increases with increasing temperature. $\theta_{o_{sub}}$ shown in Figure 3.4b is in good correspondence to that of Figure 3.3, up to 700 K. This suggests that oxygen adsorption continues till the threshold subsurface coverage is attained under the present experimental conditions. Titkov et al [13] suggests the oxygen atoms that diffuses into the subsurfaces stays in the top 2 nm. Especially, the oxygen diffusion moves into deeper surfaces at higher temperature within the above 2 nm. Above findings in combination with our results of up to $\theta_{o_{sub}}$ = 0.4 ML suggests the nature of surface Pd atoms are likely to change significantly, especially electronically, in the presence of oxygen atoms. A simple flashing of Pd(111) to 1150 K in vacuum, desorbs any subsurface oxygen [6]. This scenario may be viewed as a precursor to metastable oxide phase, and likely the surface layers is decoupled electronically from the bulk and responsible for high temperature activity reported herewith. Metastable oxide formation observed by Zemlyanov et al [12] through high pressure in-situ XPS on Pd(111) surfaces at oxygen pressure above 10^{-3} mbar supports the above discussion. In contrast to oxygen adsorption at high temperatures, no net CO-adsorption was observed above 525 K and it is in good agreement with the earlier results [20-22].

3.3.4. Transient state (TS) and steady state (SS) kinetics-temperature dependence

Figure 3.5a, b and c shows the temperature dependence of reactants (CO and O_2) adsorption and product CO_2 desorption, respectively, with a CO + O_2 beam composition of 1:1 on Pd(111) surface. Same flux (F_{CO+O_2} = 0.32 ML/s) was maintained for all reactions, unless otherwise specified. A careful analysis of the TS kinetic data indicates

that there are three temperature regimes, and there is a considerable change in CO + O_2 reaction pattern from one region to another and they are listed below:

(1) *Below 500 K*: A profound decrease in CO partial pressure on shutter removal indicating large CO uptake on clean Pd(111) surfaces, and the same continues depending on the beam composition and temperature and hence CO_2 production also varies. Indeed large CO adsorption is evident from the substantial CO uptake from the beam at lower temperatures, and it is a characteristic of strong CO-chemisorption regime. Extent of O_2 adsorption is not as high as that of CO, and it is also the same with CO-rich beams. The above observation is due to high S_{CO}(0.6-0.95) than S_{O_2}(<0.5), and higher saturation θ_{CO} (0.5 ML), than θ_o (0.25 ML) below 500 K [20, 39]. This leads to some poisoning of the active sites by adsorbed CO, and it increases with F_{CO}. This observation is in agreement with that of Goodman et al [22]. However, oxygen-rich (and hence lower F_{CO}) beams displays continuous adsorption of O_2 along with CO (albeit low F_{CO}) and hence the maximum rate regime shifts to relatively lower temperatures with oxygen-rich compositions. CO and O_2 adsorption, and CO_2 desorption display a dynamic changes in the TS, which continues up to a minute, before it reaches the SS. A main characteristic of the present TS is indicated by the over-production of CO_2, which may be defined as the TS CO_2 production rate well above the SS rate [40] (shown as hatched area in Figure 3.5c for 450 K trace), especially with CO-rich beams. This particular behaviour is not observed with O_2-rich beams as well as at reaction temperatures above 500 K.

(2) *Between 500 and 650 K*: This temperature regime is marked by a well defined and constant oxygen adsorption from the beginning till the reaction end. Especially around stoichiometric CO:O_2 compositions (2:1 to 1:2), the rate of oxygen uptake almost remains the same from TS on clean Pd(111) surface to SS. Change in oxygen partial pressure observed at the beginning of the reaction as well as for the beam oscillation in the SS exhibits the similar values support the above conclusion. Nonetheless, the extent of oxygen adsorption changes with other beam compositions. As expected, rate of CO adsorption decreases at the start of the reaction in the TS with increasing temperature. Although no direct CO adsorption is discernible from the CO adsorption traces, high CO_2

production rate hints increasing reactive sticking coefficient of CO (rs_{CO}) from the start of TS to the SS. CO_2 production is instantaneous in this temperature regime (500-650 K) and this behaviour is observed with O_2-rich beams at lower temperatures. Maximum CO_2 production rate is observed for any beam composition between 500 and 650 K.

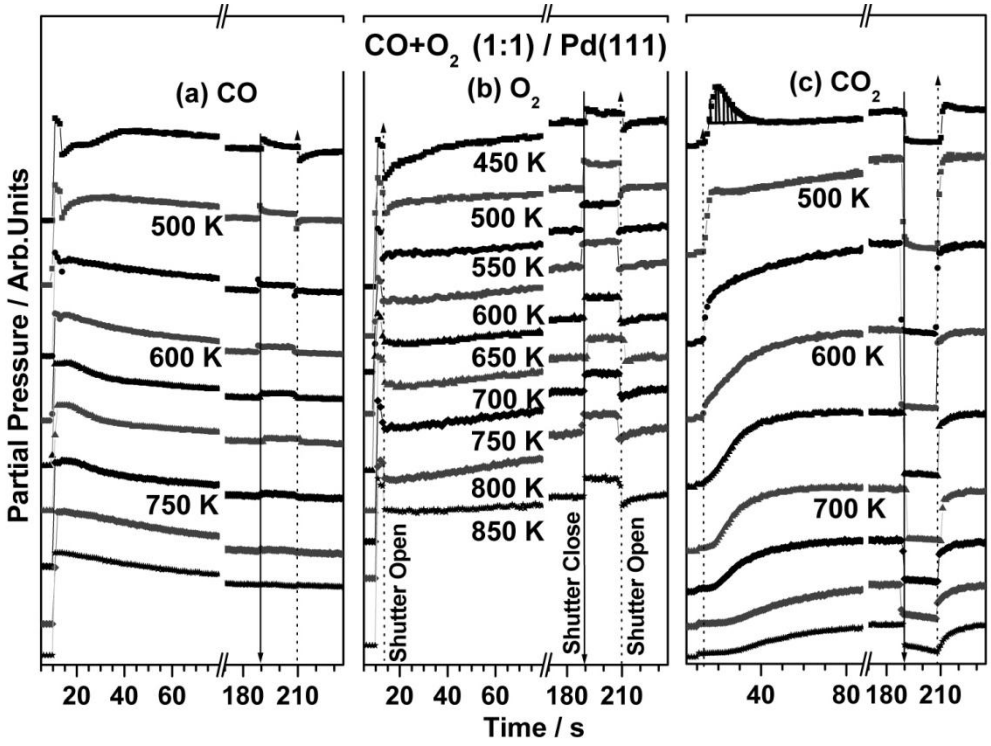

Figure 3.5 Time evolution of the partial pressures of (a) CO, (b) O_2, and (c) CO_2 during the transient and steady state of the CO + O_2 (1:1) experiments on Pd(111) as a function of substrate temperature. Hatched area in c indicates the over production of CO_2 in the transient state compared to the average SS CO_2 rate.

(3) *Above 650 K*: Although oxygen adsorption kinetics is similar to the above regime, there is no direct/reactive CO adsorption as well as CO_2 production observed immediately at the time of shutter removal, above 650 K in the TS. A significant time delay (Γ) in CO adsorption and simultaneous CO_2 production was observed to be underscored, and Γ increases with increasing temperature. Γ is defined as the time required to begin CO_2 production and the onset of reactive CO adsorption and it is directly measured from the raw results. Although plenty of CO (and O_2) from reaction mixture impinges on the Pd(111) surface from t = 13 s onwards, CO_2 production begins

later, for example, at t = 28 s at 850 K; however continuous oxygen adsorption in the TS from t = 13 s, without CO adsorption and CO_2 production, marks the onset of oxygen build-up, well above the saturation θ_o (up to 0.4 ML), which decreases with increasing temperature [20]. It is very likely that the excess oxygen build up might diffuse into subsurfaces, as shown in the earlier section.

3.3.5. Transient state (TS) and steady state (SS) kinetics-beam composition dependence

Figure 3.6 shows the beam composition dependence of CO + O_2 reactions on Pd(111) surfaces at 800 K. CO:O_2 composition varies from 7:1 to 1:10. An unambiguous dip in the partial pressure of O_2 immediately after shutter opening shows O_2 adsorption with all CO:O_2 compositions, which indicates the nature of the surface changes from metallic Pd(111) to O-covered Pd(111). Notably, there is no CO adsorption (and CO_2 production) was observed with CO rich beams. Γ decreases systematically from 77 s for CO:O_2 ratio of 7:1 at 800 K to 0 s for oxygen rich compositions above 1:4. Above decrease in Γ is due to an increase in F_{O_2} with increasing oxygen content in the beam, and hence the rate of oxygen supply increases which results in the faster diffusion of oxygen to subsurfaces. As noted in previous section, CO adsorption begins only on Pd(111) surfaces that contains oxygen atoms on the surface as well as subsurfaces. This indicates that filling the subsurface levels with oxygen atoms seems to be a prerequisite for CO adsorption. At the end of initial delay (Γ), a slow increase in CO adsorption and CO_2 production in the TS suggests a simultaneous increase in the coverage of oxygen atoms and CO molecules, especially with CO-rich beams. This demonstrates that the oxygen atoms deposited during Γ diffuses mostly to the subsurfaces and hence there is no effective reaction, even though high F_{CO} was available from the beam.

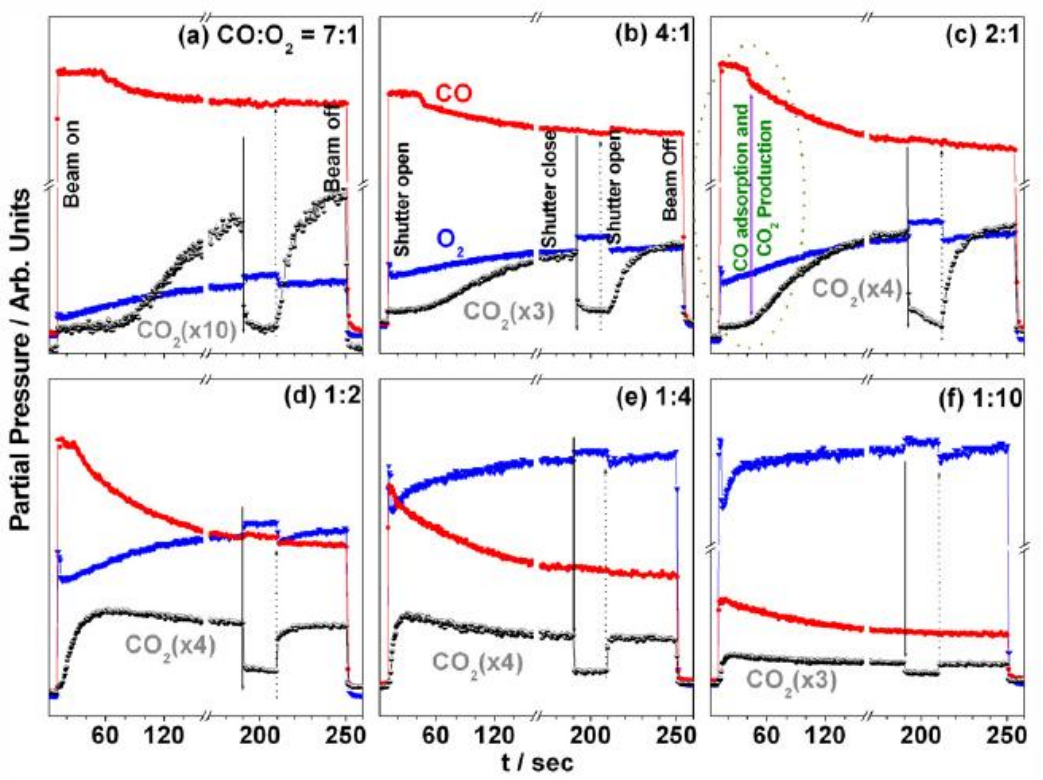

Figure 3.6 Temporal evolution of the beam compositions of (a) $CO:O_2$ (7:1), (b) (4:1), and (c) (2:1), (d) (1:2), (e) (1:4), (f) (1:10) during the transient state of the $CO + O_2$ reaction at 800 K on Pd(111). Steady state reached fast with oxygen rich beams is to be noted.

Above observations, lead to a question on the role of subsurface oxygen towards CO adsorption and $CO + O_2$ reactions. It is known that oxygen chemisorption is relatively strong and the heat of adsorption is 55 kcal/mole [20], and it is likely to change the nature of metallic Pd to Pd-O. With sufficient amount of oxygen in the subsurfaces, the electronic nature of palladium is to change from metal (Pd^0) to mildly oxidized ($Pd^{\delta+}$), and δ depends on the amount of oxygen in the subsurfaces. Some amount of metastable Pd_xO_y formation on the surface and immediate subsurfaces cannot be ruled out. In order to further probe on this aspect several experiments have been carried out which is presented in the coming sections.

Figure 3.7 shows a plot between time delay in CO_{ads} and simultaneous CO_2 production (Γ) in seconds and $CO:O_2$ beam ratio. CO rich beams show relatively large delay in CO_2 production (and CO adsorption) among the beam compositions. The above

time delay decreases with decreasing reaction temperature and with increasing O_2 content in the beam. Particularly, above stoichiometric ($CO:O_2$ = 1:2) and oxygen-rich compositions hardly shows any time delay in CO_2 production at any temperature regime. A systematic decrease in Γ with increasing oxygen content suggests an enhanced rate of oxygen diffusion into subsurfaces at high F_{O_2}. Especially with decreasing F_{CO}, attaining the threshold subsurface oxygen coverage $\theta_{O_{sub}}$ becomes faster. Expectedly oxygen lean beams take longer time to attain $\theta_{O_{sub}}$.

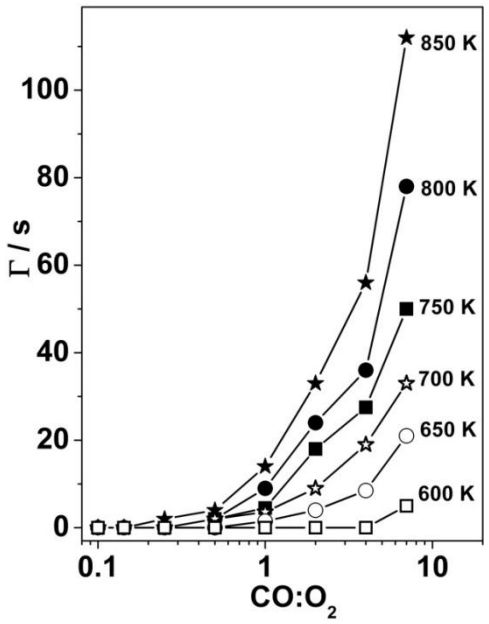

Figure 3.7 Time delay in the CO adsorption as well as CO_2 production is plotted for different temperatures and $CO:O_2$ ratio. Confirm the subsurface diffusion of oxygen and the results are discussed through a variety of experiments.

Time delay also increases linearly as a function of $CO:O_2$ composition, especially at high temperature, say >700 K due to decreasing S_{O_2}. This may be attributed to competition between oxygen diffusion into subsurface and oxygen desorption, since oxygen desorption begins around 750 K [25]. Earlier studies have determined that CO adsorption on Pd(111) displays high initial sticking coefficients S_{CO}^{0} of the order of 0.96 at 350 K, and decreases with increasing temperature [20, 22, 34]. The adsorption kinetics for CO, however, does change significantly in the presence of oxygen. Initial adsorption of reactants on clean Pd(111) surfaces in a competitive environment is an interesting and

necessary data to understand TS as well as SS kinetics. Figure 3.8 displays the dependence of (a) S_{CO}^0 and (b) $S_{O_2}^0$ as a function of temperature for all $CO:O_2$ ratios. It is to be noted that although the total flux was kept constant in all of these experiments, flux of either of the reactants change with the beam composition. CO beam at low temperatures (<425 K) shows high S_{CO}^0 values (around 0.95) comparable to that of on clean Pd(111) surface (Figure 3.8a). From 425 K and above, there is a gradual decrease in S_{CO}^0 with increasing temperature, and above 550 K, sticking coefficient becomes immeasurably small.

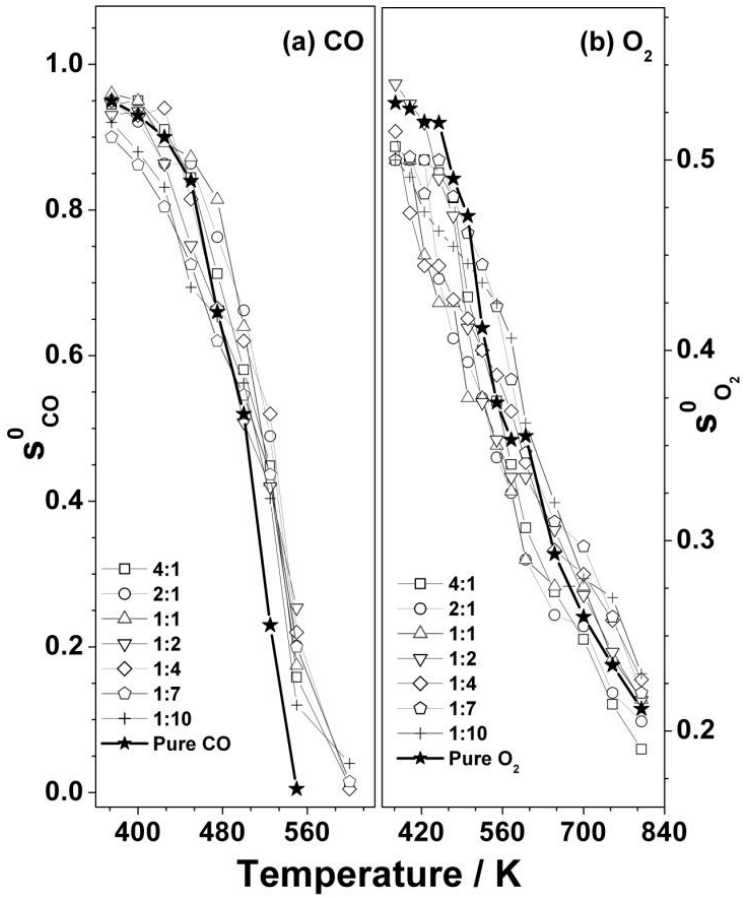

Figure 3.8 Initial sticking coefficients of (a) CO and (b) oxygen from CO + O_2 mixed molecular beams on Pd(111) surface as a function of reaction temperature and $CO:O_2$ compositions measured with CO and O_2 also plotted for comparison.

An important observation to be highlighted here is the qualitative trend in decreasing S_{CO}^0 with increasing temperature remains the same for all beam compositions

and it is independent of oxygen content. Variation observed in S_{CO}^0 values from CO + O_2 mixture, and pure CO-beam is within 5% and suggests that oxygen have no significant influence on the S_{CO}^0 from CO + O_2 mixture. Between 350 and 500 K, a significantly lower S_{CO}^0 was observed with O_2-rich beams. Figure 3.8b shows a similar temperature dependence plot for $S_{O_2}^0$ for different CO:O_2 beam compositions. $S_{O_2}^0$ decreases with increasing temperature and there is a good agreement with the data reported by Engel et al [20] on clean Pd(111). However, CO-rich beams show somewhat lower $S_{O_2}^0$ values than O_2-rich beams for entire temperature range. Appreciable $S_{O_2}^0$ value observed indicates the oxygen desorption plays a lesser role, in contrast to increasing CO desorption rate with temperature >550 K. There is a subtle difference observed between $S_{O_2}^0$ and S_{CO}^0 dependence on temperature is the highly linear decrease with the former from ~0.5 at 375 K to 0.25 around 750 K. It is also to be noted here that a similar linear trend was observed with S_{CO}^0 above the desorption maximum of CO (450 K).

Figure 3.9 shows plots for (rs) values observed in the SS for CO (rs_{CO}) and O_2 (rs_{O_2}) from CO + O_2 mixed molecular beams for different CO:O_2 ratios and temperatures. With CO rich beams the rs_{CO} varies between 0.02 and 0.25 in the SS depending on the beam composition and temperature. CO-rich beam compositions show low rs_{CO} values around 0.03; however, increasing the oxygen content in the beam and with decreasing temperature up to 500 K the rs_{CO} value increases up to 0.25. It is to be noted that CO-rich (7:1) beam shows a decreasing rs_{CO} value with decreasing temperature and it is in good agreement with reported values [22]. The rs_{O_2} values plotted in Figure 3.9b displays a striking contrast to that of rs_{CO} pattern. Irrespective of temperature, rs_{O_2} shows similar value for a given CO:O_2 composition and this value increases with increasing CO-content in the beam. Especially rs_{O_2} for CO-rich beams shows a value between 0.2 and 0.3 indicating a significantly large adsorption of oxygen onto Pd(111) under SS conditions between 500 and 800 K. This is attributed to the large number of vacant sites available in the above temperature range, since the CO desorption rate is very high. Nonetheless, with O_2-rich beams this cannot be true, since there is significant to high θ_o due to high F_{O_2} values.

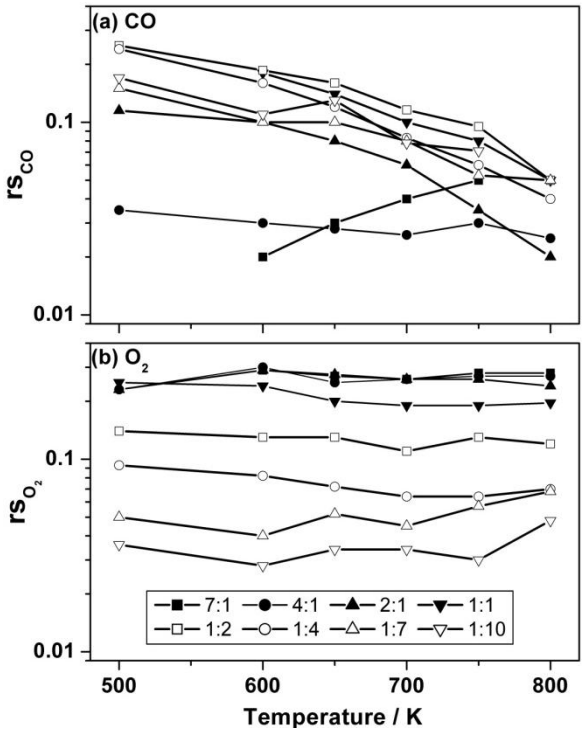

Figure 3.9 Reactive sticking coefficient of (a) CO and (b) O_2 measured under steady state reaction conditions for all CO:O_2 compositions between 500 and 800 K.

Hence a relatively steep decrease in rs_{O_2} observed with increasing O_2-content in the CO + O_2 beams. High rs_{O_2} values observed with CO-rich beams in the SS are comparable to that of $S_{O_2}^0$ (see Figure 3.8b), and underscores the high adsorption probability as on clean Pd(111) surface, even at high temperatures (>600 K). Similar rs_{O_2} values observed for a given beam composition also supports the onset of CO oxidation reaction at high temperatures only after attaining $\theta_{o_{sub}}$ Under present experimental conditions, if oxygen diffusion to subsurfaces continues beyond $\theta_{o_{sub}}$, rs_{O_2} is also expected to increase with increasing temperature, which is not observed. Hence, it is clear that $\theta_{o_{sub}}$ does not change with oxygen content in the reaction mixture, but only with temperature and supports our view on the electronic decoupling of the surface layers from bulk Pd.

3.3.6. Beam switching experiments

Beam switching experiments has been performed using 5-way valve with beam alteration between O_2 and CO to explore the concept of oxygen diffusion into the subsurface and its influence on CO-oxidation. Figure 3.10 shows the CO + O_2 reaction with CO:O_2 ratio of 1:4 at 750 K for 100 s, and then the reaction surface was cooled and titrated with CO-beam at 500 K to measure θ_o that remains on the surface.

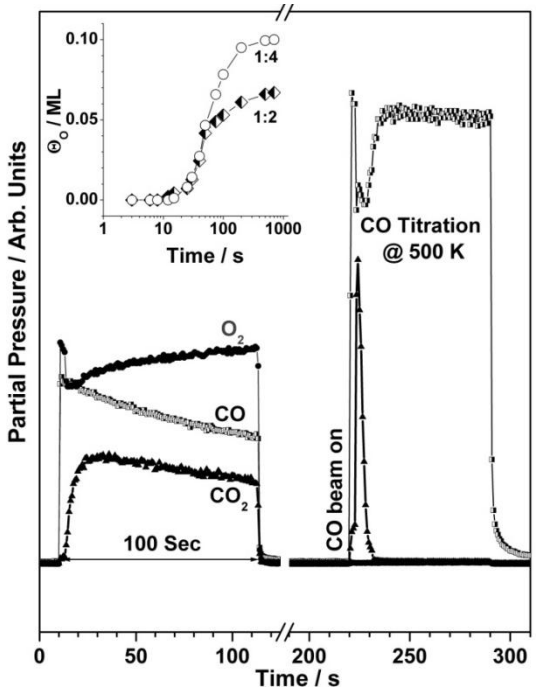

Figure 3.10 CO:O_2 =1:4 reaction was measured on Pd(111) at 750 K, followed by CO titration at 500 K. CO + O_2 beam dosing time was varied between 3 to 800 sec. Inset shows Θ_o measured from CO-titration after reaction was carried out with 1:2 and 1:4 compositions for different length of time. 1:7 and 1:10 compositions also show a result similar to that of 1:4.

This reaction was measured as a function of CO + O_2 exposure time (up to 800 sec) followed by CO-titration. It is to be highlighted that similar measurements with CO-rich beams (7:1 and 1:1) up to an exposure time of 1000 s did not yield any CO_2 during CO-titration, which indicates that the surface adsorbed oxygen had been utilized for CO oxidation and that there is no significant surface θ_o build-up. Any oxygen desorption would be negligible since oxygen desorption at low coverage begins around 800 K and

above. Inset in Figure 3.10 shows the θ_o measured from CO titration after reaction was carried out with 1:2 and 1:4 compositions for different CO + O_2 exposure time. Similar measurements with oxygen rich compositions show similar values as that of 1:4. Up to a reaction time of 12 s, no measurable θ_o was observed with any of the beam. However, an increase in θ_o with increasing reaction time is observed and approaches a saturation level in the SS, between 200 and 500 s.

A maximum of 0.07 ML with 1:2 composition and 0.1 ML with all other oxygen-rich compositions was observed. No observation of measurable θ_o up to a reaction time of 12 s clearly indicates a preferential subsurface diffusion of oxygen as well as an effective utilization of any surface oxygen towards CO_2 production in the TS. These results also suggest the necessity to populate the subsurface levels with oxygen before the onset of reaction on the surface. No surface θ_o found after the reaction with CO-rich compositions underscore the initial deposition of oxygen atoms on the surface exclusively diffuse into the subsurfaces. Only after reaching the $\theta_{o_{sub}}$ CO_2 production begins.

Figure 3.11 shows CO + O_2 reaction carried out on Pd(111) with (a) 4:1 composition at 700 K and (b) 2:1 composition at 750 K. In the first-half the reaction was measured till the onset of CO_2 desorption and stopped, and the same reaction was re-measured on the same surface, without any cleaning. On re-measuring, a great decrease in delay in CO_2 desorption (and CO_{ads}) was observed (solid arrows) from the point of shutter removal. Even though there was about 75-80 sec time delay after the first-half reaction, a fast CO_2 production begins when the second half experiment was carried out indicates that the amount of oxygen that diffused into the subsurface in the first half of the experiment is retained to a large extent. Even when the above time delay was extended up to 600 s, there was no change in second half experiment and indicates the oxygen diffused into the subsurface remained intact. Above experiments suggests the necessity to populate the subsurface states with oxygen before the onset of actual reaction on the surface.

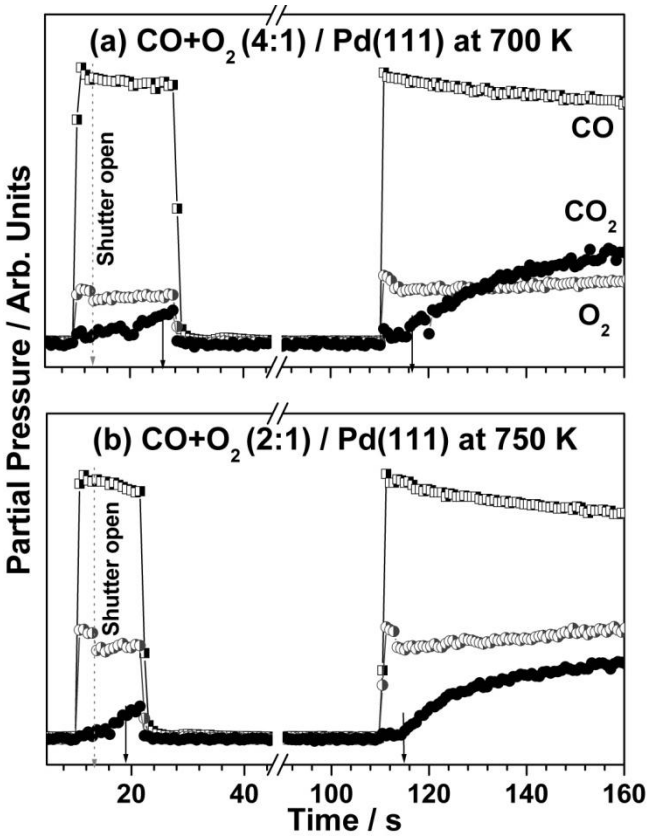

Figure 3.11 CO + O_2 reaction measured on Pd(111) surfaces with (a) 4:1 composition at 700 K and (b) 2:1 composition at 750 K. In the first-half the reaction was measured till the onset of CO_2 desorption and stopped for a while, and the same reaction was re-measured on the same surface.

In continuation to the earlier experiment in Figure 3.11, pulsed oxygen dosing for different periods of time followed by CO dosing/titration for 30 s and simultaneous CO_2 production is shown in Figure 3.12a. Oxygen pulsing time increased gradually from 5, 10, 20, and 30 s. No CO_2 desorption was observed for the first two CO pulses, after oxygen pulses. However, a gradual increase in CO_2 production was observed with latter oxygen pulses followed by CO-pulses. In fact, in another experiment (not shown) with continuous 55 s oxygen pulse too did not produce any CO_2 upon CO titration; however a subsequent oxygen pulse for 10 sec, did produce CO_2 upon CO titration. Indeed a sum of oxygen dosing time (t = 65 s) after which CO_2 production starts is in agreement with the delay time for $CO:O_2$ ratio of 8:1 (Γ = 60 s).

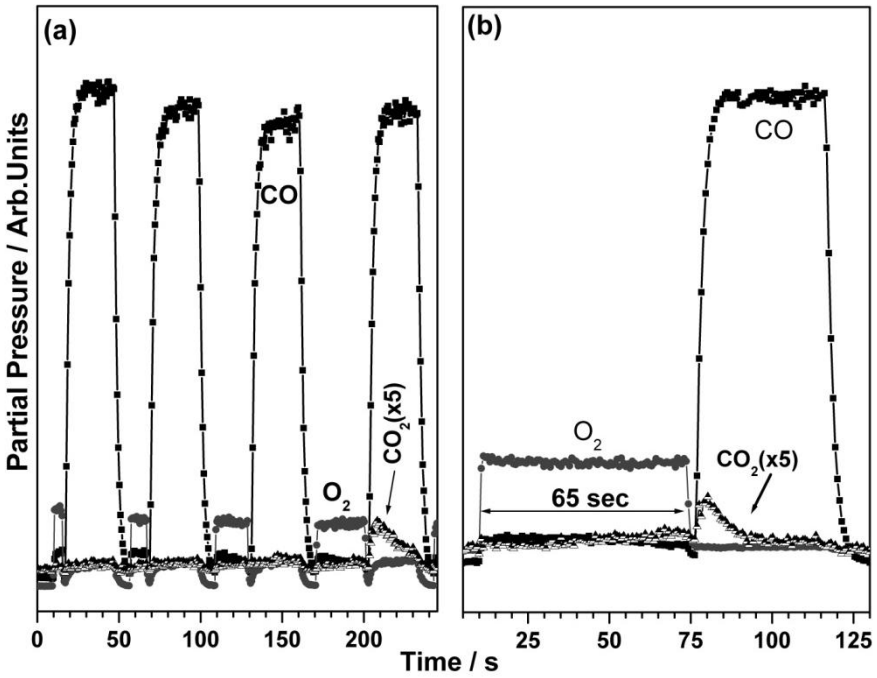

Figure 3.12 (a) Pulsed oxygen (closed circles) dosing for different time interval (5 - 30 s) followed by CO pulses (open circles) for 30 s and corresponding CO_2 production (open triangle) at 750 K on Pd(111). (b) 65 s oxygen pulse followed by 40 s CO pulse at 750 K on Pd(111). Ratio of CO:O_2 was maintained at 8:1 for the above reactions.

This confirms that the oxygen that adsorbed initially diffuse into the subsurfaces and filling the subsurface levels. It is only after attaining $\theta_{O_{sub}}$ CO adsorption and CO_2 production starts from the surface. As O_2-lean beam requires more time to fill the subsurface states, it is observed unambiguously, rather than with O_2-rich beams which fills the subsurface states rapidly.

Figure 3.13 provides a summary of the results obtained in the SS kinetic experiments reported here for CO_2 production rate against reaction temperature. A few interesting points are worth highlighting from this figure: (1) There is an optimum reaction temperature range, between 500 and 550 K, where a maximum in rate is reached for CO:O_2 beam compositions that are closer to stoichiometric composition (CO:O_2). (2) The above optimum temperature range broadens to wider temperature range, somewhere between 450 and 750 K for CO:O_2 beam compositions that are either CO-rich or O_2-rich compositions. (3) There is also an optimum CO:O_2 ratio, somewhere between 2:1 and

1:2, which maximizes the reaction rate. Although value of this ratio is close to 1:1, compositions that are closest are not far behind in rate. (4) It is interesting to note the comparable rate for 1:7 and 7:1 (and 10:1) compositions between 600 and 800 K, and it suggests the low flux reactant component decides the overall rate of the reaction. Alternatively, it may be viewed that the reaction rate becomes lesser sensitive to beam composition at high temperatures, as the rate is comparable between 4:1 and 1:4 (similarly between $CO:O_2$ = 2:1 and 1:1).

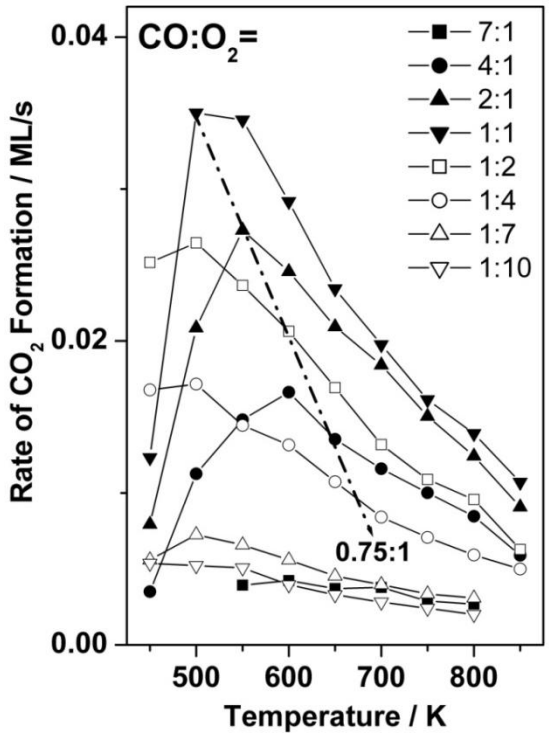

Figure 3.13 Steady-state rate of the CO + O_2 reaction as a function of temperature for various beam compositions. The stoichiometric ratio (2:1 to 1:2) shows a maximum steady-state rate in all temperature ranges and the dotted line shows the CO_2 production trend from 500 to 700 K for CO + O_2 (0.75:1) reported by Ertl et al [4] (*J. Chem. Phys.* **1978**, *69*, 1267). Considerable higher rate is observed from the Pd(111) surfaces that contains subsurface oxygen compared to clean Pd(111).

(5) Lower rate observed at 450 K with CO-rich compositions (7:1 to 2:1) compared to the highest rate with O_2-rich compositions (1:2 to 1:10) underscores a significant CO-poisoning in the former case. All of the above observations demonstrate that the reaction rate is effectively controlled by both the surface temperature and the beam composition

below 600 K. Nonetheless, the rate becomes less dependent on the reaction temperature and reactants composition >600 K. Indeed, as the temperature increases ≥600 K a gradual delay in CO-desorption rate sets-in, and simultaneously the overall reaction rate also increases with CO-rich beam compositions. An immediate attainment of SS and a higher SS rate for a stoichiometric 1:1 $CO:O_2$ composition is observed and we attribute this behavior to a near-stoichiometric (1:1) coverage of both CO and oxygen atoms on the surface under the present experimental conditions in the SS. Measurement of ratio of adsorption rate of reactants (CO/O) Figure 3.14 shows a value very close to one for the high rate regime for all CO-rich and stoichiometric beam compositions (2:1 to 1:4). There are some deviations observed, especially, in the low temperature regime is exclusively due to CO-poisoning. At higher temperatures, oxygen adsorption (step 2) is dominant and it is one of the fast steps in the overall reaction. Almost same CO/O value observed for oxygen-rich compositions between 450 and 600 K, hints the rate determining step is CO-adsorption.

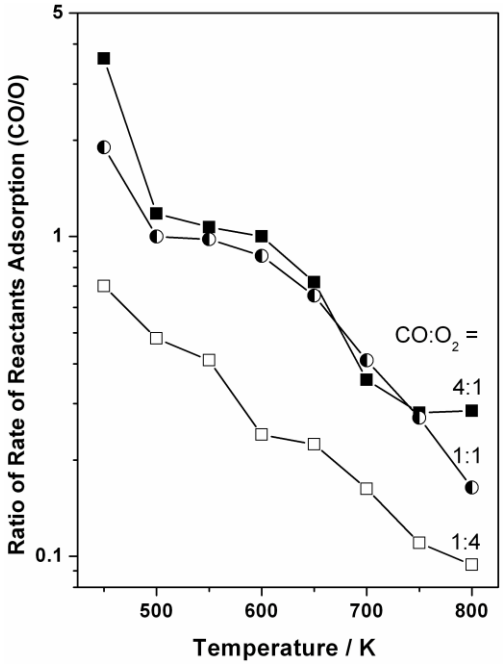

Figure 3.14 Ratio of rate of adsorption of CO to oxygen measured from the SS kinetic data for 1:4, 1:1 and 4:1 compositions between 400 and 800 K.

The kinetic data for the TS of the CO oxidation with oxygen on Pd(111) surfaces presented here generally reinforce the conclusions reached by Engel and Ertl and others [20, 27, 28].

3.3.7. Polycrystalline Palladium

$CO + O_2$ reaction was measured on a polycrystalline Pd-metal surface with CO-rich compositions at high temperatures, and a typical results is given in Figure 3.15 with $CO:O_2 = 4:1$ at 700 K. Same beam flux was used as in earlier experiments in Figures 3.5 and 3.6. This is to show that the oxygen subsurface diffusion is a phenomenon that occurs on all Pd-surfaces and not restricted to Pd(111) facet. Interestingly there is no delay in CO adsorption and CO_2 production was observed at surface temperatures <700 K for any $CO:O_2$ compositions.

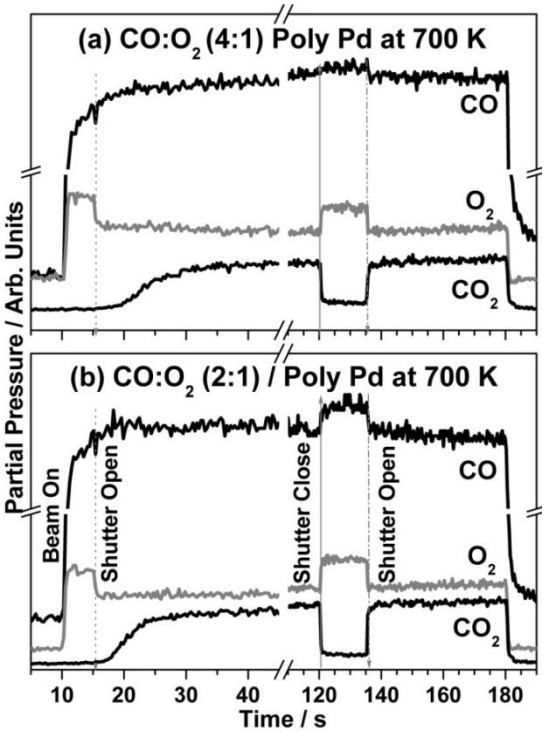

Figure 3.15 Isothermal kinetic data from polycrystalline palladium with $CO:O_2 = 4:1$ at 700 K. A large decrease in the delay time observed on polycrystalline palladium is to be contrasted with large delay time on Pd(111) under same conditions.

Although small, but clear CO adsorption was observed at 700 K, however no CO_2 production begins immediately after shutter opening. It is well known that strong CO adsorption occurs on defect sites and hence some marginal CO adsorption was observed on polycrystalline Pd even at 700 K [34]. Oxygen adsorption continues at the same rate from the time of shutter removal to end of the experiment. Importantly, CO_2 formation begins only after a delay time (Γ) of about 4 seconds. It is also to be noted that the SS was reached quicker on polycrystalline Pd compared to that of Pd(111). Although no delay in CO_{ads} was observed, the delay in CO_2 desorption supports the oxidation activity begins only after the nature of the surface changes to mildly oxidized with threshold oxygen coverage in the subsurfaces, as in Pd(111). Though onset of CO_2 production was delayed as in Pd (111), but occurred sooner on polycrystalline Pd than Pd (111) under the same beam compositions and temperatures. This is attributed to faster oxygen diffusion into subsurfaces through defect sites on polycrystalline Pd. It is likely that the defects on Pd(111) might also be responsible for O-diffusion into the subsurface.

3.3.8. Unusual transient kinetics- discussion

The kinetic data presented here provide new information on the mechanism of catalytic oxidation of CO by oxygen over palladium surfaces, especially from the TS kinetic data of CO + O_2 reaction with CO-rich beam compositions at temperatures >600 K. An unambiguous oxygen adsorption, with no net CO-adsorption and CO_2 production, on the Pd(111) surface with CO-rich beams is evident from the results shown in Figures 3.5, 3.6, 3.11 and 3.12. Above initial oxygen adsorption mostly diffuses to subsurfaces to populate the subsurface states to a threshold coverage. A slow and gradual increase in CO adsorption on the Pd(111) surface covered with oxygen in subsurfaces and surface could be seen with CO-rich compositions after a delay time Γ and a simultaneous CO_2 production. Meanwhile, the direct oxygen adsorption from the beam during the above delay period demonstrates the change in nature of substrate from clean metal to oxygen-covered surfaces, which is likely to be mildly oxidized. Generally the reaction data presented earlier hints the maximum surface oxygen coverage of 0.25 ML at 500 K to subsurface and surface oxygen coverage together between 0.3 to 0.6 ML at ≥600 K.

Nature of such surface might resemble to that of a precursor to a metastable Pd_xO_y, and this is to be explored by spectroscopic studies. As usual to any TS kinetics, there is a continuous change in CO:O ratio on the surfaces from the beginning of reaction till the reaction reaches the SS. An onset in CO-adsorption and CO_2 production, immediately after the above delay period correlates very well and indicating that there was no net CO adsorption till the end of delay time Γ. It is to be noted that the rate of oxygen adsorption remains the same from the beginning till the MB was shut off, and suggests a first order dependence with respect to oxygen coverage. No direct CO uptake at the time of shutter removal from CO-rich beams is in neat agreement with no net CO-adsorption on clean Pd(111) surfaces >550 K, due to high rate of CO-desorption [22, 43]. All of the above observations unambiguously demonstrate that CO-adsorption capacity is significantly high on oxygen covered Pd(111) that contains significant subsurface oxygen coverage and at high temperatures.

We make the following suggestions for the delayed CO-adsorption (CO_2 desorption) observed in the results discussed above. A decrease in both the attractive O-O as well as repulsive O-CO interaction might be a possibility, which also inevitably leads to CO_2 production. The above scenario was observed in the case on Pt(111) [44] and hence CO-adsorption within the oxygen islands was possible. This indicates the nature of oxygen covered Pd surface changes considerably and favorably towards oxidation at high temperatures. STM and LEED studies also shows subsurface oxygen on Pd(111) surfaces [7, 8, 14, 16]. However, some possibility of metastable Pd_xO_y formation in the TS cannot be ruled out. A change in surface structure due to reconstruction after threshold oxygen coverage is an important point to be mentioned [12]. Phenomenon like, '*capture zone effect*' might be invoked to explain the CO-adsorption on oxygen-covered surfaces at high temperatures. Such effect has been reported on Pd supported on either Al_2O_3, Fe_2O_3 or MgO [42, 45] but not on metallic Pd-surfaces.

3.3.9. Reaction mechanism aspects

Our present study essentially tries to find out the influence of the interaction of oxygen with Pd(111) surfaces and a special emphasis is given for transient kinetic analysis. Since

the SS rate equation has been dealt by many groups, it is not discussed here. In the discussion of the results presented here, it is important to remember that, as opposed to the case of the SS regime, the kinetics in the TS does not require that all the steps in the mechanism display equal rates. In simple terms, as the metal surface goes from a clean metal in the beginning of the reaction to the SS, both the surface concentration and the rates of individual steps change in absolute and relative terms and hence the variations in rates over time seen in Figures 3.1, 3.5 and 3.6. CO oxidation reaction above 500 K goes through the following mechanism:

$$S \xrightarrow{k_1} e^- + S^+ \quad (1)$$

$$O_{2gas} + 2* \xrightarrow{k_2} 2O_{ads} \quad (2)$$

$$O_{ads} \xrightarrow{k_3, \geq 500K} O_{sub} \quad (3)$$

$$S^+ \xrightarrow{k_4, O_{Sub}} S^{\delta+} + * \quad (4)$$

$$CO_{gas} + * \xrightarrow{k_5} CO_{ads} \quad (5)$$

$$CO_{ads} + O_{ads} \xrightarrow{k_6} CO_{2\,ads} \xrightarrow{fast} CO_{2gas} \quad (6)$$

S, S^+ and $S^{\delta+}$ stands for surface, oxidized and mildly oxidized surfaces. It should be remembered here that direct CO adsorption is not possible ≥550 K on a Pd(111) surface. Therefore, CO_2 production rate at high temperatures is entirely dependent on the CO-adsorption capacity, which is induced by oxygen coverage on subsurfaces and surfaces, and hence significant oxygen adsorption should occur and sustain. It is presumed that Pd(111) surfaces lose considerable amount of surface electron cloud at high temperatures. Hence it makes the surface electronic nature significantly different at high temperature compared to the low temperature (<500 K) Pd(111) surfaces, so that the electron deficient CO molecules ($^{\delta+}$C-O) are repelled from the Pd(111) surfaces. At the same time, the modification of the electronic state of the surface highly favors O_2 molecules to adsorb on the surface and considerable quantity of the adsorbed O-atoms diffuse into the subsurface

region [8]. It is a well known fact that most adsorbate can change the work function of the surface. It is also known that the dissociative oxygen adsorption leads to negatively charged ($O^{\delta-}$) adsorbate, and hence the saturation coverage does not exceed 0.25 ML at <500 K. However the same factor recovers electron density from the bulk at high temperatures and makes the top atomic layers mildly oxidized. Thus the electron cloud is slowly recovered back on the Pd(111) surfaces similar to the lower temperatures surface with the help of surface as well as subsurface oxygen. It makes CO adsorption possible at higher temperatures, and begins producing CO_2 molecules (Figures 3.5 and 3.6). Alternatively, the electron rich pockets/islands might also be created due to oxygen adsorption on the surface [7, 8, 14], in which (and around) CO-adsorption takes place and leading to CO_2. Above mentioned illustrates into a simplified jellium model [46]. Here delocalized electron gas is surface electron density and background positive charge created due to diffusion of oxygen into subsurfaces and hence temporary Pd-O bonds formation.

Hence, the possibilities further expand: (a) background positive charge created due to subsurface diffusion of oxygen leads to a dent or decrease in surface electron density, and the same was observed in STM studies of the O/Pd(111) system, but at lower temperatures [14, 16]. (b) Upon further oxygen adsorption, there is oxygen islands formation which creates electron rich regimes around it. (c) CO adsorption takes place in that regime and CO_2 production. Step b expands gradually as more and more oxygen islands forms, and hence an increase in CO adsorption in the TS kinetic regime and CO_2 production.

Hence the rate of the reaction at the high temperatures can be formulated as:

$$R(CO_2) = k_6 \theta_{CO} \theta_O \tag{7}$$

θ_O depends on equations 2 and 3.

$$\theta_O = \frac{k_2 s_O^0 \theta_{vac} F_{O_2}}{k_3 \theta_{sub}} \tag{8}$$

Similarly, θ_{CO} depends on steps, 1, 3, 4 and 5

$$\theta_{CO} = \frac{k_4 k_5 s^0_{CO} \theta_{sub} F_{CO}}{k_1 k_3 \theta_{sub}} = \frac{k_4 k_5 s^0_{CO} F_{CO}}{k_1 k_3} \quad (9)$$

Hence CO_2 production rate for the CO oxidation reaction on Pd(111) surfaces in the TS can be expressed as:

$$R(CO_2) = k_6 \frac{k_4 k_5 s^0_{CO} F_{CO}}{k_1 k_3} \frac{k_2 s^0_O \theta_{vac} F_{O_2}}{k_3 \theta_{sub}} = \frac{k_2 k_4 k_5 k_6 s^0_{CO} s^0_O \theta_{vac} F_{CO} F_{O_2}}{k_1 k_3^2 \theta_{sub}} = K \frac{s^0_{CO} s^0_{O_2} \theta_{vac} F_{CO} F_{O_2}}{\theta_{sub}} \quad (10)$$

where $K = k_2k_4k_5k_6/k_1k_3^2$. The factor that really affects the above rate equation is the S_{CO}, which increases gradually as the subsurface states are getting populated increasingly towards the threshold coverage. The Arrhenius plots for stoichiometric CO:O_2 compositions leads to an activation energy (E_a) around 15 Kcal/mole especially below 500 K where there is no oxygen diffusion into subsurfaces occurs. At higher temperatures (>550 K), E_a is somewhat higher around 21 Kcal/mole. It may be attributed to the change in the electronic nature of the surface layers due to oxygen diffusion. More detailed analysis will be reported elsewhere.

3.4. Low-temperature CO oxidation results

Room temperature or low temperature CO oxidation is also very important, as in the case of above high temperature CO oxidation. Earlier, low temperature CO oxidation has been observed on gold clusters (Au_{10}) or nano particles of gold (2-5nm) supported on metal oxides by Haruta [49], and Hutchings [50]. They could observe CO oxidation even below room temperature with these catalysts. However, the idea of low temperature CO oxidation with modification in the subsurfaces of Pd has not been explored. The main idea is to dose the oxygen systematically at high temperature (900 K) to ensure the oxygen migration towards the subsurfaces prior to CO + O_2 reactions around ambient temperatures. In our earlier reports we investigated the simultaneous impact of CO + O_2 on Pd(111) surfaces ≥500 K. Net CO adsorption ≥600 K with significant sticking coefficient (S_{CO}) is observed only after subsurface modified (SM) of Pd(111) through

exclusive O_2 adsorption (from CO + O_2 mixture) followed by diffusion into subsurfaces to a threshold O subsurface coverage $\theta_{o_{sub}}$ [34]. This helps to broaden the CO oxidation regime to high temperatures and to increase the rate compared to clean Pd(111) surfaces. On clean Pd(111) surfaces, hardly there is any CO oxidation observed ≥750 K due to high rate of CO desorption. Contrary to high temperature, CO chemisorbs very strongly on clean Pd(111) surfaces and poisons the Pd-surfaces, and hardly any sustainable CO oxidation activity observed below 375 K [48]. Nonetheless, at RT, SM Pd(111) surfaces demonstrate that CO poisoning is lifted (at least, partially) with O_2 (CO)-rich CO:O_2 compositions. Indeed the former is directly relevant to RT oxidation under practical conditions in many places, such as, living rooms, public places.

3.4.1 Preparation of modified Pd(111) surfaces

Clean Pd(111) is modified by exposing to O_2 MB at 900 K with a flux (F_{O_2}) of 1 ML/s for different time intervals from 5 to 110 min. It is to be noted that S_{O_2} is significant at 900 K on Pd(111) due to highly competitive diffusion of O atoms into subsurfaces, rather than desorption. Oxidation was carried out on the above SM Pd(111) with different CO:O_2 ratios (7:1 to 1:11) between 300 and 525 K. Between two experiments the surface and subsurface was cleaned for O-atoms by H_2 treatment at 873 K for up to 6 h. It is to be noted that H atoms diffuses into subsurfaces and reacts with O-atoms to be desorbed as H_2O. We found that this procedure is more effective than the conventional Ar^+ sputtering [34].

A typical CO oxidation experiment was carried out by starting the experiment at 300 K with F_{CO+O_2}= 0.32 ML/s and after recording the steady state (SS) raw kinetic data, the crystal temperature was ramped to next higher temperature and the same procedure was repeated. All the reactants and products were followed by mass spectrometry. F_{CO+O_2}= 0.32 was kept constant for all experiments, unless specified. CO + O_2 reaction carried out earlier on clean Pd(111) surfaces and the results is considered as bench mark.

Figure 3.16 shows the CO_2 production between 300 and 525 K with four different CO:O_2 ratios after SM of Pd(111) to different extent and compared to that of clean

Pd(111) surfaces. Extent of surface modification is given by the time exposed to F_{O_2} at 900 K; $\theta_{o_{sub}}$ increases linearly [34], and between 50 and 60 min. of O_2 pre-dosing the $\theta_{o_{sub}}$ reached a maximum value around 0.5 ML, and no further increase in $\theta_{o_{sub}}$ observed. In the steady state (SS) molecular beam was deliberately blocked and unblocked several times to measure the SS rate of the reaction at different temperatures. During beam blocking a decrease (increase) in CO_2 (reactants) partial pressure observed was due to the stopping of reaction, which directly gives the reaction rate in Figure 3.16, of course after calibration of mass spectrometer with known pressure values [34].

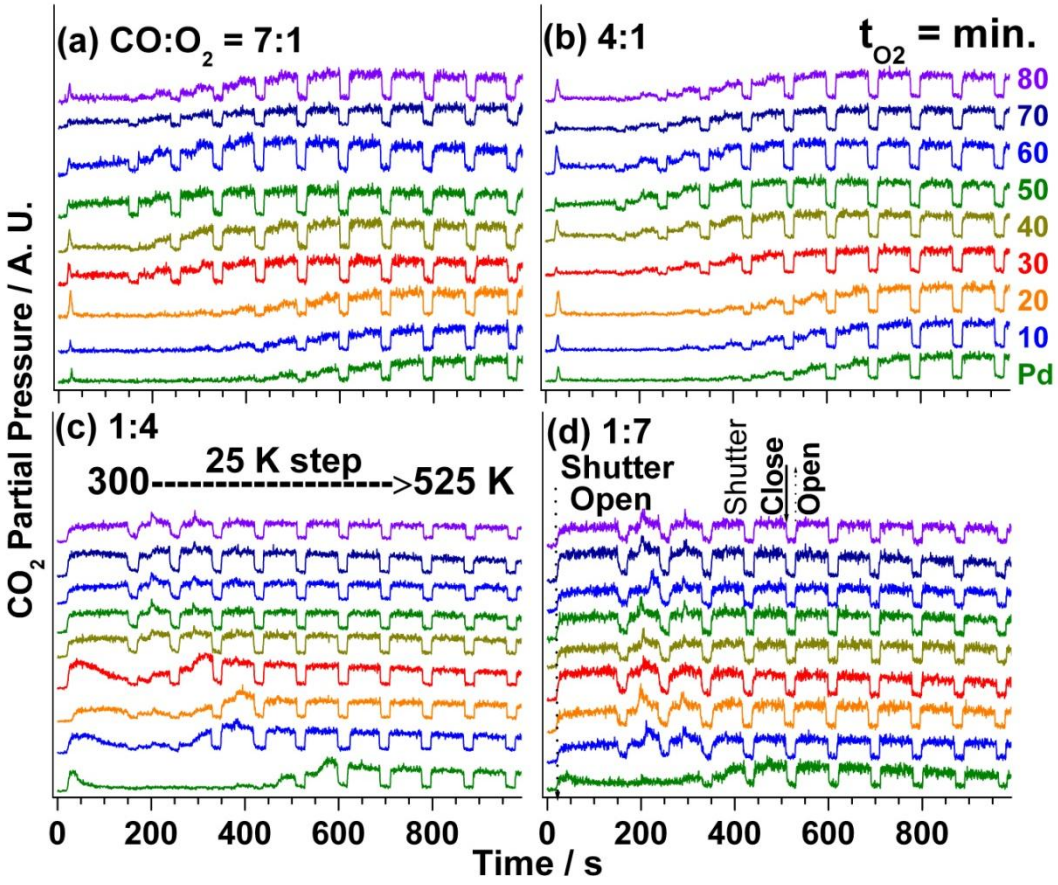

Figure 3.16 Time evolution of CO_2 desorption on surface modified Pd(111) between 300 and 525 K with different $CO:O_2$ ratios (a) 7:1, (b) 4:1, (c) 1:4, and (d) 7:1. Extent of surface modification is indicated by O_2 pre-dosing time on top-right side. Steady state (SS) rate was measured by beam oscillation in the SS. CO oxidation started at 300 K, continued up to 525 K and each time the temperature ramped by +25 K. Note the change in transient kinetics for CO and O_2-rich $CO:O_2$ compositions.

On clean Pd(111) surface the rate maximum (R_{max}) is observed around 500 K, depending on $CO:O_2$, and it is in good agreement with earlier results [4, 34, 48]. However, the R_{max} for SM Pd(111) broadens and shifts to lower temperatures with higher time of O_2 pre-dosing.

Few important points from Figure 3.16 are worth highlighting here: (a) As the surface modified progressively, from clean metal to increasingly covered with O in subsurfaces, the reactivity broadened towards lower temperature for all $CO:O_2$ ratios. CO_2 production increases gradually and sustainable SS CO_2 production could be observed for all $CO:O_2$ ratios. (b) R_{max} for O_2-rich $CO:O_2$ compositions (1:4 and above) show similar rate between 300 and 525 K for oxygen pre-dosing of ≥30 min; however rate increases gradually at 300-325 K with increasing O_2 pre-dosing. (c) O_2 pre-dosing for >60 min does not show any further improvement in activity, rather a fluctuation in activity in certain cases, likely due to surface structural changes [4, 6, 8, 14, 16, 19, 47, and 51]. (d) A gradual change in transient kinetics observed at 300 K from no activity to sustainable activity from clean Pd(111) to SM Pd(111) surfaces, respectively. A fast change in transient kinetics with O_2-rich $CO:O_2$ compositions could be seen under the above conditions.

Figure 3.17 shows the SS rate of CO oxidation described in Figure 3.16. This set of results un-obviously demonstrates that indeed there is sustainable catalytic oxidation activity after SM of Pd(111). Especially, O_2-rich $CO:O_2$ compositions shows the similar rate for a given composition at all temperatures indicating the sustainable high CO conversion to CO_2. Our preliminary experiments demonstrate that this activity is further extended, at least, up to 273 K with O_2-rich compositions. Compared to clean Pd(111) surfaces, SM Pd(111) shows higher activity, especially ≤400 K, for all $CO:O_2$ ratios is to be noted. R_{max}, generally observed around 500 K on clean Pd(111), shifts to lower temperatures progressively for a given beam composition. For eg. R_{max} of 4:1 (1:4) $CO:O_2$ composition shifts from 525 K (475 K) on clean Pd to 400 K (375 K) after 50-60 min O_2 pre-dosing.

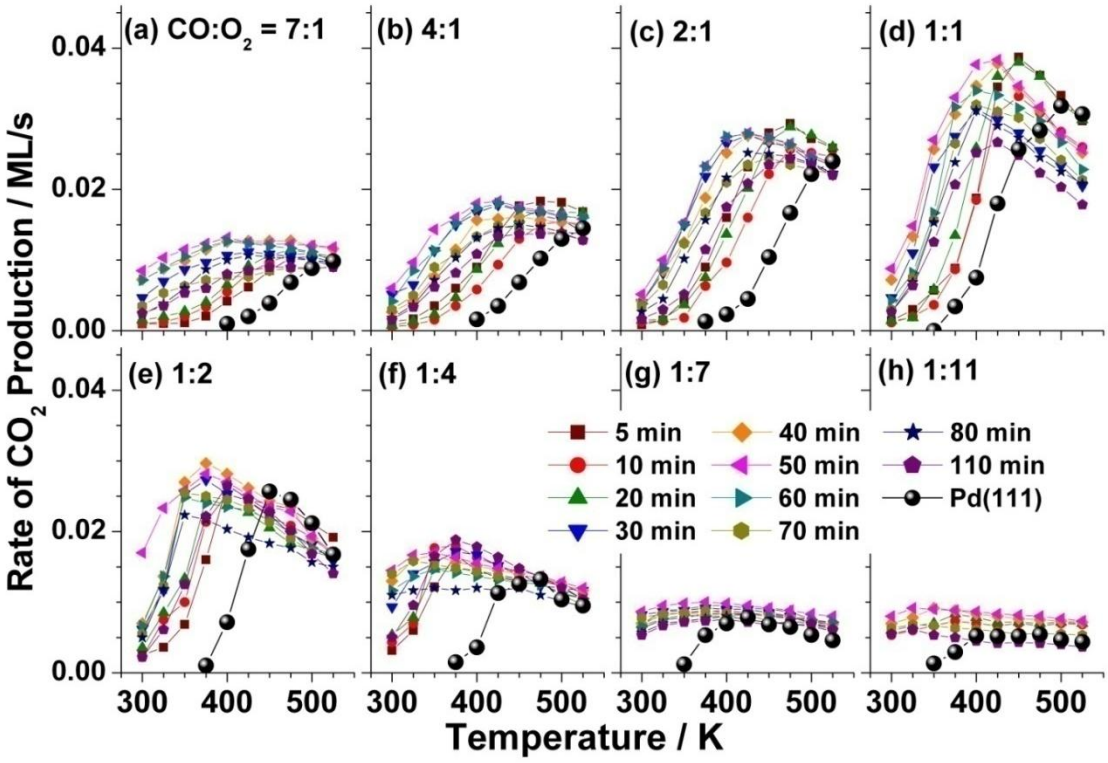

Figure 3.17 Steady state rate measured for the reactions described in Figure 3.16 for different $CO:O_2$ ratios (a) 7:1, (b) 4:1, (c) 2:1, (d) 1:1, (e) 1:2, (f) 1:4, (g) 1:7, and (h) 1:11. Note a significant increase in oxidation capacity at low temperatures with all $CO:O_2$ ratios on SM Pd(111) compared to clean Pd(111) surfaces.

This highlights the effectiveness of SM towards O_2-lean as well as rich $CO:O_2$ ratios. As expected the low flux component decides the overall rate along with the extent of oxidized surface [51].

Selected measurement at 273 K has been carried out at least for 1 h to confirm the sustainability of the reaction as well as to demonstrate the non-consumption of subsurface oxygen. It is to be noted that subsurface oxygen only influences the surface electronic properties and hence catalytic activity of SM Pd, and does not get consumed by CO oxidation. In fact the reaction cannot sustain for more than 2 min if subsurface O atoms were to be consumed for CO-oxidation. No subsurface diffusion of atomic oxygen occurs below 500 K rules out the possibility of exchange of surface to subsurface oxygen at temperatures below 500 K.

While analyzing the adsorption trend of reactants on SM Pd(111) surfaces under SS conditions, origin for the above activity was uncovered. It is evident that there is sustainable CO adsorption under SS at 300 K, irrespective of the $CO:O_2$ compositions. For beam oscillations under SS conditions, there is a good change in CO and O_2 partial pressure demonstrate that the activity is due to intrinsic nature of SM Pd, and no external factors influences. Indeed it is surprising to note that there is no CO poisoning on SM Pd(111) at 300 K even with CO-rich compositions. With O_2-rich compositions also significant CO adsorption observed in the SS highlight the reactivity of SM Pd(111) surfaces has changed dramatically. We suggest the following based on the above experimental observations: (1) O-diffusion into Pd subsurfaces modifies the electronic nature of surfaces to be oxidized ($Pd^{\delta+}$) in nature and the extent of δ should increase with $\theta_{O_{sub}}$ (2) Electronically modified surface active sites are available for exclusive CO adsorption. (3) CO_{ads} on $Pd^{\delta+}$ is more reactive (rather than poisoning) due to the negligible possibility of back donation of electrons from $Pd^{\delta+}$ and hence weakening of CO bond strength. This is likely to be the reason for lifting of CO poisoning at low temperatures on $Pd^{\delta+}$ (4) Mobility of CO is still high at 300 K after SM.

3.4.2. Steady state (SS) kinetics-temperature dependence

From the figures 3.16 and 3.17, the steady state rate of CO oxidation increases gradually towards (300 K) low temperature, when the subsurface oxygen concentration is increased, for proper comparison, clean metal data included in all the four beam compositions. In all the beam compositions even in CO-rich conditions at low temperature CO poisoning effect was not observed, which is in direct contrast to that of clean Pd(111) surfaces. With O_2-rich compositions also significant CO adsorption observed in the SS highlight the reactivity of SM Pd(111) surfaces has changed dramatically. A decrease of 100-150 K for R_{max} and activity broadening to lower temperature up to 273 K, indicates a decrease of activation energy by 20-30 KJ/mole.

Reference clean Pd data showed hardly any CO_2 at room temperature for all the compositions, whereas with modification in subsurfaces, CO_2 steady state rate was observed at 300 K with >30 min of O_2 dosage. The R_{max} shifting to lower temperature

with more O_2 dosage, and in O_2-rich conditions the steady state rate of 300 K trace is almost same as 525 K. This demonstrates the sustainable activity throughout the temperature range.

3.4.3. Steady state (SS) kinetics-beam composition dependence

The CO_2 production steady state rate gradually increase with increase in temperature for both CO-rich (7:1) and (4:1) in figure 3.16 (a) and (b) conditions, especially with O_2 dosing time >30 minutes. In contrast, the steady state rate of CO_2 production is almost same from 300 to 525 K for O_2-rich conditions (1:4) and (1:7) in Figure 3.16 (c) and (d). In general, the rate of CO_2 production gradually increases with increase in O_2 dosing time for all the beam compositions especially it is more pronounced in O_2-rich conditions. For all the 4 compositions reference data is given for clean Pd.

3.5. Summary and conclusions

CO oxidation reaction on Pd(111) surface, polycrystalline Pd, SM Pd(111) with oxygen in the subsurfaces of Pd with molecular beams at wide range of temperatures (from 273 K to 850 K) for a variety of beam compositions ranging from 7:1 to 1:11 gave some interesting information about the reaction. A revisit to CO oxidation on Pd(111) surfaces was to explore the influence of subsurface oxygen on overall kinetics, and particularly transient state kinetics.

1) Interesting information derived from the above studies is the necessity to fill up the subsurface layers with oxygen atoms to threshold coverage $\theta_{o_{sub}}$Time delay and $\theta_{o_{sub}}$ in CO-adsorption (and/or CO_2 production) increases with increasing temperature and with CO-rich compositions. Onset of CO adsorption with significant S_{CO} (up to 0.25) on the Pd-surfaces, that is covered with significant subsurface oxygen, underscores a change in the electronic state of Pd-surfaces towards mildly oxidized (or $Pd^{\delta+}$) state and likely an electronic decoupling occurs between bulk and top few surface atomic layers.

2) $\theta_{O_{sub}}$ was measured up to 0.3 ML between 500 and 850 K before the onset of CO adsorption; however, $\theta_{O_{sub}}$ increases from insignificant value <500 K to 0.4 ML at 900 K with pure O_2-beam. With significant $\theta_{O_{sub}}$ on the subsurfaces of Pd(111).

3) The rate of CO_2 production in the steady-state is considerable, even at high temperatures (700-850 K), and a broadening of the active CO-oxidation regime to high temperature on SM Pd(111) surfaces.

4) Pd(111) surfaces has been modified systematically by dosing oxygen at 900 K to populate the subsurface diffusion of oxygen into Pd layers. The dosing time varied from 5 to 110 minutes.

5) It is clearly demonstrated that room temperature or even below, CO oxidation is possible with modified Pd(111) surfaces.

6) Sustainable CO_2 production was observed up to 1 hr to make sure that; the subsurface oxygen is not utilized in the CO oxidation.

3.6. References

1. http://en.wikipedia.org/wiki/Carbon_monoxide
2. http://en.wikipedia.org/wiki/Carbon_monoxide_poisoning
3. (a) Shelef, M.; Graham, G. W. *Catal. Rev. Sci. Eng.* **1994**, *36*, 433. (b) Kreuzer, T.; Lox, S. E.; Lindner, D.; Leyrer, J. *Catal. Today.* **1996**, *29*, 17. (c) Taylor, K. C. *Catal. Rev. Sci. Eng.* **1993**, *35*, 457. (d) Shelef, M. *Chem. Re*v. **1995**, *95*, 209. (e) Belton, D. N.; Taylor, K. C. *Curr. Opin. Solid State Mater. Sci.* **1999**, *4*, 97. (f) Shelef, M.; McCabe, R.W. *Catalysis Today* **2000**, *62*, 35.
4. (a) Engel, T.; Ertl. G. *J. Chem. Phys.* **1978**, *69*, 1267; (b) Engel, T. *J. Chem. Phys.* **1978**, *69*, 373.
5. (a) Zaera, F.; Gopinath, C. S. *Phys. Chem. Chem. Phys.* **2003**, *5*, 646. (b) Zaera, F.; Gopinath, C. S. *Chem. Phys. Lett.* **2000**, *332*, 209. (c) Permana H,; Ng, K. Y. S.; Peden, C. H. F.; Schmieg, S. J.; Lambert, D. K.; Belton, D. N., *Catal. Lett.* **1997**, *47*, 5. (d) Zaera, F.; Gopinath, C. S. *J. Chem. Phys.* **1999**, *111*, 8088.

6. Leisenberger, F. P.; Koller, G.; Sock, M.; Surnev, S.; Ramsey, M. G.; Netzer, F. P.; Klötzer, B.; Hayek. K. *Surf. Sci.* **2000**, *445*, 380.
7. (a) Klőtzer, B.; Hayek, K.; Konvicka, C.; Lundgren, E.; Varga, P. *Surf. Sci.* **2001**, *482*, 237. (b) Gabasch, H.; Unterberger, W.; Hayek, K.; Klőtzer, B.; Kresse, G.; Klein, C.; Schmid, M.; Varga, P. *Surf. Sci*. **2006**, *600*, 205.
8. (a) Zheng, G.; Altman, E. I. *Surf. Sci.* **2000**, *462*, 151. (b) Zheng, G.; Altman. E. I. *Surf. Sci.* **2002**, *504*, 253. (c) Zheng, G.; Altmann. E. I. *J. Phys. Chem. B* **2002**, *106*, 1048.
9. Kan, H. H.; Shumbera, R. B.; Weaver, J. F. *Surf. Sci*. **2008**, *602*, 1337.
10. Wickam, D.T.; Banse, B. A.; Koel, B. *Surf. Sci.* **1991**, *243*, 83.
11. Bondzie, V. A.; Kleban, P.; Dwyer, D. J. *Surf. Sci.* **1996**, *347*, 319.
12. Zemlyanov. D.; Kiss, B. A.; Kleimenov, E.; Teschner, D.; Zafeiratos, S., Hävecker, M.; Knop-Gericke, A.; Schlogl, R.; Gabasch, H.; Unterberger, W.; Hayek, K.; Klotzer, B. *Surf. Sci.* **2006**, *600*, 983.
13. Titkov, Alexander I.; Salanov, Alexey N.; Segrey, V.; Boronin, K.; Andrey, I. *Rean. Kinet. Catal. Lett.*, **2005**, *86*, 371.
14. (a) Ketteler, G.; Ogletree, F.; Bluhm, H.; Liu, H.; Eleonore, L. D.; Hebenstreit.; Salmeron, M. *J. Am. Chem. Soc.*, **2005**, *127*, 18269. (b) Rose, M. K.; Borg, A.; Dunphy, J. C.; Mitsui, T.; Ogletree, D. F.; Salmeron, M. *Surf. Sci*. **2004**, *561*, 69.
15. Voogt, E. H.; Mens, A. J. M.; Gijzeman, O. L. J.; Geus, J. W. *Surf. Sci*., **1997,** *373*, 210.
16. Han, J.; Zemlyanov, D. Y.; Ribeiro, F. H. *Surf. Sci.* **2006**, *600*, 2730 and 2752.
17. Peterlinz, K.A.; Sibener, S.J. *J. Phys. Chem.* **1995**, *99*, 2817.
18. Thirunavukkarasu, K.; Thirumoorthy, K.; Libuda, J.; Gopinath. C. S. *J. Phys. Chem. B* **2005,** *109*, 13283.
19. (a) Lundgren, E.; Gustafson, J.; Mikkelsen, A.; Andersen, J. N.; Stierle, A.; Dosch, H.; Todorova, M.; Rogal, J.; Reuter, K.; Scheffler, M. *Phys. Rev. Lett*. **2004**, *92*, 046101. (b) Todorova, M.; Reuter, K.; Scheffler, M. *J. Phys. Chem. B* **2004**, *108*, 14477.

20. (a) Engel, T.; Ertl, G. *Adv. Catal*. **1979**, *28*, 1. (b) Ladas, S.; Imbhil, R.; Ertl, G. *Surf. Sci.* **1989,** *219*, 88.
21. Nakao, K.; Ito, S.; Tomishige, K.; Kunimori, K. *J. Phys. Chem. B* **2005**, *109*, 17579.
22. (a) Min, B.K.; Santra, A.K.; Goodman, D.W. *Catal. Today* **2003,** *85*, 113. (b) Szanyi, J.; Kuhn, W. K.; Goodman, D. W. *J. Phys. Chem.* **1994,** *98*, 2978. (c) Gao, F.; McClure, S.M.; Cai. Y.; Gath. K.K.; Wang, Y.; Chen, M.S.; Guo, Q.L.; Goodman. D.W. *Surf. Sci.,* **2009**, *603*, 65.
23. Fukui, K.; Miyauchi, H.; Iwasawa, Y. *J. Phys. Chem.***1996**, *100*, 18795.
24. Rzenicka, I. I.; Ma, Y.; Cao, G.; Matsushima, T. *J. Phys. Chem. B.* **2004**, *108*, 14232.
25. Gopinath, C. S.; Zaera, F. *J. Catal.* **2001**, *200*, 270.
26. (a) Johánek, V.; Schaürmann, S.; Laurin, M.; Gopinath, C. S.; Libuda, J.; Freund, H. J. *J Phys Chem B* **2004**, *108*, 14244. (b) Zaera, F.; Wehner, S.; Gopinath, C. S.; Sales, J. L.; Gargiulo, V.; Zgrablich, G. *J. Phys. Chem. B.* **2001,** *105*, 7771.
27. Salo, P.; Honkala, K.; Alatalo, M.; Laasonen, K. *Surf. Sci.* **2002,** *516*, 247.
28. Nakai, I.; Kondoh, H.; Shimada, T.; Resta, A.; Andersen, J. N; Ohta, T. *J. Chem. Phys.* **2006,** *124*, 224712.
29. Zhang, C.J.; Hu, P. *J. Am. Chem. Soc*. **2001**, *123*, 1166.
30. Hicks, R. F.; Qi, H.; Young, M. L.; Lee, R. G. *J. Catal.* **1990**, *122*, 295.
31. (a) Lyubovsky, M.; Pfefferle, L. *Appl. Catal. A.* **1998**, *173*, 107. (b) Velu. S.; Suzuki, K.; Gopinath, C. S.; Hattori, T.; Yoshida, H. *Phys. Chem. Chem. Phys.* **2002**, *4*, 1990.
32. (a) Lampert, J. K.; Shahjahan Kazi, M.; Farrauto, R. J. *Appl. Catal. B.* **1997**, *14*, 211. (b) Corro, G.; Vázquez-Cuchillo, O.; Banuelos, F.; Fierro, J. L. G.; Zomoza, M. *Catal. Commun.* **2007**, *8*, 1977.
33. Nagarajan, S.; Thirunavukkarasu, K.; Counsell, J.; Gilbert, L.; Gopinath, C. S.; Bowker, M. *J. Phys. Chem. C*. **2009**, *113*, 9814.
34. (a) Gopinath, C. S.; Thirunavukkarasu, K.; Nagarajan, S. *Chem. Asia. J.* **2009**, *4*, 74. (b) Nagarajan, S.; Thirunavukkarasu. K.; Gopinath, C. S. *J. Phys Chem. C.*

2009, *113*, 7385. (c) Thirunavukkarasu, K.; Nagarajan, S.; Gopinath, C. S. *Appl. Surf. Sci.* **2009**, *256*, 443. (d) Nagarajan, S.; Gopinath, C. S. *J. Ind. Inst. Sci*, **2010**, *90*, 245.

35. Markovits, A.; Minot, C. *Chem. Phys. Lett.* **2008**, *458*, 92.
36. Thirunavukkarasu, K.; Thirumoorthy, K.; Libuda, J.; Gopinath, C. S. *J. Phys. Chem. B* **2005,** *109*, 13272.
37. Thirunavukkarasu, K.; Gopinath, C. S. *Catal. Lett.* **2007**, *119*, 50.
38. Ramsier, R. D.; Gao, Q.; Waltenburg, N. H.; Lee, K.-W.; Nooij, O. W.; Leerts, L. Yates, J. T., Jr. *Surf. Sci.* **1994**, *320*, 209.
39. Surnev. S.; Sock. M.; Ramsey, M. G.; Netzer, F. P.; Wiklund, M.; Borg, M.; Anderson, J. N. *Surf. Sci*. **2000**, *470*, 171.
40. (a) Gopinath, C. S.; Zaera, F. *J. Phys. Chem. B.* **2000**, *104*, 3194. (b) Zaera, F. *J. Phys. Chem. B.* **2002**, *106*, 4043. (c) Zaera, F. *Acc. Chem. Res*. **2002**, *35*, 129.
41. (a) Dellwig, T.; Hartmann, J.; Libuda, J.; Meusel, I.; Rupprechter, G.; Unterhalt, H.; Freund, H.-J. *J. Mol. Catal. A: Chem.* **2000,** *162*, 51. (b) Johanek, V.; Laurin, M.; Hoffmann, J.; Schauermann, S.; Grant, A. W.; Kasemo, B.; Libuda, J.; Freund, H-J. *Surf. Sci.* **2004,** *561*, L218.
42. (a) Becker, C.; Henry, C.R. *Surf. Sci.* **1996,** *352-354*, 457. (b) Laurent, P.; Conrad, B.; Henry, R. *Appl. Surf. Sci.* **2000**, *164*, 156.
43. Unterhalt, H.; Rupprechter, G.; Freund, H-J. *J. Phys. Chem. B.* **2002**, *106*, 356.
44. Wintterlin, J.; Voelkening, S.; Janssens, T. V. W.; Zambelli, T.; Ertl, G. *Science* **1997,** *278*, 1931.
45. (a) Schalow, T.; Brandt, B.; Starr, D. E.; Shaikutdinov, S. K.; Schauermann, S.; Laurin, M.; Libuda, J.; Freund, H.-J. *Angew. Chem. Int. Ed.* **2006**, *45*, 3693. (b) Johánek, V.; Laurin, M.; Grant, A. W.; Kasemo, B.; Henry, C. R.; Libuda, J. *Science* **2004**, *304*, 1639.
46. Somorjai, G. *Introduction to Surface Chemistry and Catalysis*, A Wiley Interscience publication, **1994,** p-363.
47. Teschner, D.; Borsodi, J.; Wootsch, A.; Révay, Z.; Hävecker, M.; Knop-Gericke, A.; David Jackson, S.; Schlögl, R. *Science* **2008**, *320*, 86.

48. Jones, I.; Z. Bennett, R.; A. Bowker, M. *Surf. Sci.* **1999**, *439*, 235.

49. (a) Haruta, M. *Journal of New Materials for Electrochemical Systems* **2004**, *7*, 163. (b) Haruta, M. Catalysis Today **1997**, *36*, 153.

50. Hutchings, G. *Nature Chemistry* **2009**, *1*, 584.

51. Imbihl, R.; Ertl, G. *Chem. Rev.* **1995,** *95*, 697.

Chapter 4

NO + CO + O_2 Reactions on Pd(111) Surfaces

4.1. Introduction

The nitric oxide emission from automobile exhaust and power plants is one of the key environmental issues in the 21st century and it is directly affecting the living beings in many ways. Regulations for the control of NO_x emissions in automobiles have dramatically increased all over the world [1-4]. TWC employed in automobile converts pollutants (NO_x, CO, C_xH_y) to innocuous gases (N_2, H_2O) and less harmful gases (CO_2), and controls the pollutants [5]. Improvements in automobile IC engines and the developments in fuel quality led to fuel-efficient vehicles. Nonetheless, problems exist particularly in the reduction of NO to N_2, especially under net oxidizing conditions with fuel-efficient lean-burn engines [6].

In the last decade palladium only TWC converters (Pd supported on Al_2O_3, CeO_2, ZrO_2, SiO_2, La_2O_3 (or a combination of two-three supports)) were introduced increasingly, and it replaced the traditional Rh-Pt TWCs, due to its significant performance to reduce NO in net oxidizing conditions, its relatively low cost and higher abundance than Rh. Metals like Pt and Rh are found to be passive in oxygen rich conditions due to irreversible oxide formation [7-10]. However, there is no such poisoning effect observed on Pd surface, even in the oxygen rich conditions. Hence an understanding of NO_x reduction reactions under net oxidizing conditions on palladium catalysts is attracting more attention for the last one decade. Due to the complex nature of catalyst materials, the molecular level understanding and the micro kinetic details are yet to be understood. Hence, fundamental studies on single crystal surfaces for TWC reactions, especially with Pd are a necessity. Modern IC engines are operating at high air to fuel ratio, and consequently more oxygen is found in the

exhaust too. NO reduction is highly challenging in such oxygen rich conditions. It is important to note that Pd remain active in such high oxygen content, because of reversible oxidation capacity, and no oxygen poisoning was observed even with oxygen rich conditions makes palladium to be better catalyst. Oxygen interaction with palladium has been studied and its influence on oxidation catalysis has been explored by few groups [11-19].

NO:CO and NO:CO:O_2 reactions were carried out on noble metal single crystal surfaces by very few groups [20-23]. Zaera et al studied NO:CO reactions extensively on Rh(111) surfaces and it has been found that maximum N_2 production was observed between 500 and 600 K [24, 25]. The addition of O_2 inhibits the rate of production of N_2 as well as CO_2 under the reaction conditions. This behavior was explained by the poisoning of surface active sites from the dissociative adsorption of oxygen. The addition of excess CO also inhibits the rate of production of both N_2 and CO_2, below 500 K due to CO poisoning nature. The addition of O_2 to CO rich beams enhances the conversion of NO to N_2. The added O_2 helps to remove the excess CO from the surface. Zaera et al [25, 26] observed that the maximum product formation (N_2, CO_2) occurs at stoichiometric ratio of NO and CO on Rh(111) surfaces. Thirunavukkarasu et al [27] found that significant N_2 production was observed around 500 K upon catalytic decomposition of NO on Pd(111).

Goodman et al [28-30] carried out NO + CO reactions on Pd(111) and Pd(100) surfaces and it showed higher activity than Pd(100) for CO_2 and N_2O. Matsushima et al [31, 32] identified three different nitrogen removing process, which is in the NO:CO:O_2 reaction on Pd(110).

$$(1)\ N_2O_{(ads)} \rightarrow N_{2(g)} + O_{(ads)},$$

$$(2)\ N_2O_{(ads)} \rightarrow N_2O_{(g)},$$

$$(3)\ 2N_{(ads)} \rightarrow N_{2(g)}$$

Although there are few reports on the SS and the TS behavior of the NO:CO:O_2 reaction on Rh surfaces [4], and few Pd based powder catalysts [33-36],

to the best of our knowledge, there are no reports on Pd(111), especially with technically relevant conditions such as high temperatures and a wide range of NO:CO:O_2 ratios. NO dissociation under net-oxidizing conditions and beam switching experiments, between O_2-lean and rich compositions to manage NO reduction addressed in this chapter. Isothermal experiments with the NO:CO:O_2 reaction on Pd(111) surfaces were conducted in a molecular beam instrument (MBI) between 400 and 800 K and with xNO:yCO:zO_2 hereafter (x : y : z) and the composition of individual components varied from x = 1, 2, 4, and 6; y = 2, 4, and 7; z = 1, 2, 4, and 7.

4.2. Experimental section

Isotopically labeled ^{15}NO (SG Spectra Gases 99 %), CO and oxygen (Inox air products ltd, 99.9%) were all used without any further purification. The mass spectrometer signals of reactants and products are calibrated independently, by leaking the corresponding pure component. Since only ^{15}N-labelled NO was used in this work, ^{15}NO, $^{15}N_2$, ^{15}N and $^{15}N_2O$ will be simply referred to as NO, N_2, N, N_2O, respectively, hereafter. All the rates obtained are believed to be accurate to within 5% error; the main source of systematic errors originating from the mass spectrometer calibration and the contribution of the background gases to the overall measured reaction rates. In relative terms, the reported values were reproducible to within 5% for a given beam composition, beam flux, and surface temperature. More Details about the MBI used for the experiments is available in (Chapter 2 sections 2.2, 2.3 and 2.4).

4.3. Results

4.3.1. General considerations

All kinetic experiments reported here for NO:CO:O_2 reaction on Pd(111) surfaces were carried out in a manner identical to that of reported in Chapter 2 sections 2.2, 2.3 and 2.4 and also in our earlier publications [11-14]. The clean Pd(111) surface is first heated to a pre decided temperature, and then exposed to an effusive molecular

beam with required NO:CO:O_2 ratio, while the partial pressure of the different gases of interest are followed by QMS as a function of time.

Figure 4.1 shows a typical raw kinetic data obtained in this manner. Figure 4.1 shows the evolution of partial pressure traces of NO, CO, O_2, CO_2, N_2, and N_2O for a beam of NO:CO:O_2 (2:2:1) directed on Pd(111) surfaces at 550 K. The partial pressures of all the relevant species were recorded as a function of time. The various steps in all the experiments are explained below with reference to the above data:

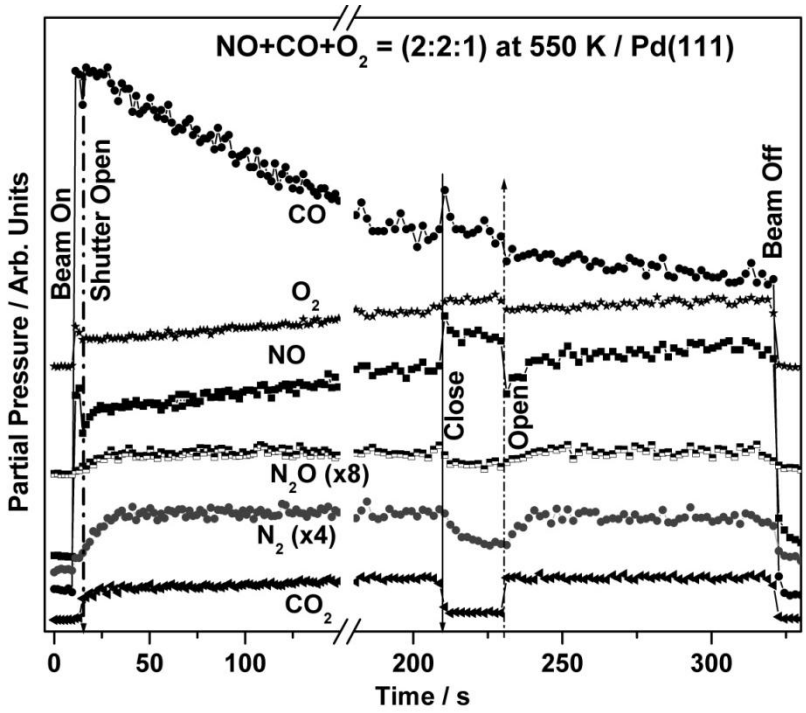

Figure 4.1 An effusive collimated NO:CO:O_2 molecular beam (of 2:2:1) is directed onto a clean Pd(111) surface as the temperature kept at 550 K and the partial pressures of all the reactants (NO, CO, and O_2) and products (N_2, N_2O and CO_2) are followed as a function of time. The beam was blocked at 210 sec and unblocked at 230 sec in order to measure the SS rates due to the gases in the beam directly, as they are proportional to the drop in partial pressure of the products and/or the rise in partial pressure of the reactants from their SS values. Note the instantaneous changes in CO_2 signal with blocking and unblocking of the beam, in contrast with the slower response of the N_2 and N_2O trace.

(1) At t = 10 s, a molecular beam of a mixture of the reactants was turned on; an immediate increase in reactants partial pressures could be seen. Some adsorption of

the reactants from the background cannot be avoided at this stage. It is also to be mentioned here that shutter is in place and blocking the beam reaching Pd(111) surface.

(2) At around t = 13 s, the shutter was opened ((dashed arrow) in Figure 4.1) to allow the beam to interact directly with the Pd(111) surface kept at 550 K. An immediate decrease in the partial pressure of the reactants was observed indicating the adsorption of the reactants on the Pd(111) surface. This data is helpful to explore the competitive adsorption characteristics of reactants from a mixture of reactants. An increase in the partial pressure of the products, $^{15}N_2$ (30 amu), CO_2 (44 amu) and $^{15}N_2O$ (46 amu) were also observed. The changes observed from the time the shutter is opened (t = 13 s) until the SS is reached is termed as the TS, and SS normally reaches within 1 min under the present experimental conditions.

(3) In the SS, the reaction rate was measured by blocking the beam deliberately for 20 s (between t = 210-230 s) with the shutter. An increase (decrease) in the partial pressure of all reactants (products) and a clear decrease in the partial pressures of N_2 and CO_2 was observed. Although a decrease in the partial pressure of N_2O was observed it is not like other products. A slow increase in NO partial pressure (up to 10%) was due to NO adsorption on the UHV chamber walls, which decreases with time, and does not indicate a change in the NO flux (F_{NO}) on Pd(111). An increase in the overall partial pressure of NO and O_2 was observed, while blocking the beam in the SS; a sharp change in the CO partial pressure was observed only at the blocking and unblocking of the beam, but an overall increase was not observed during the beam blocking time. Above observation and other results presented in this chapter highlight the net adsorption is significantly influenced by the reaction conditions. The measured changes in the partial pressures of products allows to directly determine the SS reaction rates. A sharp decrease in the CO_2 partial pressure was observed when the beam was blocked, whereas a slow decay in partial pressure was observed for the N_2 and N_2O.

(4) At t = 230 s the shutter was opened to resume the SS. This is mainly to observe the resumption of SS ad there is no anomoly in that. Immediately on shutter opening CO, O_2 and CO_2 intensity reverts back instantly; however N_2 and N_2O gradually

increases and the time required to reach the SS depends on reaction conditions. In the present case shown in Figure 4.1, it takes about 10 s to reach the SS value again. Large NO adsorption, resembling to that of TS, occurs, which is in contrast to CO and O_2. The reaction was followed to continue for some more time.

(5) At about *t* =320 s, the beam was turned off to stop the reaction. After the pressure of the UHV chamber reached the initial background level, the sample temperature was ramped to 1000 K at a heating rate of 10 K/s to record the TPD of all the relevant species. The coverage by the nitrogen atoms that remained on the Pd(111) surface was calculated by integrating the area of the N_2 desorption peak observed in the TPD.

A systematic study of the NO + CO + O_2 reaction kinetics on Pd(111) surfaces was carried out by following the above procedure as a function of temperature and, NO:CO:O_2 composition. During the reaction measurements, the total pressure in the chamber increases to about (1-2) x 10^{-8} Torr and that induces some additional adsorption/reaction apart from the direct beam onto Pd(111). As shown in Figure 4.1, the reactants pressure increase in the same manner, whether the beam was blocked or not, except while opening/closing the shutter. CO_2 shows an increase in pressure and displays that there is reaction to some extent due to background adsorption of reactants. In the case of N_2 (amu 30) a significant increase in background pressure is mostly due to 1% ^{14}NO (amu 30). Indeed, at low temperature (<450 K) measurements, where there is no net reaction, show a rise in partial pressure of amu 30 is exclusively due to ^{14}NO (refer Figure 4.2a). It was difficult to make out any contribution due to the very poor signal/noise associated with the data of N_2O production. However, at the time of shutter opening/closing, a good change in partial pressure of all the products (including N_2O) demonstrate that major contribution is due to molecular beam. Further, the extent of CO_2 production due to background adsorption is not more than 5% of the CO_2 produced from the direct beam. However, a similar measurement for $^{15}N_2$ was not reliable as the background is largely due to ^{14}NO. For the above reason, the background contribution is not included in the results reported. In order to understand the NO reduction under net oxidizing conditions, wide range of temperature and beam compositions are studied and next section

describes the temperature dependence of NO:CO:O_2 reaction with (1:1:2) beam compositions.

4.3.2. Temperature dependence

Figure 4.2 displays the raw data for time evolution of the TS and SS kinetics of (a) one of the reactant NO uptake, (b) CO_2 (c) N_2 and (d) N_2O production at different temperatures between 450 and 800 K on the Pd(111) surface to a 1:1:2 NO:CO:O_2 beam. There is no significant N_2 production can be observed at 450 K, whereas a small, but, sustainable CO_2 production occurs at 450 K, with significant CO_2 production in the TS. Isothermal kinetic results from surfaces exposed to NO:CO beams under comparable conditions [27] have also indicated that the desorption of N_2 starts above 450 K, hence it can be concluded that the presence of oxygen in the beam does not significantly changes the threshold temperature of catalysis.

A clear NO uptake observed at the time of shutter opening at t = 140 s, indicating a possibility of adsorption-desorption equilibrium at T = 450 K, which is in good agreement with TPD results of NO/Pd(111) system [39]. Above 450 K, the SS production of CO_2, N_2 and N_2O, increase rapidly with temperature until reaching a maximum value between 550 and 600 K. Notice that no net NO adsorption is observed above 600 K; very similarly, no significant N-containing products (N_2 and N_2O) were also observed ≥600 K. In contrast sustainable CO_2 production was observed even at 800 K although the extent of CO_2 production decreases >600 K. Notice also that the kinetics observed in the SS for beam oscillation (immediately after shutter closing as well as opening) are quite different for N-containing products and CO_2. Changes in CO_2 pressure are instantaneous upon blocking and unblocking of the beam, whereas the N_2 and N_2O pressure changes slowly. The main conclusion from this observation is that the recombination of nitrogen atoms is likely to be rate limiting due to the lateral diffusion for the whole process under the experimental conditions. Another important observation is a strikingly different TS kinetics for CO_2 and N_2 production. For instance, between 500 and 650 K, the N_2 production rate increases abruptly in TS and then slowly stabilizes to the SS. However, CO_2

production increases gradually to the SS, without any large CO_2 production as seen at 500 and 450 K. This is likely due to the change in competitive adsorption of reactants as well as desorption of products due to change in surface composition of various species.

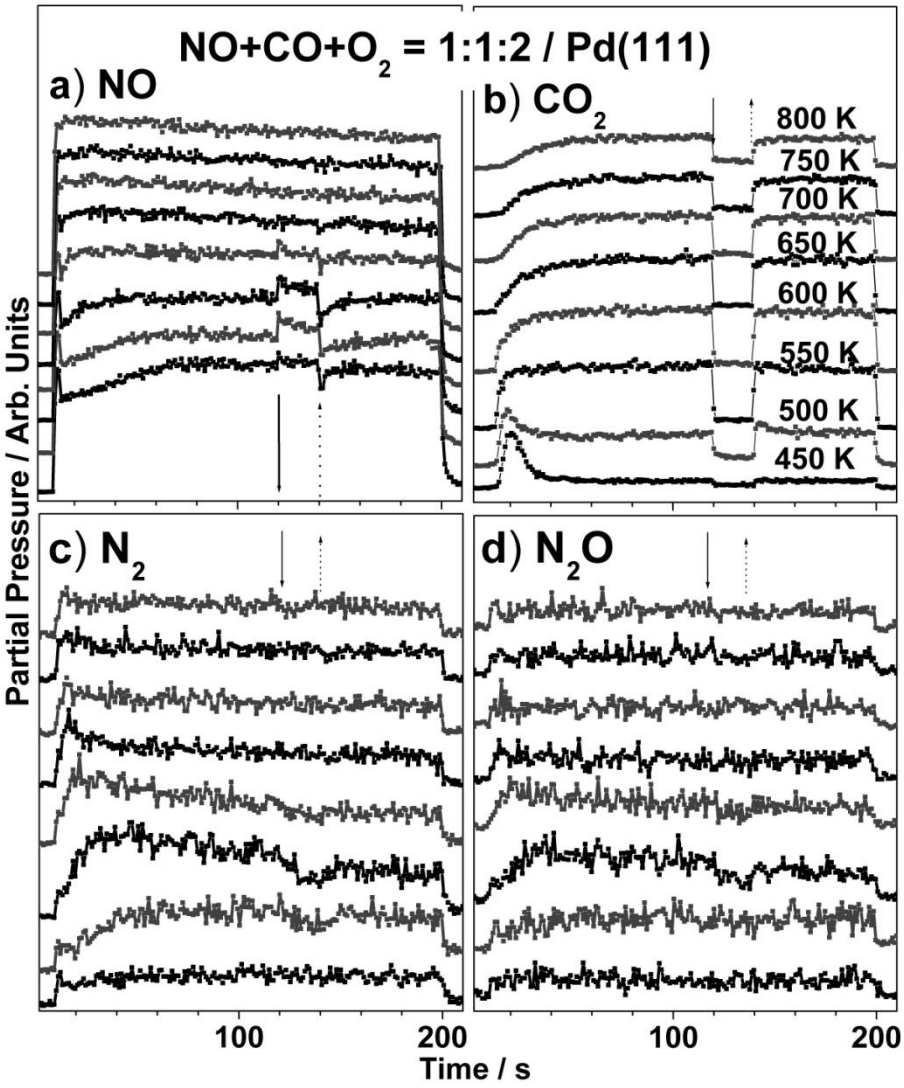

Figure 4.2 Time evolution of the partial pressure of the products, (a) NO, (b) CO_2, and (c) N_2 and (d) N_2O uptake in kinetic experiments such as that described in Figure 4.1 for the compositions of (1:1:2) NO:CO:O_2 at given temperature. CO_2 production occurs at all temperatures, but N_2 and N_2O formation observed only between 500 and 600 K. Shutter open and shutter close is indicated by dotted and solid arrows, respectively in all the figures.

Fast increase in N_2 production highlights the favorable dissociation of NO followed by N+N recombination. Slow increases in CO_2 production underscores the relatively slow net O_2 uptake under competitive adsorption conditions, and hence slow CO_2 generation in TS. Figure 4.2 demonstrates that the overall reaction rate increases with increasing temperature until reaching a maximum between 550 and 600 K and decreases with further increase in temperature.

4.3.3. Beam composition dependence

Figure 4.3 displays the rate of products formation of (a) CO_2, (b) N_2, and (c) N_2O on Pd(111) during the exposure of $NO:CO:O_2$ = (2:1:z) composition with z varying between 0, 1, 2, 4, and 7 at temperature between 450 and 800 K.

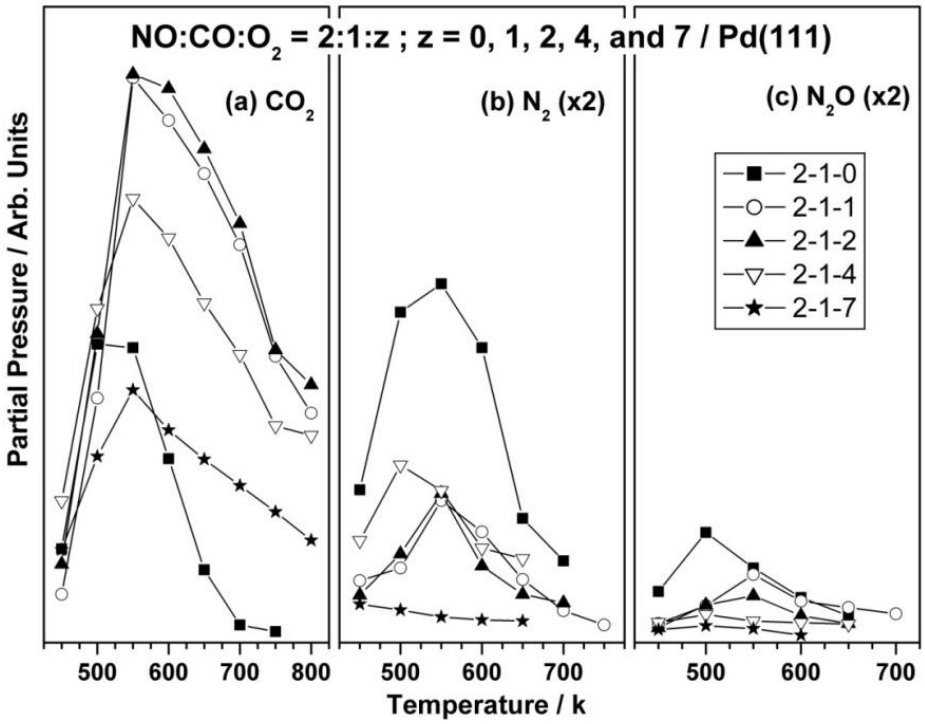

Figure 4.3 Temperature dependence of the SS rates for the formation of products, (a) CO_2, (b) N_2, and (c) N_2O during the conversion of $NO:CO:O_2$ mixtures on Pd(111) as a function of beam composition. The beam composition was (2:1:z) with z = 0, 1, 2, 4 and 7. The SS rate measurement observed from the raw kinetic data. SS rate increased from 450 K reaches maximum at 550 K and decreases for all the beam composition with respect to CO_2. The intensity of N_2 and N_2O was multiplied by a number 2, to project it in a clear way.

CO_2 production observed from 450 to 800 K with the rate maxima observed at 550 K for all beam compositions. Below 450 K, there is no sustainable CO_2 production was observed, except in the TS regime and very similar to Figure 4.2. SS rate observed for N_2 with 2:1:1 and 2:1:2 compositions is almost identical hinting no significant influence of oxygen at lower and comparable levels to that of NO-content. SS rate of CO_2 for 2:1:0 composition is lesser than 2:1:1 and 2:1:2 hints the limited O-supply by NO-dissociation. A sudden jump in the rate of CO_2 production at 550 K and above with 2:1:1, 2:1:2 and 2:1:4 compared to 2:1:0 highlights the competitive O_2 adsorption. Indeed a steep fall in N_2 production >550 K demonstrates the decrease in NO dissociation due to predominant θ_o on the surface. However, an overall decrease in the CO_2 rate was observed for oxygen rich 2:1:4 and 2:1:7 compositions due to decreasing F_{CO} relative to F_{O_2}.

There is a shift in the rate maxima was observed with respect to CO_2 production from 500-550 K with 2:1:0 to 550-600 K with increase in oxygen content in the 2:1:2 beam. N_2 production was also observed in the range of 450 and 600 K, with the maximum production observed in the absence of oxygen content in the beam. The overall production of N-containing products decreases with increase in oxygen. Very similar to CO_2, N_2 rate pattern also shows similar values for 2:1:1 and 2:1:2 compositions suggesting a sustainable catalytic NO decomposition without significant influence of oxygen at lower/comparable levels to that of NO content. The rate maxima observed at 550 K with 2:1:1 and 2:1:2 compositions, shifts to lower temperature with increase in the oxygen content for 2:1:4. Rate maxima for 2:1:4 is 500 K, whereas it decreases for 2:1:7. Similar trend is observed in N_2O also. The reason for rate maxima shift to lower temperature for N-containing products is likely due to the repulsive force exerted by more chemisorbed oxygen at 550 K with oxygen rich conditions, which decreases NO interaction with the Pd-surface. Further with increasing O_2-content, NO-flux decreases and this is another reason for an overall decrease in the rate of N-containing products.

4.3.4. Transient kinetics

Figure 4.4 shows the temporal evolution of partial pressure of (a) NO uptake, (b) CO_2, (c) N_2 and (d) N_2O formation for 2:1:z of NO:CO:O_2 at 500 K. The beam composition varied from O_2-lean (2:1:1) to O_2-rich (2:1:7) conditions. The following points are worth mentioning in this section:

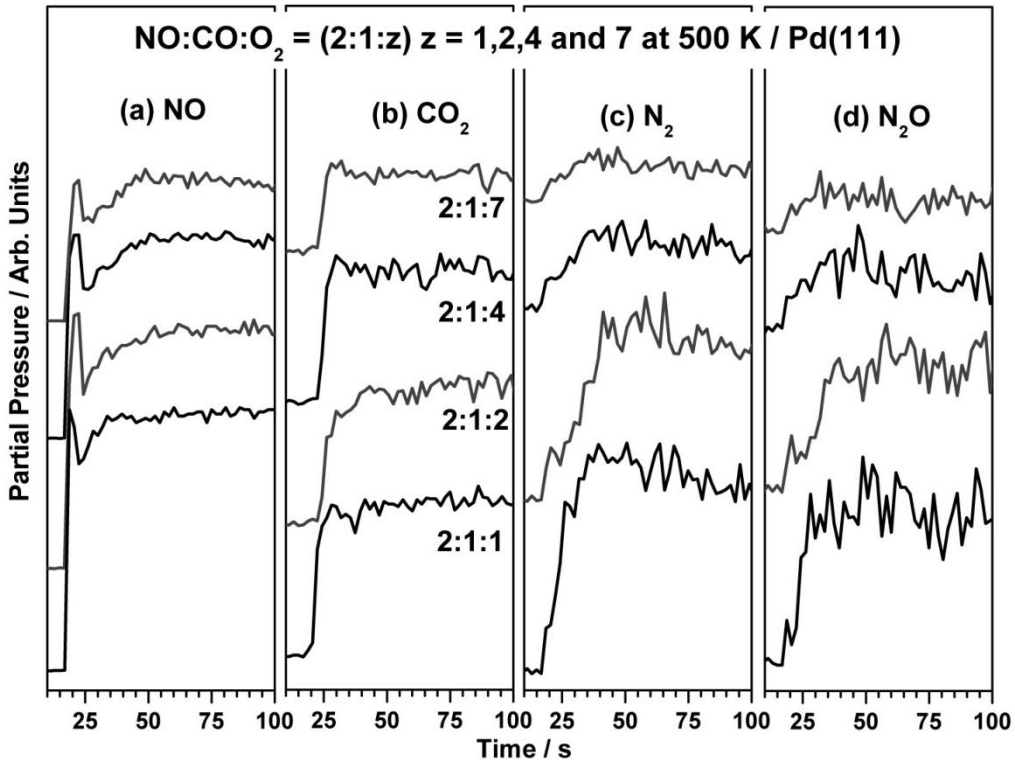

Figure 4.4 shows the transient state temporal evolution of partial pressures of (a) NO, (b) CO_2, (c) N_2 and (d) N_2O from 2:1:z where z = 1, 2, 4 and 7 of NO:CO:O_2 composition at 500 K.

(1) As the oxygen content increases in the beam, the intensity of the NO decreases, which is expected, as the total partial pressure of the beam is constant. (2) The TS rate of production of CO_2 does not alter much with O_2 content and similar trend is observed in SS rate also (see Figure 4.3). However, N-containing products like N_2 and N_2O decreases drastically when O_2 content increased, a similar trend is observed in SS rate also (see Figure 4.3). (3) At high O_2 content in the beam chemisorbed oxygen coverage (θ_o) also increases, and this hinders the NO adsorption and hence a decrease in the N-containing products (Figure 4.4 (c) and (d)). (4) when the shutter is

initially opened at t = 20 sec, CO_2 production is observed instantaneously, irrespective of the beam compositions. The N-containing products showed significant delay in TS, especially the delay is more pronounced in oxygen rich conditions. Similar trend is observed in Figure 4.1 and 4.2. The above point demonstrates the formation of N+N recombination step is to be the slowest and hence the rate determining step. The above points demonstrates the importance of oxygen free surfaces, for sustainable NO dissociation under SS condition. (5) Inspite of increasing O_2-content in the beam, unambiguous adsorption of NO in the TS on clean Pd(111) occurs. Indeed we utilize this aspect for managing NO reduction through beam oscillation between O_2-lean and O_2-rich conditions.

4.3.5. Steady state kinetics

Figure 4.5 displays the time evolution of (a) CO_2 (b) N_2 (c) N_2O production traces during exposure of the Pd(111) surfaces to NO:CO:O_2 beams with 1:7:*z* compositions (*z* = 0, 1, 2 and 4) at crystal temperatures between 500 and 600 K. Although the reaction has measured between 400 and 800 K, for the sake of clarity 500, 550 and 600 K data showed in Figure 4.5 for all the products at all of the beam compositions. The rate of CO_2 production is maximum at 550 K when z = 0; however it shifts to 500 K with increasing O_2 content. The sustainable CO_2 production observed even up to 800 K, when z = 1, 2 and 4. The N-containing products (N_2 and N_2O) shows a reverse trend. Considerable TS and SS N_2 and N_2O observed when 1:7:z (z = 0 and 1).

NO adsorption on Pd surfaces dominates, when there is no oxygen content in the beam (z = 0); at temperatures from 500 to 600 K; whereas in the presence of oxygen the rate of production of N_2 and N_2O decreases drastically and very little SS rate observed in the case of 500 K and 550 K data for (z = 1 and 2). When the O_2 concentration increased further, N_2 and N_2O production not observed in SS. The rate of N-containing products decreases as the temperature increases from 500 to 600 K for z = 0, 1 and 2.

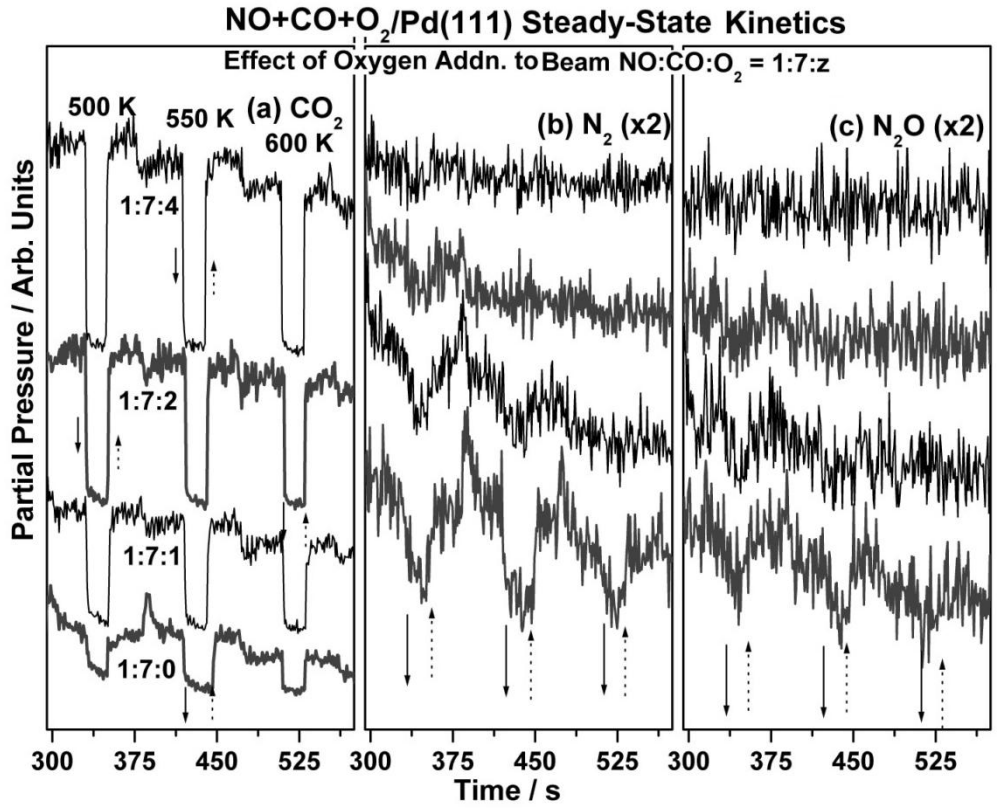

Figure 4.5 Time evolution of the partial pressure of products (a) CO_2, (b) N_2, and the (c) N_2O at temperatures between 500 and 600 K. 1:7:z where z = 0, 1, 2 and 4 NO:CO:O_2 ratios were used in this set of experiments with z varying from 0 to 4. CO_2 production observed at all temperatures, but N-containing products ceases at high temperatures (especially above 600 K) with increasing oxygen concentration. As in Figure 4.1, a slow response seen at N-containing products for z = 0 and 1, upon blocking and unblocking of the beam.

This is attributed to oxygen poisoning the surface for further NO adsorption. Inspite of significant amount of oxygen present in the beam, N-containing products observed in the SS is to be underscored. This is attributed to relatively strong adsorption characteristics of NO, compared to O_2 at temperatures $\leq$ 550 K.

4.3.5.1. SS kinetics with NO variable

In order to understand the SS rate phenomena associated with NO + CO + O_2 reaction, three types of variations in the reactants compositions are included. SS rate has been measured by varying one of the reactants in the beam by fixing other two as constant. Here is an example shown for the NO:CO:O_2 beam with NO content as a

variable. Figure 4.6 displays the time evolution of the (a) CO_2 (b) N_2 and (c) N_2O production in SS during exposure of the Pd(111) surfaces to NO:CO:O_2 beams with (x:1:2) compositions, where (x = 1, 2, 4 and 6) at 550 K.

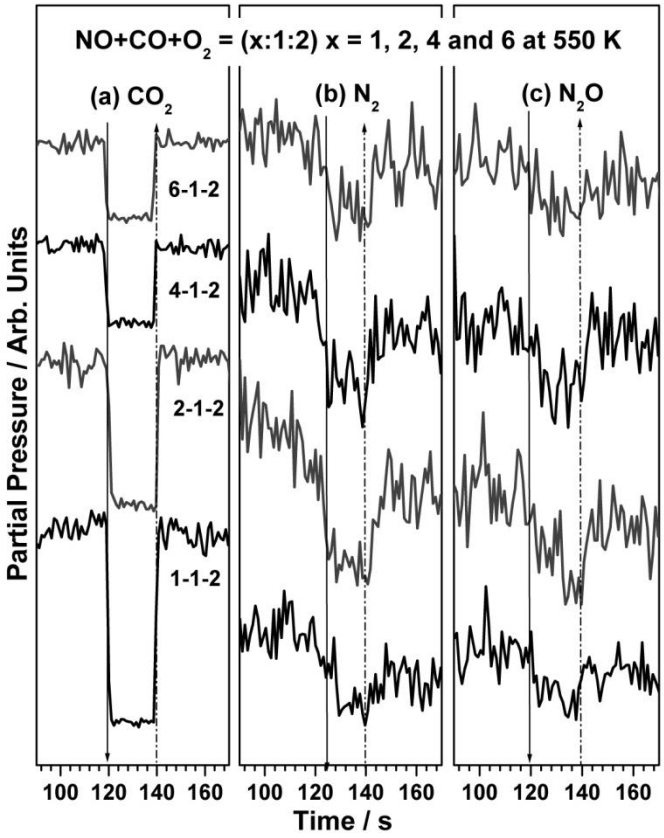

Figure 4.6 Time evolution of the partial pressure of SS rate of the products, (a) CO_2 (b) N_2 and (c) N_2O, carried out at 550 K on Pd(111) with the beam composition of NO:CO:O_2 (x:1:2) x = 1, 2, 4, 6 CO_2 production decreases with increase in the NO content, but N_2 formation increases in (2-1-2) and then decreases with increasing NO concentration. As in Figure 4.1, a slow response is seen for N_2 trace upon blocking and unblocking of the beam. N_2O formation initially increases from (1:1:2) to (2:1:2).

At t = 120 s (140 s) the shutter is deliberately blocked (opened) to measure the SS rate of the reaction. As discussed in earlier, the CO_2 response is immediate upon shutter operation, whereas N-containing products display slow decay (4 to 5 sec) to reach new SS. Above delay is more pronounced in (x:1:2) where x = 1 and 2. When the NO content is increased in the beam, CO_2 production decreases, as expected.

However, the maximum N_2 and N_2O was observed for (2:1:2), indicating a significantly large NO conversion and N_2 yield at x = 2.

4.3.5.2. SS kinetics with O_2 variable

Temperature dependence of the SS rate has been measured for the NO:CO:O_2 (2:1:z) composition with increasing oxygen content (z = 0 to 7) in (Figure 4.7). CO_2 production has been observed between 450 and 750 K with all values of z, expect z = 0, where SS rate measured only up to 700 K).

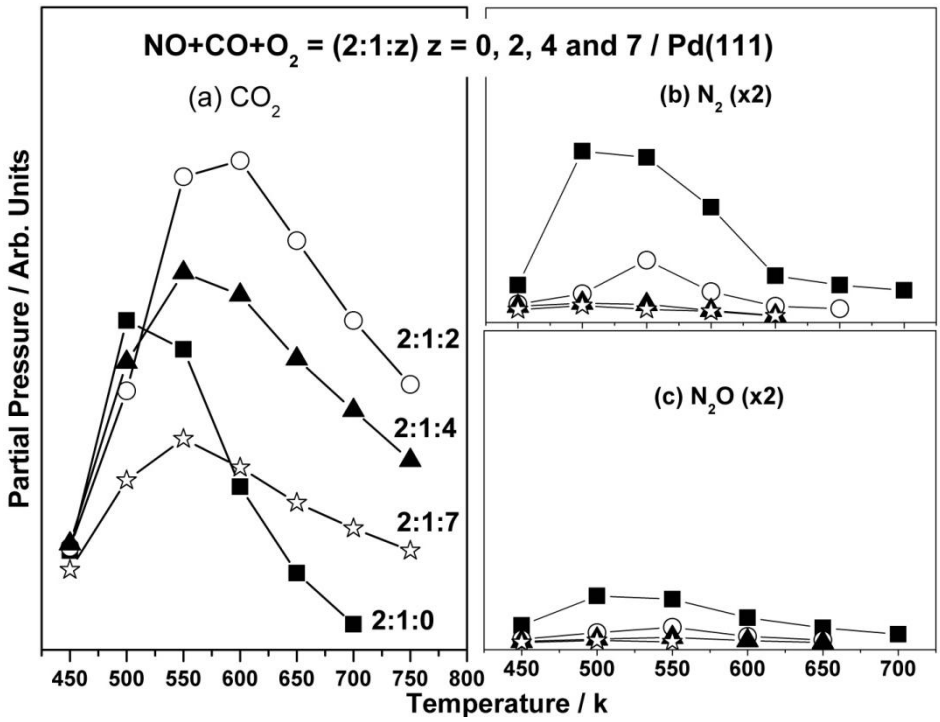

Figure 4.7 SS rate of the NO:CO:O_2 with the ratio (2:1:z) z = 0, 2, 4, 7 on Pd(111) as a function of temperature. The ratio (2:1:2) shows a maximum SS rate in the case of CO_2 and (2:1:0) show maximum SS rate for N-containing products. The maximum production observed at 550 K with respect to all products except (2:1:0) composition.

When there is no oxygen content in the beam (2:1:0) composition, the CO_2 production shows maximum around 500 K, and the rate decreases drastically. Two important reasons are (a) desorption rate increases above 550 K, for both CO and NO molecules, and hence (b) decreasing availability of oxygen for oxidation of CO to CO_2. As the oxygen concentration increases, (1:1:2) composition shows the maximum

CO_2 production between 550 and 600 K. As the oxygen content increases further, (z = 4 and 7), the rate of CO_2 decreases due to decrease in F_{CO} and the surface is increasingly covered by oxygen atoms >600 K. Rate of N-containing products could be measured up to 700 K in the case of 2:1:0 composition; however, the rate decreased dramatically observed between 500 and 600 K with gradual oxygen addition to the beam. In general, the maximum N_2 and N_2O was observed for z = 0, and SS rate decreases with increase in oxygen content in the beam. Both N-containing products showed maximum rate at 500 K, when there is no oxygen and it shifted to high temperature (550 K) when oxygen content is present in the beam.

4.3.5.3. SS kinetics with CO variable

SS kinetic data measured for (a) CO_2, (b) N_2 and (c) N_2O production as a function of composition (and temperature) for the 1:*y*:3 NO:CO:O_2 beams are plotted in Figure 4.8. The purpose of varying CO is to observe the effect of fuel-lean and fuel-rich conditions by adding CO (2, 5, 8, 11 and 14) to the beam. In this set of experiments, the maximum rate of reaction shifts toward higher temperatures as more CO is added to the beam. Other important points to be noted are: (1) the extent of CO_2 production at 400 K in the SS decreases with increase in CO from y = 2 to 14. CO coverage (θ_{CO}) on the Pd(111) surface dominates, at this temperature and hence a decrease in the CO_2 production. The rate maximum was observed at 450 K for y = 2 and it shifts gradually to 550 K with increasing addition of O_2 to the beam. (2) With respect to N-containing products, significant N_2 and N_2O production starts only when the crystal temperature is between 450 and 550 K. When the Pd(111) sample is ramped from 400 to 450 K, the N_2 desorption rate increases abruptly, and then stabilized to its new SS. This is mainly due to desorption of the strongly bound nitrogen that builds up on the surface due to dissociative adsorption of NO at ≥400 K [39].

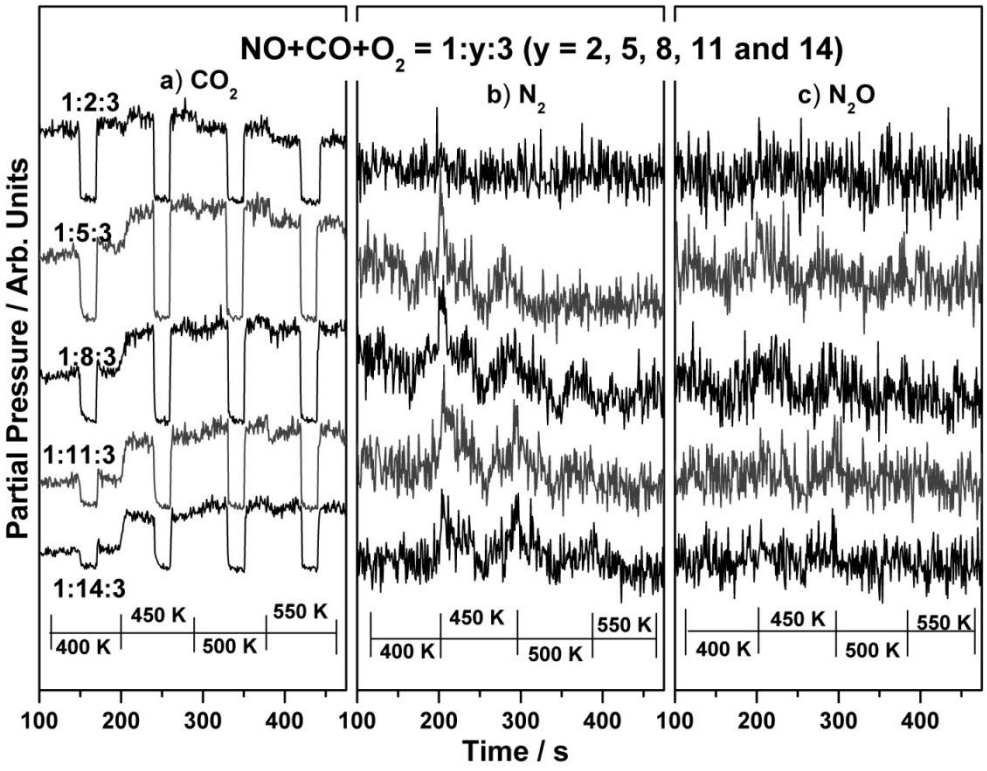

Figure 4.8 Effect of addition of CO to the activity of Pd(111) towards the conversion of NO:CO:O_2 mixtures. The dependence of SS kinetics of formation of the products, (a) CO_2, (b) N_2 and (c) N_2O, as shown here as a function of reaction temperature for a set of beams with 1:y:3 of NO:CO:O_2 ratios, with y = 2, 5, 8, 11 and 14.

This desorption observed during temperature ramping decreases between 450 and 500 K. Significant SS N_2 production observed for all O_2-rich beam compositions ($y \geq 5$) at 450 K and 500 K is to be noted. This is attributed to the high rate of CO oxidation and hence the oxygen deprived Pd-surfaces enhances NO dissociation, inspite of decreasing F_{NO} from y = 2 to 14.

4.3.6. O_2:NO ratio

Figure 4.9 provides the information about SS rate for the products (a) CO_2 and (b) N_2 with different oxygen content in the beam for 1:1:z composition. (1) Maximum CO_2 production was observed between 550 and 600 K for all z values (z = 1, 2, 4 and 7). (2) The rate of CO_2 production is almost similar for 500 and 800 K for (z = 2, 4 and 7) values.

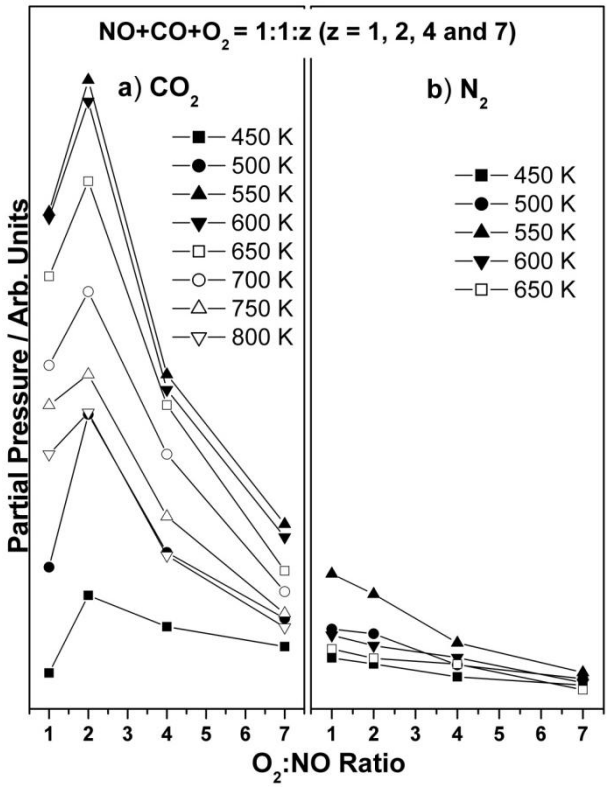

Figure 4.9 Composition dependence of the SS rates of formation of the products, (a) CO_2 and (b) N_2 during the conversion of NO:CO:O_2 (1:1:z) z = 1, 2, 4, 7 mixtures on Pd(111) as a function of reaction temperature.

(3) The maximum rate of CO_2 production was observed with z = 2 for all temperature range (450 to 800 K) and the rate decreases with increase or decrease in oxygen content; For oxygen rich (1:1:7) composition the difference between the rate maximum and rate minimum is the lowest, whereas for (1:1:2) composition the rate variation was observed to be at the maximum, among the reactants composition plotted in Figure 4.9. The rate increases with increase in the oxygen content and then decreases further after (1:1:2) compositions. In the case of N_2 production, the rate decreases with increase in oxygen flux as expected. The maximum rate with respect to N_2 was observed at (1:1:1) for all temperatures (450 to 650 K).

4.3.7. O_2:CO ratio

Figure 4.10 shows SS rate of the products CO_2 and N_2 for the beam compositions NO:CO:O_2 = (1:y:1) where y = 1, 2, 4, 6. Maximum CO_2 production was observed at 600 K for all beam compositions and the beam ratio (1:2:1) provides maximum rate in

all temperature range between 450 and 800 K. However, reaction rate decreases further for CO rich (y = 4 and 2) conditions. Changes observed in the rate of CO_2 production are very similar to that of N_2. Minimum rate observed at 450 K with respect to CO_2, whereas minimum rate for N_2 was observed at 700 K.

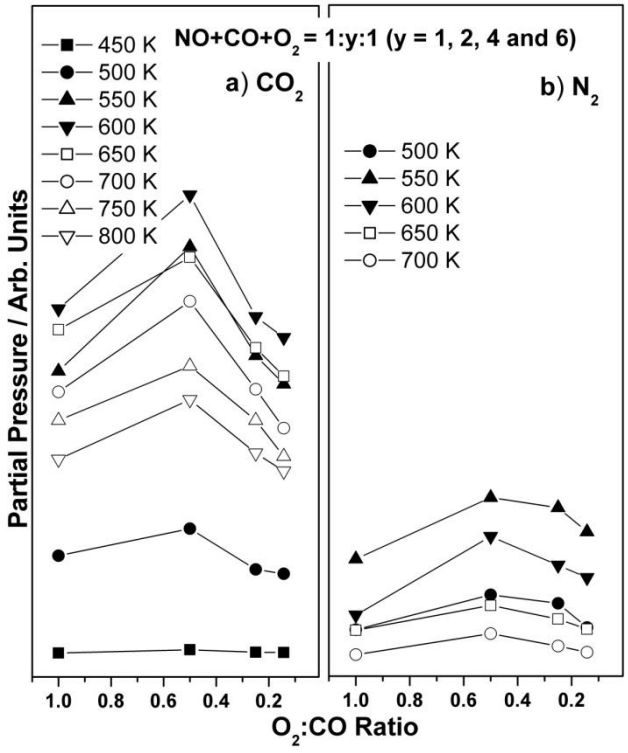

Figure 4.10 Effect of the change in CO:O_2 ratio to the activity of Pd(111) toward the conversion of NO:CO:O_2 mixtures. The dependence of the SS rates of formation of the products, CO_2 (a) and (b) N_2 is shown here as a function of reaction temperature for a set of beams with NO:CO:O_2 (1:y:1) ratios, with *y* varying from 1, 2, 4, 6. (a) Optimum rates are seen under conditions leading to stoichiometric coverages on the surface (1:2:1). At 600 K, the rate maxima for all beam compositions were observed. (b) Rate maxima for N_2 also observed at (1:2:1) and at 550 K for all beam compositions.

When the CO concentration increases above the stoichiometric ratio, the rate of CO_2 production decreases drastically as it poisons the crystal at low temperature. However, with increasing CO concentration, the rate of N-containing products showed higher SS rate compared to stoichiometric composition (y = 1) and the beam composition is (1:1:1). The above point demonstrates that, the CO molecules effectively utilize the chemisorbed oxygen atoms for oxidation to CO_2, which makes

the Pd surface increasingly free from oxygen. This allows more NO to dissociate on the surface. In general, the rate of N-containing products formation decreased at high temperatures, especially above 600 K due to favor of CO+O_2 reactions which dominates the Pd surfaces.

4.4. Beam switching experiments

Real world three-way catalysts employed in the automobiles face a significant fluctuation in the composition of the auto exhaust depending on the driving conditions. Although we cannot go into the minute details of all the possible fluctuations, two extreme situations are easy to be modeled based on either the oxygen (fuel) rich (lean) or poor (rich) conditions. Most of the above mentioned fluctuations should be between the above two extreme conditions. Reversibility between the above two conditions is mandatory for the best performance of TWCs.

Fast molecular beam switching experiments has been performed (Figure 4.11, 4.12) to simulate the above conditions as well as to observe the changes in reactivity, simultaneously. First of all, an excellent reversibility between end to end conditions on Pd(111) surface was observed. It is worth noting from the Figure 4.3-4.5 and 4.7 that, irrespective of O_2 content in the reactant mixture, NO adsorption was clearly observed with moderate to high rate of N_2 production in the TS. However, rate of N_2 production in the SS decreases, when the oxygen content is high. These points highlights the fast (slow) adsorption kinetics associated with NO (O_2) in the TS and gradual changes in adsorbate (N and O) composition as the reaction proceeds from the start of the reaction to the SS. Our aim was to make use of this observation to maximize NO reduction under net oxidizing conditions. Although we made few attempts to maximize NO reduction, a successful attempt is described below to maximize NO reduction under net maximizing conditions by fast oscillation of reactants between O_2-rich and O_2-lean compositions. By using the five-way valve setup described in the experimental section, the behavior of the system under oscillatory conditions could be probed directly [24, 25].

4.4.1. Temperature dependence

A number of kinetic runs were performed where the Pd surface was alternatively exposed to oxygen-rich and oxygen-lean beams. In the example presented in Figure 4.11, an initial beam of 3:6:1 NO:CO:O_2 ratio was alternated with a second beam of 3:4:3 compositions while varying the surface temperature between 500 and 700 K. Figure 4.11 displays the raw experimental data for the partial pressures of (a) NO, (b) CO_2, (c) N_2 and (d) N_2O and as a function of time and temperature. This data is normalized to the same $F_{NO+CO+O_2}$. This normalization was required to compensate for the drop in backing pressure behind the doser induced by pumping of the intermediate volume common to the two gas reservoirs every time the beam was switched. By using five-way valve setup described in chapter 2, section 2.2 [37, 38], the behavior of the system under oscillatory conditions can be measured directly.

The surface of Pd has been exposed to number of kinetic runs with oxygen lean and oxygen rich conditions. When the beam is altered from O_2-lean to O_2-rich composition (Figure 4.11), the rate of CO_2 production for O_2-rich composition increases almost twice that of O_2-lean beam. However, the rate of N-containing products like N_2 and N_2O decreases marginally with respect to TS and SS at 500 K. When the beam is altered continuously between O_2-lean and oxygen-rich, the intensity of CO_2 TS gradually increased in O_2-lean beams and the intensity of N_2 in TS increases in O_2-rich conditions. The above effect is more pronounced at high temperatures. When the temperature is raised to 550 K, the overall rate of production of all products (CO_2, N_2, N_2O) increases with respect to both O_2-lean and O_2-rich compositions has been observed especially at short oscillation time at t = 330-390 s. The intensity difference between N-containing products between O_2-lean and O_2-rich compositions in the SS increases gradually when the temperature is raised. N-containing products (N_2 and N_2O) observed both in TS and SS up to 650 K, on both oxygen-lean (3:6:1) and oxygen-rich condition (3:4:3).

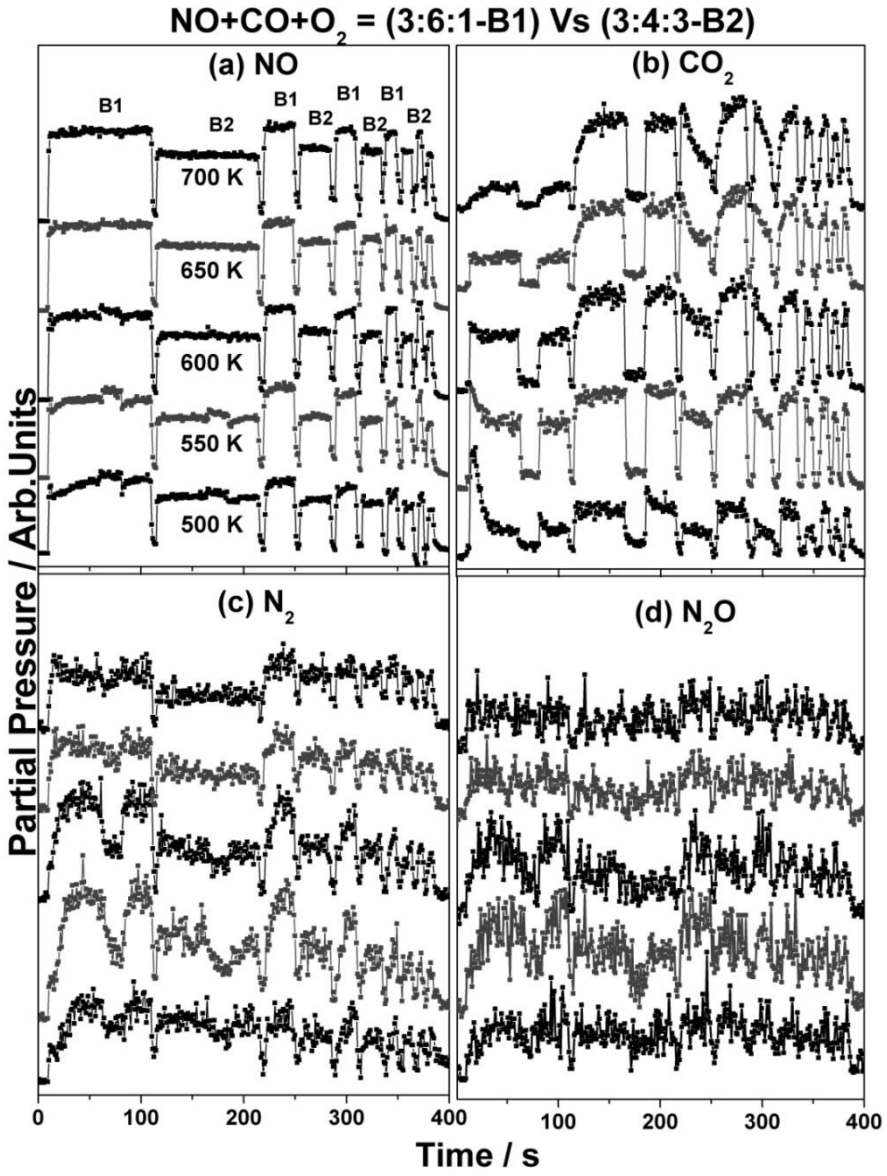

Figure 4.11 Temperature dependence of beam switching experiments with NO:CO:O_2 (3:6:1) (O_2-lean-B1) and (3:4:3) (O_2-rich-B2) products are shown here. CO_2 was observed at all temperature range and in both beams B1 and B2. B2 CO_2 production was always more when compared to B1 as it is oxygen rich. N_2 was observed in B1 for 550, 600 and 650 K and in B2 550 and 600 K. N_2O was observed for 550, 600 and 650 K and in B2 550 and 600 K. NO reductions can be achieved in oxygen rich conditions due to fast beam switching kinetics, but in the case of oxygen rich beams N_2 production observed only in transient conditions.

First set of SS experiments at t <200 s, clearly indicates that the NO reduction efficiency of the Pd surface deteriorates under net oxidizing conditions, apparently because of the inhibiting effect that O_2 exerts on the NO adsorption; In contrast, CO

oxidation enhances with O_2-rich beams in TS and SS. The latter part is in contrast to that of Rh(111) surfaces [7], which displays a decrease in CO_2 production with O_2-rich beam hinting the O_2-poisoning effect towards CO adsorption. High CO_2 production with O_2-rich beams on Pd(111) surfaces, highlighting the high tolerance of Pd-surfaces towards poisoning by oxygen atoms. It is also clear from the data in Figure 4.11 that the changes induced by changing the beam composition are completely reversible: the original SS reactivity of the catalyst is easily regained by restoring the same beam composition.

4.4.2. Beam composition dependence

Beam composition dependence of NO:CO:O_2 reactions has been studied using beam switching experiments and the results are shown in Figure 4.12. The beam one (B1) is (1:4:5) NO:CO:O_2 O_2-rich composition, and the beam two (B2) is varied from (1:9:z) where z = 0, 4 and 8. The above compositions are chosen to understand the effect of beam without oxygen (z = 0), moderate oxygen content (z = 4) and oxygen rich content (z = 8). CO_2 SS rate was observed for all the beam compositions. When z = 0, the CO_2 production was observed exclusively from chemisorbed CO on the surface and adsorbed oxygen from NO dissociation, which results in lesser CO_2 intensity in B2. When z = 4, the intensity of CO_2 in both B1 and B2 similar, since the oxygen content is same in both B1 and B2.

When z = 8, the intensity of B2 become more as it is oxygen rich. In the case of N_2, the SS rate was not observed in B1 for all the three reactions, as it is oxygen-rich (1:4:5) composition, whereas a definite SS rate was observed for all B2 compositions; but it decreases when oxygen content increases. Fast beam switching kinetics between oxygen-rich and oxygen-lean provides the information about transient CO_2 and N_2 production. Two important conclusions can be drawn from the Figures 4.11 and 4.12. (a) Inspite of difference in SS rate of CO_2 production for O_2-lean and O_2-rich compositions, under fast beam oscillation conditions they tend to show comparable rate of CO_2 formation.

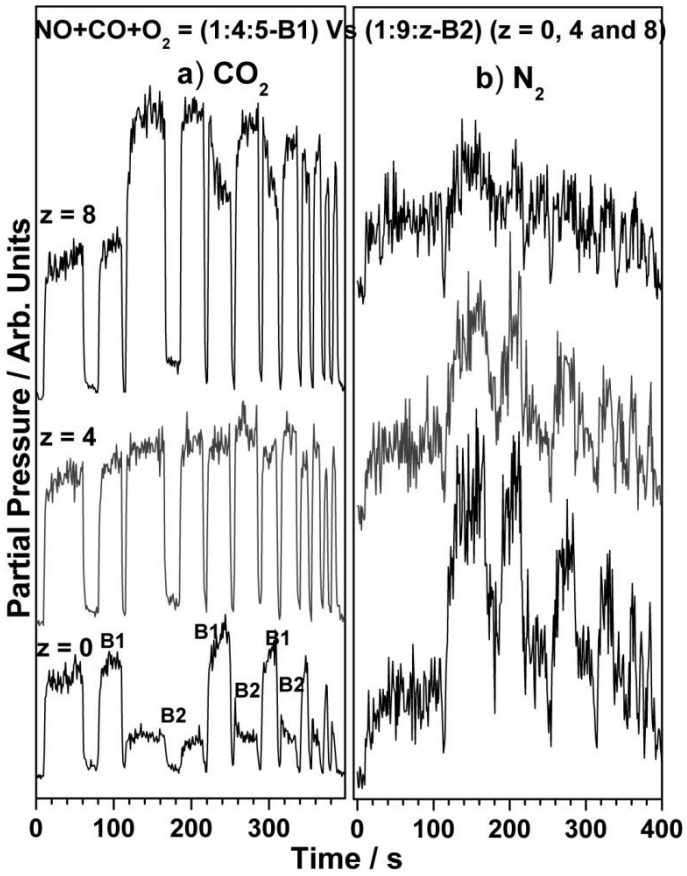

Figure 4.12 Beam composition dependence of beam switching experiments with NO:CO:O_2 (1:4:5) (B1) and (1:9:z) (B2) where z = 0, 4 and 8 compositions are shown here. (a) When z = 0 transient and SS rate of CO_2 was more in the case of O_2-rich whereas in the B2 the intensity reduced to one third. When z = 4 both B1 and B2 CO_2 intensities are similar as the oxygen content is close to same. In the case of z = 8, the intensity are reversed, whereas the fast beam switching between the two compositions end up in the equal intensities. (b) SS was not observed in all the (1:4:5) B1 whereas clear SS rate observed for all the z values in B2, which demonstrate that oxygen has been consumed by CO and NO uptake is possible. NO reduction can be achieved in oxygen rich conditions also due to fast beam switching kinetics, but N_2 production observed only in transient condition for oxygen rich beams.

(b) The above point suggests the fast removal of O-atoms from the surface, irrespective of beam composition and allowing NO decomposition to occur, in the TS. The above experiments demonstrate that oxygen free surfaces needs to maintain to achieve the effective NO reduction.

4.5. Discussion

The kinetic data reported here focus on the effect of variation in each reactants in the reactants mixture of NO:CO:O_2 on Pd(111) surfaces. In general, it is observed that the addition of oxygen inhibits the NO dissociation, as chemisorbed oxygen occupies the active site, restricting NO reduction in a net oxidizing environment. Especially the repulsive interaction between oxygen and NO prevents their co-existence on Pd surfaces. It is also known that NO dissociation requires two adjacent vacant sites; which makes NO dissociation increasingly difficult under net-oxidizing conditions. Net oxidizing SS conditions invariably leads Pd surface to be enriched with O atoms and this decrease the NO adsorption due to above repulsive interaction. In particular, the deposition of oxygen on palladium surfaces >600 K can alter the adsorption properties and the Pd is found to be mildly oxidized [11]. The behavior of Pd-based systems supported on alumina and ceria-zirconia was investigated with stoichiometric C_3H_6:NO:CO:O_2 composition by Garcia et al [33] underscore the importance of oxidation state of Pd on supported catalysts. It has been found that PdO like species get reduced to metallic Pd on Al_2O_3, but not on ceria-zirconia supported catalyst. Changes in adsorption dynamics were observed due to a competition among NO, CO, and O_2 molecules for adsorption sites and it varies with reactants compositions, surface composition of adsorbed species and the reaction temperature [40]. Both CO and NO exhibit a large extent of adsorption with high sticking coefficient below 550 K; however, oxygen adsorption is predominant above 550 K and extended even up to 900 K on Pd(111) surfaces with significant sticking coefficient [11-14]. Oxygen may inhibit the adsorption of the other reactants, but also removes adsorbed CO as CO_2 and hence helping (but not poisoning), the overall NO reduction reaction. In contrast to the above, Rh(111) surface is poisoned with O_2-rich compositions and it hinders CO oxidation [4]. In the case of CO-rich conditions, it is involved in the removal of excess oxygen chemisorbed on the surfaces, especially below 500 K. Other effects like the influence of NO on CO:O_2 reaction need to be considered to understand the overall reactivity of the NO:CO:O_2 mixture. Results obtained in the present kinetic studies of the ternary NO:CO:O_2 mixture on Pd(111) system is analyzed in light of the above points.

4.5.1. Influence of O_2 on NO + CO reactions

From the results derived from Figures 4.3, 4.4, 4.7, 4.9, 4.11 and 4.12 with increase in the oxygen content in the beam always results in lesser N_2 production in the SS. However, CO_2 production increases as oxygen content increases. Oxygen does not seem to poison the surface irrespective of CO flux, which in turn produces CO_2. Indeed this conclusion is in good agreement with our earlier results (Chapter 3) and also in [11] on CO:O_2 reaction as well as with that of Schalow et al on Pd/Fe_2O_3 [41]. Though initial sticking coefficient (S_{CO}^{o}) of CO on clean Pd(111) is negligible above 550 K, it increases with increasing subsurface O-coverage on Pd(111) from NO:CO:O_2 mixture ≥550 K. Indeed this is the reason why Pd(111) surface is active for oxidation at 750 K with O_2-rich compositions (see Figure 4.7) On the other hand, O-atoms occupy the adsorption sites and NO adsorption capacity decreases with increasing temperature as well as with increasing oxygen coverage on the surface. Hence a retardation for NO decomposition on Pd(111) surface was observed due to oxygen at high temperatures (>550 K). NO decomposition also increasingly contributes to the rate determining step as observed for NO:CO/Pd(111) systems. The conclusion with respect to the O_2 on NO:CO is, the presence of oxygen significantly decreases the adsorption as well as dissociation of NO over CO adsorption on Pd(111) resulting a decrease in the N-containing products (N_2 and N_2O). The suggestion is to maintain relatively oxygen free surface to achieve the NO reduction on Pd(111) surfaces under SS conditions.

4.5.2. Effect of NO on CO + O_2 reactions

The role of NO on the overall NO:CO:O_2 reaction could be better understood from the experiments carried out below 600 K. In 1993, Graham et al [34, 35] compared the rate of CO_2 production from three different reactions, NO + CO + O_2, NO + CO, and CO + O_2 on Pd(100) at a partial pressure of 1 torr and between 430 and 580 K. The rate in both CO:O_2 and CO:NO follows Arrhenius behavior. The rate of NO:CO was two orders of magnitude lower than CO:O_2 and hence NO:CO:O_2 rate is not different from the latter. Interestingly, the rate of CO_2 production was found to be higher with NO:CO:O_2 than CO:O_2 below 480 K. The situation regarding the NO + CO + O_2

reaction provides a greater contrast between Pd and Rh. In the case of Rh(111), the addition of NO to CO + O_2 has been found to greatly reduce the rate of CO_2 formation [34, 35]. Lambert et al [42] observed 100% NO_x conversion in the presence of CO and H_2 as a reductant on Pd nano particles supported on TiO_2/Al_2O_3. The NCO formation on Pd is critical on titania, whereas alumina promotes the hydrolysis of NCO to NH_3, which in turn reduces NO_x. Figure 4.6 and 4.9 provides some information about the role of NO in NO:CO:O_2 reactions. It has to be remembered here that NO dissociation starts around 400 K, but still not complete at 475 K. Further, under the reaction conditions the equilibrium coverage of CO and oxygen should be high and hence finding two adjacent vacant sites for NO-dissociation is difficult. Rate of CO-desorption increases above 475 K, and hence sizeable NO dissociation occurs at 500 K and starts contributing to the overall reaction. Alternatively, significant amount of NO that adsorb and dissociates at the time of initial shutter opening and makes the oxygen and nitrogen atoms available for CO oxidation and N+N recombination. It is well known that N+N recombination is a diffusion controlled process, which is a slow process as well as rate-control step. Figures 4.1, 4.2, 4.6, 4.11 and 4.12 demonstrates that, when shutter operation is performed CO_2 partial pressure reaches the new SS instantaneously, whereas N-containing product takes at least few sec (up to 5 s) delay.

The presence of oxygen adsorbate retards the NO dissociation and hence a sizeable molecular NO available on the surface makes the N_2O formation possible. Increasing oxygen content increases CO_2 production rate at all the temperatures investigated. However, when we compare these rates of CO_2 formation for NO:CO:O_2 reaction with CO:O_2 reaction, lower rates were observed $\leq$475 K. Relatively large oxygen adsorption above 600 K, leading an increasingly oxygen covered Pd(111) decreases the NO adsorption changes the nature of the overall reaction increasingly towards CO:O_2 reaction at high temperatures.

4.5.3. Fast beam switching experiments and comparison of the present results with NO + CO + O_2/Rh(111) surfaces

The reducing activity of the catalysts normally poisoned by oxygen under oxygen-rich conditions, which can be recovered by the exposure of fuel-rich mixtures. It appears

that surface-reducing agents (CO in the present case, VOC in most practical engines) can effectively remove the surface oxygen as CO_2 (Figure 4.8). Hence, the duration of the fuel-rich pulses used to reduce the catalyst becomes critical. Fast beam switching experiments has been performed between O_2-lean and O_2-rich conditions on Pd(111) systems to understand the effectiveness of NO reduction under net oxidizing environments. The above concept is to simulate the automobile exhaust which is altered between O_2-lean and O_2-rich conditions. Few points are worth to highlight in this section: (a) The Surprising thing to be noticed here is an increase in the SS CO_2 production, even though the F_{CO} decreased to 40% in oxygen-rich conditions (compared to 60% CO in oxygen-lean conditions) in Figure 4.11. Expectedly, a large increase in both N_2 and N_2O production was observed with fuel-rich conditions in the SS. Nonetheless, more interesting is the observation of large N_2 production in the TS with oxygen-rich compositions. As mentioned in the results section, relatively clean or less-oxygen-covered Pd-surfaces help in NO dissociation in the TS. However, subsequent oxygen-rich beam builds up significant oxygen coverage on Pd and hence SS NO-dissociation decreases. Nonetheless, the above significant oxygen coverage helps for fast CO-oxidation in the TS with O_2-lean beam and simultaneously significant NO-reduction could be achieved in the TS. By alternating the composition between O_2-rich and O_2-lean compositions, oxygen build-up on Pd surface could be minimized, which also helps towards NO dissociation. Although the above method might not reach 100% efficiency towards NO-reduction, by fast and appropriate cycling between the oxygen-rich and oxygen-poor exhaust compositions, a better NO-reduction management is possible.

Making use of a significantly large NO-dissociation on relatively oxygen-free Pd-surface is the key finding from this experiment. The aim of the present work is to manage NO_x reduction in a better way, especially under the conditions in real world automobile exhausts. In order to achieve complete combustion of fuel, the modern IC engine operates at high air, which is the recent development in the IC engine technology. Further, oxygen uptake increases gradually, as evidenced by gradual increase in CO_2. This is the observation in the TS could help to maximize NO

reduction under net oxidizing conditions by oscillating reactants between O_2-rich and O_2-lean compositions.

The new information and the reaction mechanism have been derived from NO:CO:O_2 on Pd(111) systems. The surface was found to be primarily covered with CO as well as NO below 400 K and in CO rich beams, which affects the net NO reduction as well as overall reaction. Oxygen was the dominant surface species above 600 K and in oxygen-rich conditions, which directly affects NO dissociation. There are few observation and comparison could be made between the present results on Pd(111) with that of on Rh(111). In the case of Rh(111), no N_2O was produced in the reactions reported [4, 7], whereas the presence of N_2O in all beam composition has been observed in Pd(111) surfaces, but the intensity of N_2O is roughly 8 times lesser than N_2 production. Based on SS kinetic measurements observed by Gopinath et al for Rh(111) with isotopic label switching, that N_2 production under the conditions of the catalytic reaction is likely to involve the formation of a N–NO intermediate [43-45]. This intermediate is presumed to be common for the production of both N_2 and N_2O, and the selectivity between the two pathways must be dominated by the relative probabilities for N–NO decomposition (to N_2 + adsorbed O) versus molecular desorption. The main supporting evidence for the claim comes from the slow response of the N_2 partial pressure trace while blocking and unblocking of the beam seen below 600 K (Figures 4.1, 4.2, 4.3 and 4.6), which is applicable for Rh(111) also. One of the most important observations from the Gopinath et al [7] that there is a build-up of a critical coverage of nitrogen atoms on the Rh surface before N_2 desorption can be seen. In the case of Pd(111), N_2 formation limits the rate of the overall reaction below 525 K [29]. However, NO dissociation step contributes in a major way toward the rate determining step above 525 K [29]. The fast responses of the NO, CO, and CO_2 partial pressure traces to changes in the beam flux under SS conditions demonstrate that both NO dissociation and CO_2 formation are faster than N_2 production under most relevant reaction conditions for both Rh(111) and Pd(111).

4.6. Conclusions

An investigation of NO:CO:O_2 reactions was carried out on Pd(111) using mixed molecular beam in a wide range of temperatures between 400 and 800 K and beam compositions. The beam compositions varied from stoichiometric to CO, NO rich beams with respect to NO, CO and O_2. Maximum reactivity was found between 500 and 600 K for all beam composition ranges. The kinetic data were presented to understand the role of oxygen in this chapter and the main effect of the oxygen addition to the NO:CO mixture is to inhibit the NO-dissociation rates in the SS and clearly enhance the rate of CO_2 production under most circumstances. Surface oxygen decreases the net NO adsorption and dissociation above 600 K and maintains the CO-oxidation rates. The overall reaction was largely controlled by the N+N recombination below 525 K and NO-dissociation also increasingly contribute to the rate determining step with increasing temperature and oxygen content in the beam. The rate of formation of CO_2, and N_2 does not vary much with CO flux was observed. Pd(111) surface shows reversible nature with respect to oxygen-rich and oxygen-lean conditions. Large NO-dissociation occurs on relatively oxygen-free Pd-surfaces (oxygen lean) or only in TS on oxygen rich conditions, which is observed through fast beam switching for better de-NO_x management.

4.7. References

1. Shelef, M. *Chem. Rev.* **1995**, *95*, 209.
2. Belton, D. N.; Taylor, K. C. *Curr. Opin. Solid State Mater. Sci.* **1999**, *4*, 97.
3. Taylor, K. C. *Catal. Rev. Sci. Eng.* **1993**, *3*, 457.
4. Shelef, M.; Graham, G. W. *Catal. Rev. Sci. Eng.* **1994**, *36*, 433.
5. Twigg, M.V. *Phil. Trans. R. Soc. A*, **2005,** *363*, 1013
6. Jobson, E. *Top. Catal.* **2004**, *28*, 191.
7. Gopinath, C. S.; Zaera, F. *J. Catal.* **2001**, *200*, 270.
8. Suhonen, S.; Valden, M.; Hietikko, M.; Laitinen, R.; Savimaki, A.; Harkonen, M. *Appl. Catal, A* **2001**, *218*, 151.
9. Weaver, J. F.; Chen, J-J.; Gerrard, A. L. *Surf. Sci.* **2005**, *592*, 83.
10. Shumbera, R. B.; Kan, H. H.; Weaver, J. F. *Surf. Sci.* **2007**, *601*, 4809.

11. Nagarajan, S.; Thirunavukkarasu, K.; Gopinath C. S. *J. Phys. Chem. C.* **2009**, *113*, 7385.
12. Thirunavukkarasu, K.; Nagarajan, S.; Gopinath C. S. *Appl. Surf. Sci* **2009**, *256*, 443.
13. Gopinath, C. S.; Thirunavukkarasu, K.; Nagarajan, S. *Chem. Asia. J.* **2009**, *4*, 74.
14. Nagarajan, S. Gopinath, C. S. *J. Indian. Inst. Sci.* **2010**, *90*, 245.
15. Zheng, G.; Altman, E. I. *Surf. Sci.* **2000**, *462*, 151.
16. Zheng, G.; Altman, E.I. *Surf. Sci.* **2002**, *504*, 253.
17. Zheng, G.; Altman, E. I. *J. Phys. Chem. B* **2002**, *106*, 1048.
18. Teschner, D.; Pestryakov, A.; Kleimenov, E.; Haevecker, M.; Bluhm, H.; Sauer, H.; Knop-Gericke, A.; Schloegl, R. *J. Catal.* **2005**, *230*, 186.
19. Ketteler, G., Ogletree, D.F., Bluhm, H., Liu, H., Hebenstreit, E.L.D., Salmeron, M., *J. Am. Chem. Soc.*, **2005**, *127*, 18269.
20. Ramsier, R. D.; Gao, Q.; Waltenburg, H. N.; Yates, J. T., Jr. *J.Chem. Phys.* **1994**, *100*, 6837.
21. Bertolo, M.; Jacobi, K.; Nettesheim, S.; Wolf, M.; Hasselbrink, E.*Vacuum* **1990**, *41*, 76.
22. (a) Bertolo, M.; Jacobi, K. *Surf. Sci.* **1990**, *226*, 207. (b) Rainer, D. R.; Vesecky, S. M.; Koranne, M.; Oh, W. S.; Goodman, D. W. *J. Catal.* **1997**, *167*, 234 and references therein.
23. Ozensoy, E.; Goodman, D. W. *Phys. Chem. Chem. Phys.* **2004**, *6*, 3765, and references therein.
24. Gopinath, C. S.; Zaera, F. *J. Catal.* **2001**, *186*, 387.
25. Zaera, F.; Gopinath, C. S. *J. Mol. Catal. A* **2001**, *167*, 23.
26. Zaera, F.; Gopinath, C. S. *J. Chem. Phys.* **1999**, *111*, 8088.
27. Thirunavukkarasu, K.; Thirumoorthy, K.; Libuda, J.; Gopinath, C. S. *J. Phys. Chem. B* **2005,** *109*, 13272.
28. Vesecky, S. M.; Chen, P.; Xu, X.; Goodman, D. W. *J. Vac. Sci. Technol. A* **1995**, *1*, 1539.
29. Szanyi, J.; Goodman, D. W. *J. Phys. Chem.* **1994**, *98*, 2972.

30. Szanyi, J.; Kuhn, W. K.; Goodman, D. W. *J. Phys. Chem*. **1994**, *98*, 2978.
31. Ma, Y. S.; Rzeznicka, I. I.; Matsushima, T. *Appl. Surf. Sci.,* **2005**, *244*, 558.
32. Ma, Y. S.; Rzeznicka, I. I.; Matsushima, T *Cat. Lett.,* **2005**, *101*, 109.
33. García, M. F.; Juez, A. I.; Arias, A. M.; Hungría, A. B.; Anderson, J. A.; Conesa, J. C.; Soria, J. *J. Catal.* **2004,** *221*, 594.
34. Graham, G. W.; Logan, A. D.; Shelef, M. *J. Phys. Chem (Letters),* **1993**, *97* 5445.
35. Graham, G. W.; Logan, A. D.; Shelef, M. *J. Phys. Chem.* **1994**, 98, 1746.
36. Fisher, G. B.; Oh, S. H.; Dimaggio, C. L.; Schmieg, S. J.; Goodman, D. W.; Peden, C. H. F.*In Proceedings 9th International Congresson Catalysis*; Phillips, M. J., Ternan, M., Eds.; The Chemical Institute of Canada: Ottawa, **1988**; p 1355.
37. Thirunavukkarasu, K.; Gopinath, C. S. *Catal. Lett.* **2007**, *119*, 50.
38. Nagarajan, S.; Thirunavukkarasu, K.; Gopinath, C. S.; Counsell, J.;Gilbert, L.; Bowker, M. *J. Phys. Chem. C.* 2009, *113*, 9814.
39. Thirunavukkarasu, K.; Thirumoorthy, K.; Libuda, J.; Gopinath, C. S. *J. Phys. Chem. B.* **2005**, *109*, 13283.
40. Gopinath, C. S.; Zaera, F. *J. Phys. Chem. B.* **2000**, *104*, 3194.
41. Schalow, T. Brandt, B.; Starr, D. E.; Laurin, M.; Shaikhutdinov, S. K.; Schauermann, S.; Libuda, J.; Freund, H-J. *Angew. Chem. Int. Ed.* **2006**, *45*, 3693.
42. Macleod, N.; Cropley, R.; Keel, J. M.; Lambert, R. M. *J. Catal.* **2004,** *221*, 20.
43. Zaera, F.; Gopinath, C. S. *Chem. Phys. Lett.* **2000**, *332*, 209.
44. Zaera, F.; Wehner, S.; Gopinath, C. S. *J. Phys. Chem. B.* **2001**, *105*, 7771.
45. Zaera, F.; Gopinath, C. S. *J. Chem. Phys.* **2002**, *116*, 1128.

Chapter 5

Ethanol + NO + O_2 Reactions on Pd(111) Surfaces

5.1. Introduction

Air pollution is one of the major problems in the world, and it is directly affecting the living things as well as environment. The destructive role of automobile exhausts in the air pollution is significant due to the tremendous increase in the number of vehicles all over the world. Nitric oxides (NO_x) is a main atmospheric pollutant, and responsible for the acid rain and ozone formation at ground level [1]. By adding ethanol to the gasoline air pollution might be controlled better, since ethanol is highly combustible. Addition of ethanol reduces the emission of olefins, aromatics, complex hydrocarbons and SO_x [2].

Countries like, Brazil has already implemented the ethanol blended gasoline to control the air pollution. However, there are few problems associated with ethanol and it leads to the emission of small amounts of aldehydes and/or even some amount of unburned ethanol into the environment [1]. It would be ideal if NO reduction can be managed directly with unburned ethanol or aldehydes. Miyadera et al [2] studied the NO_x reduction using ethanol on an alumina-supported silver catalyst. A variety of nitrogen containing by-products, such as N_2O, NH_3, CH_3CN, HCN, were observed. Dong et al [3] reported that a high NO_x conversion up to 90% was achieved with ethanol using a three component catalyst system, namely, Ag/Al_2O_3 + Pt/TiO_2 + Cu/TiO_2, between 350 and 450°C. They reported that NO_x conversion efficiency increases with increase in the ethanol dosage, but it cause CO emission also. Dzwigaj et al [4] studied the effect of zeolites with isolated Co^{II} and Fe^{III} species for selective catalytic reduction of NO with ethanol.

The catalytic converter employed in the automobiles increasingly uses Pd as an active ingredient, or sometimes as the only active ingredient, to tackle NO reduction, CO and VOC oxidation. De Mello et al [5] studied NO reduction with ethanol using MoO_3/Al_2O_3 and CeO_2-ZrO_2 supported Pd catalysts. TPD analysis of adsorbed NO and ethanol showed that the Pd/CeO_2-ZrO_2 catalyst has a higher ability for the dissociation of NO to N_2 and for the oxidation of ethanol to CO_2. De Mello et al [5] also compared the catalytic behavior of Pd/Al_2O_3 with Pd-Mo/Al_2O_3. It has been reported that Pd/Al_2O_3 catalyst shows more activity for NO conversion. Velu et al [6] studied the oxidative steam reforming of ethanol with CuNiZnAl mixed oxide, and observed 100% ethanol conversion at 300^0C to acetaldehyde and H_2. It is important to mention that ethanol as a fuel in modern ICE increases the oxygen content in the exhaust, and NO reduction under net oxidizing conditions becomes increasingly difficult. Very few reports are available about NO-reduction under net oxidizing conditions. Gopinath and Zaera [7] carried out CO + NO and CO + NO + O_2 reactions on Rh(111) surfaces, to show the effective NO reduction management in a net oxidizing environment by beam oscillation between fuel-rich and fuel-lean compositions. Bowker et al [8, 9] studied methanol oxidation on iron molybdate, and ethanol oxidation and acetic acid decomposition on Pd(110) surfaces. It was demonstrated that several pathways exist for ethanol decomposition and oxidation, including decarbonylation to produce methane and CO and via acetate as an intermediate species to combustion [8, 10]. These pathways were confirmed by use of high resolution XPS [10].

Literature reports show that there is very limited molecular level understanding of NO reduction using ethanol, especially under net oxidizing conditions. The purpose of this chapter is to explore this reaction in detail in order to understand more about NO reduction with ethanol on Pd-surfaces, and the possibility of managing NO-reduction under oxidizing conditions. Molecular beam methods were utilized to explore the optimum conditions for maximum NO reduction. Fast oscillation between fuel-lean and fuel rich compositions (NO + Ethanol + O_2) ensures the surface is not poisoned, particularly with oxygen; this is the key aspect towards the management of NO reduction under net-oxidizing conditions. Molecular beam methodology provides a valuable

alternative to provide fundamental information about the mechanistic and kinetic details of such reactions. The present chapter deals with the impact of ethanol on NO reduction on Pd(111) surfaces. We performed Ethanol + NO reactions with different beam compositions and in the presence of O_2 between 400 and 800 K.

5.2. Experimental section

$F_{Ethanol+NO}$ = 0.32 ML/s is the total flux of the Ethanol + ^{15}NO (and O_2) beam with a desired composition and is used in all the experiments reported here, unless otherwise specified. The NO used in all of the experiments is ^{15}N-labelled NO (^{15}NO), in order to differentiate the species that have the same mass (amu = 28 for $^{14}N_2$ ($^{15}N_2$) and CO, and amu = 44 for CO_2 and $^{14}N_2O$ ($^{15}N_2O$)). Indeed, we have also carried out the intensity of different fragments from ethanol, including amu 28, and confirmed that there is no significant contribution from amu 28. Since only ^{15}N-labelled NO was used in this work, ^{15}NO, and $^{15}N_2$ will be simply referred to as NO, N_2, respectively, hereafter. More Details about the MBI used for the experiments is available in (Chapter 2 section 2.2, 2.3 and 2.4) and also in [12, 13].

5.3. Results and discussion

Pd surfaces are active for many forms of catalysis and adsorb oxygen and NO efficiently. We have measured the initial sticking probability, S_o, (i.e. that at zero adsorbate coverage) of O_2 and NO as a function of temperature, and the results are shown in Figure 5.1. Here it can be seen that oxygen adsorbs with a S_o value of 0.32, which decreases with sample temperature. NO sticks more efficiently at room temperature, but the sticking diminishes fast with increasing temperature. However, a more significant difference exists between the two, which is very important in respect of the reactions we are interested in here, that is, NO_x conversion to nitrogen. Oxygen dissociates with a probability of 0.32, whereas NO does not dissociate and adsorbs only into the molecular state [14, 15]. Dissociation of NO only begins at more elevated surface temperatures as shown elsewhere [15], and at that point (~450 K) the sticking probability is diminishing fast with increasing temperature.

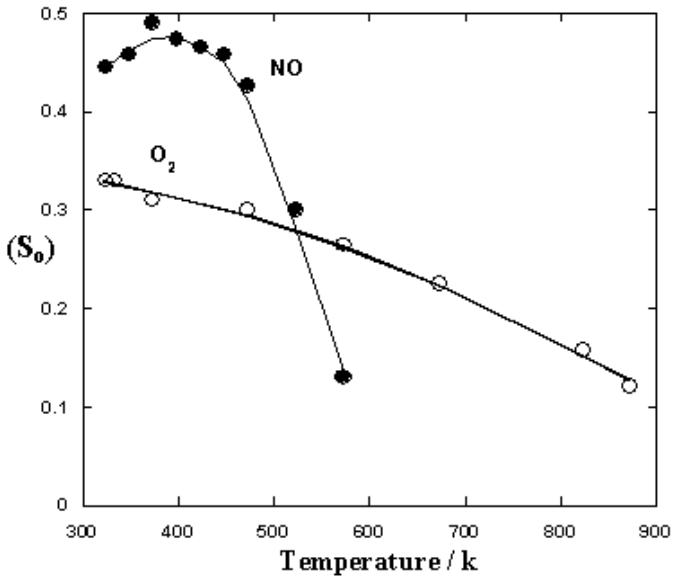

Figure 5.1 The initial sticking probabilities (S_0) of oxygen and NO on Pd(111) as a function of crystal temperature.

In contrast to the two molecules above, the adsorption of ethanol was difficult, and the sticking probability was <0.04, essentially un-measurable in molecular beam setup. This presumably indicates that there is a relatively weak interaction between the molecule and the clean Pd surface and that the dissociation is difficult at 300 K. On Pd(110) surface the adsorption was somewhat more efficient with an initial sticking probability of ~0.3 [9, 10]. In order to study the ethanol influence on NO reduction, the systematic study of the reaction of ethanol + NO, ethanol + O_2 and ethanol + NO + O_2 beams with different compositions between 400 and 800 K has been carried out on Pd(111) surfaces. As described above, no significant adsorption of ethanol was observed on clean and O-pre-covered Pd(111) surfaces below 400 K. Nonetheless, above 450 K, N_2 as well as CO, CO_2 and H_2O were observed as products during the course of the reaction; however no N_2O was observed in any of the above reactions.

Figure 5.2 Shows typical raw kinetic data observed under isothermal conditions (600 K) with a 1:1 composition of ethanol + NO on the Pd(111) surface. A certain sequence of experimental steps is followed while measuring the reaction and this is described as follows. First, at t = 10 s, the beam was turned on, however the Pd(111) surface is still blocked with the shutter at that point. An increase in reactant pressure can

be seen with a minor evolution of products due to reaction from the background on the Pd surface.

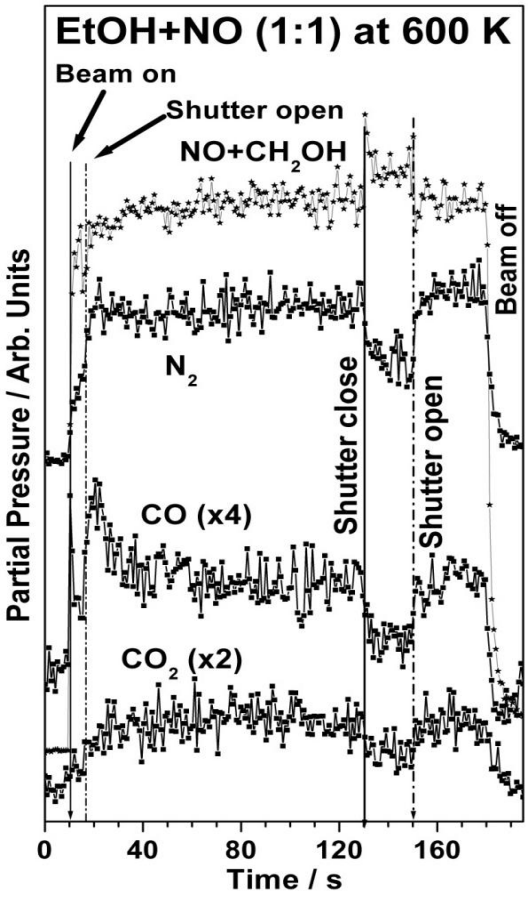

Figure 5.2 An effusive mixed molecular beam of ethanol + NO (1:1) is directed on to Pd(111) surface at 600 K. All the reactants and products masses were followed as a function of time. The beam was blocked (130 sec) and unblocked (150 sec) in the SS to measure the rate of the reaction.

At t = 13 s, the shutter was removed to allow the reactants to impinge on the Pd surface, and so products can be seen to evolve due to reaction. A sharp increase in the product formation marks the TS; before it reaches the SS around 45 s. SS rate was measured by deliberately blocking the beam for few seconds between 130 and 150 s. As might be expected there are opposite responses for the reactants and products when the beam is blocked. The reactants (represented by mass 31) increase in pressure when the beam is blocked (since they are no longer consumed in the surface reaction), whereas the products decrease due to the blocked reaction. The decrease in the partial pressure of products

gives an idea of the rate of reaction, after calibration of the various masses. After the beam was unblocked, the reaction returns to SS quickly and thereafter the reaction was stopped by turning off the molecular beam at t = 180 s. The solid and dotted lines indicate the closing and opening of the shutter, respectively, between time t = 130-150 s.

5.3.1. Ethanol + NO – temperature dependence

Figure 5.3 displays the time evolution of (a) CO, (b) CO_2 and (c) N_2 traces during exposure of the Pd(111) surfaces to ethanol + NO beams with 1:1 compositions at crystal temperatures between 550 and 650 K.

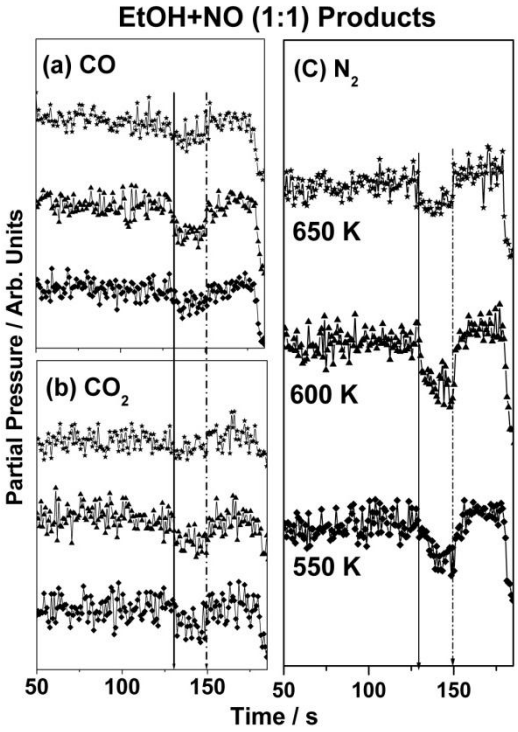

Figure 5.3 Time evolution of the partial pressure of products (a) CO, (b) CO_2 and (c) N_2, at temperatures between 550 and 650 K for ethanol + NO (1:1) beam compositions. CO_2 production was less observed at all temperatures due to the lesser O-content in the beam.

Although the reaction been has measured between 400 and 800 K, for the sake of clarity 550, 600 and 650 K data are shown in figure 5.3 for all the products.

The rate of CO_2 production is minimum at all temperatures due to low oxygen content available in the system. Dissociation species (C and H) or ethanol requires

oxygen atoms for complete oxidation to CO_2 and H_2O. Due to limited availability of O atoms from NO and ethanol, extent of oxidation is also restricted. Indeed this aspect favours NO reduction, since the surface is deprived of oxygen. The sustainable N_2 production was observed between 550 and 650 K at given ratio underscores the effectiveness of NO reduction in the presence of ethanol.

5.3.2. Ethanol + NO – beam composition dependence

A comparison of the rate of products formation (Figure 5.4 a-c) at 600 K with different ethanol + NO ratios suggests that NO dissociation increases with increasing ethanol content (an increase in the N_2 formation rate is seen).

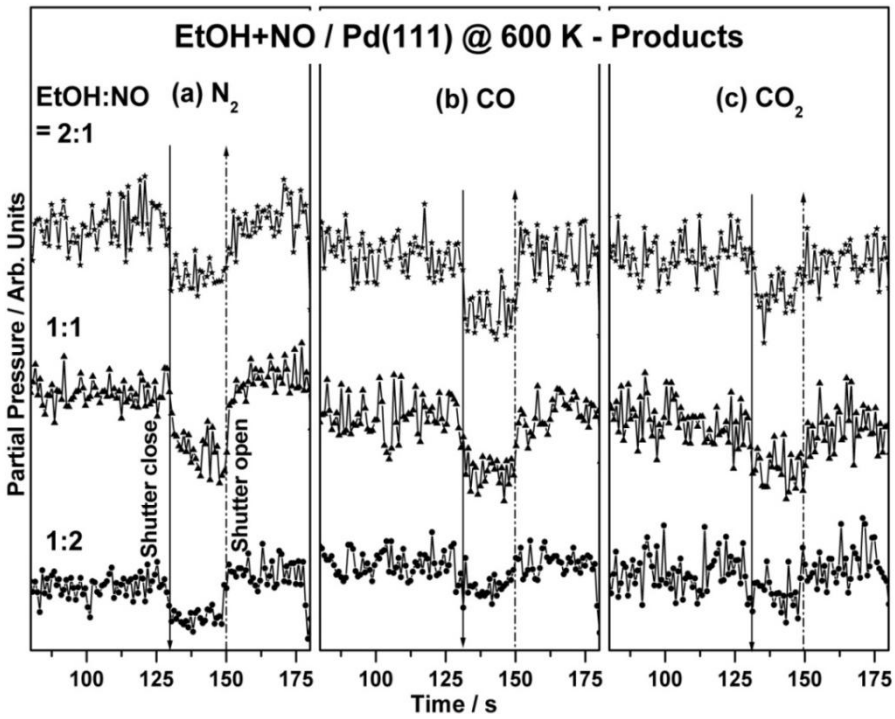

Figure 5.4 The rate of production of (a) N_2, (b) CO and (c) CO_2 from ethanol + NO reactions carried out at 600 K for three different beam compositions (1:2), (1:1) and (2:1) of ethanol + NO.

The rate of formation of all of the oxidized products, along with H_2O (not shown), also increases with increasing ethanol content. It is to be noted that the NO-content (and hence F_{NO}) decreases from 1:2 of ethanol + NO to 2:1.

In spite of that an increase in nitrogen production from 0.0065 ML/s for 1:2 to 0.01 ML/s for 2:1 underscores the effectiveness of NO-reduction. Indeed, the extent of NO conversion to N_2 or the rate of N_2 production per NO increases with increasing ethanol content in the beam. In a similar manner, rate of CO_2 (CO) production increases from 0.009 (0.002) ML/s for 0.015 (0.004) ML/s for 2:1. This observation supports the view that ethanol enhances NO dissociation and N_2 formation on Pd(111). An increase in CO and CO_2 production with increasing ethanol content suggests that both the reactants seems not to poison the surface, rather dissociate and react. Indeed it may be noted that there is a synergetic effect between the two, that is, NO dissociation (leaving oxygen on the surface) aids ethanol reaction, while ethanol reaction reduces the SS level of oxygen on the surface which would otherwise block further NO dissociation. The slow nitrogen decay/formation kinetics while blocking/unblocking the beam in the SS indicates that the nitrogen formation might be a rate-determining step for the overall reaction.

5.3.3. Ethanol + O_2 – temperature dependence

Figure 5.5 displays the time evolution of the TS and SS of (a) CH_2OH (b) CO and (c) CO_2 during the isothermal conditions at different crystal temperatures between 400 and 800 K on the Pd(111) surface to a 1:1 compositions of ethanol + O_2 beam. An important observation is the change in partial pressure of amu 31 (CH_2OH) species during beam oscillation from 400 K and above. This indicates that in the presence of a suitable co-adsorbate, adsorption of ethanol occurs and dissociates. Indeed no sizeable adsorption observed for pure ethanol on Pd(111) surface is in contrast to the above observation. It is observed that significant TS and SS rate of CO and CO_2 production was observed above 500 K and the same continued up to 800 K.

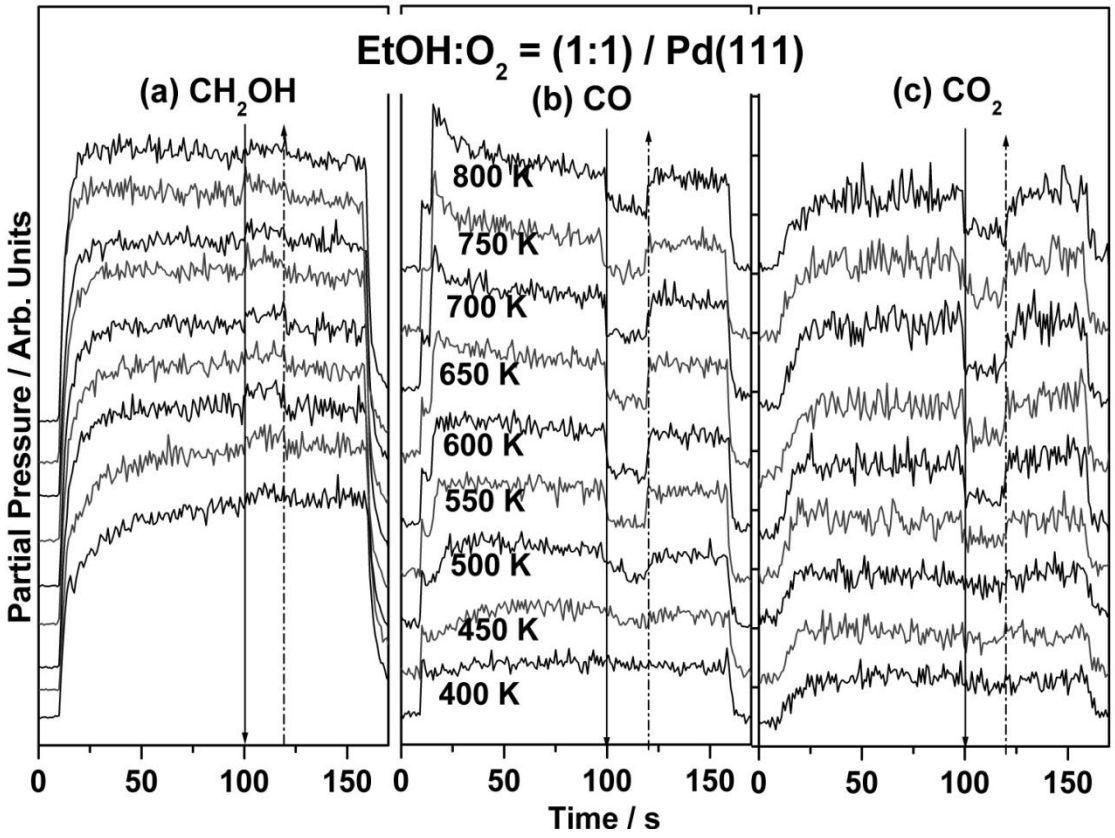

Figure 5.5 Time evolutions of partial pressures of (a) CH_2OH, (b) CO and (c) CO_2 uptake in kinetic experiments for the composition of ethanol + O_2 (1:1) ratio between 400 and 800 K on Pd(111) surfaces. Both CO and CO_2 production observed only above 500 K. At t = 100 s (120 s) shutter is closed (opened) to measure the SS rate of the reaction. Shutter close and shutter open is indicated by solid and dotted arrows, respectively in all the figures.

Maximum CO production was observed at 600 K, whereas maximum CO_2 production was observed at 700 K. A careful analysis of Figure 5.5 c reveals that ethanol adsorption and dissociation is the RDS. Fast changes in CO and CO_2 partial pressure for beam oscillation indicates that those steps are faster than ethanol adsorption and dissociation.

5.3.4. Ethanol + O_2 – beam composition dependence

Ethanol oxidation kinetics has been studied with an ethanol + O_2 beam for three different compositions to understand the beam composition dependence. Figure 5.6 shows the CO_2 and CO production at 600 K for different ethanol + O_2 compositions of 1:1, 1:2 and 1:4 on Pd(111) surface. An increase in the O_2 content, as expected, leads towards complete

oxidization to CO_2, and CO production decreases. It may be noted that ethanol content decreases from 50% in 1:1, 33% in 1:2 to 20% in 1:4. In spite of that, same rate of CO production (0.008 ML/s), but higher rate of CO_2 formation from 1:1 (0.003 ML/s) to 1:2 (0.01 ML/s) was observed.

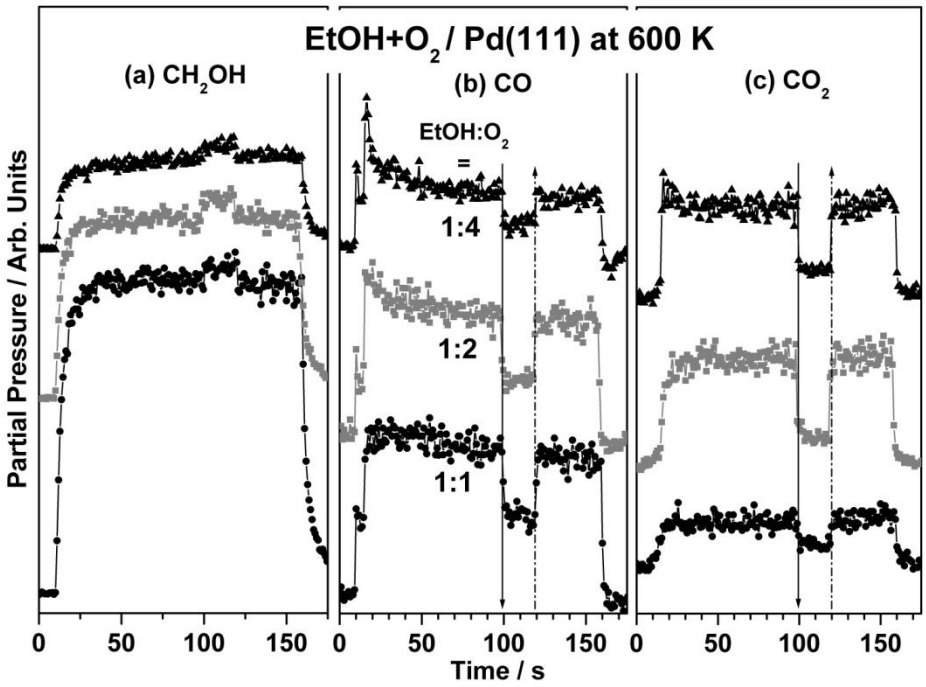

Figure 5.6 Ethanol oxidation experiments carried out with ethanol + O_2 mixed beam on Pd(111) surfaces at 600 K with three different ethanol + O_2 ratios, namely, 1:1, 1:2, and 1:4.The solid and dotted arrow indicates the shutter closing and opening, respectively. Note the change in transient evolution of CO with different beam compositions.

On further increase in oxygen content (1:4), rate of CO production decreases to 0.005 ML/s and CO_2 production remains at the same value as that of 1:2. Above changes highlights the change in trend towards complete oxidation. This also suggests that CO_2 production per ethanol molecule increases with increasing oxygen content. With 1:1 beam, more CO formation has been observed. It is also to be noted that there is some CO production at the time of beam opening and decreases even before the beam is directed onto Pd(111) surface, suggesting some amount of reaction from the background on Pd(111) surface as well as from chamber walls. However the same does not seems to occur with CO_2 or any other products. The atomic oxygen from O_2 dissociation on

Pd(111) reacts with the carbon components of ethanol to produce CO and CO_2. Oxygen dissociates very easily on Pd(111); we have measured the dissociation probability to be 0.3 at this temperature, as shown in Figure 5.1. The pattern observed in the mass spectrometer confirms that amu = 44 arise from CO_2, rather than other species such as CH_3CHO. Hence dehydrogenation and dehydration of ethanol can be ruled out as pathways under the present experimental conditions.

The rate of CO_2 production is small with a 1:1 ratio of ethanol + O_2, but there is a drastic increase in the rate of CO_2 production with 1:2 and 1:4 beams. Large CO production is observed with 1:1 ethanol + O_2, suggesting that the surface is dominated by ethanol and its fragments. However with higher O_2 content in the beam, the trend changes more towards complete oxidation and CO is lowered. It is to be noted that the extent of ethanol adsorption and sticking coefficient below 400 K is very low on Pd(111). Adsorption of ethanol on the oxygen-pre-covered Pd(111) surface is also negligible below 400 K, and underscores the poor catalytic activity below 400 K. Nonetheless, ethanol adsorption and hence the reaction rate increases above 400 K from ethanol + O_2 mixed beam and leads to oxidation. A similar observation was made with an ethanol + NO mixed beam >400 K, and no significant reaction was observed below 400 K. Generally, highest sticking coefficient for Ethanol was observed between 550-600 K, in the presence of oxygen, or NO or NO + O_2.

5.3.5. Ethanol + NO + O_2 - beam switching experiments

Generally, a fresh catalyst undergoes substantial changes at the start of a catalytic reaction, before it reaches its SS condition. Adsorbate-induced changes are the key reasons invoked to explain these initial changes [16-18], however, the dynamic changes in the composition of the adsorbate layers on the surface affect the TS kinetics in a very significant manner. Consequently, the transient behavior of a catalytic system can often provide valuable information about its performance under SS conditions. Indeed, the changes observed in Figure 5.2 hint that there is a significant change in the surface from the start of the reaction by the time it reached SS.

By utilizing the five-way valve setup described in chapter 2 section 2.2, the performance of the system under oscillatory conditions could be probed directly. A number of kinetic data were collected, in which the Pd(111) surface was alternatively exposed to O_2-lean and O_2-rich beams. Figure 5.7 shows a representative beam switching experiment, where an initial oxygen-lean beam (20 % O_2) of 1:1:0.5 ethanol + NO + O_2 was alternated with a second oxygen-rich beam (60 % O_2) of 1:1:3 composition at a reaction temperature 600 K. Figure 5.7 displays the kinetic data for the partial pressures of all (a) reactants and (b) products N_2, CO, CO_2 and H_2O as a function of time. It is to be noted that all of the mass traces were offset for background in Figures 5.7 and 5.8, mainly for better clarity. Note that there is some drop in signals intensity during subsequent dosings due to some drop in the backing pressure behind the doser every time the beam was switched on.

From Figure 5.7 it is evident that the reaction with the O_2-lean (1:1:0.5) beam displays a higher nitrogen production rate than that seen after switching to the O_2-rich (1:1:3) beam, and that the rate of oxidized products formation also increases with the O_2-rich beam. An overall decrease in nitrogen production with O_2-rich beam is due not only to the effect of extra oxygen, but the effective percentage of NO decreases compared to the O_2-lean beam, as the total flux of the beam remains the same in both cases. The NO uptake is higher with the oxygen-lean beam, as expected. Nonetheless, it is to be noted that the average product formation rate becomes comparable with fast switching kinetics, and it is clearly observed between t = 340 and 400 s. Although the SS kinetics in the first two beam switching parts show different rates of product formation, it is interesting to observe a similar rate irrespective of beam composition when the beam is alternated fast at later time. The high rate of formation of oxidized products under O_2-lean conditions highlights the efficient clean-off of adsorbed oxygen atoms (from the previous O_2-rich beam) and hence subsequent NO adsorption and decomposition. Fast switching kinetic experiments also suggests that the changes induced by changing the beam composition are completely reversible. No significant deterioration of the Pd surface towards NO-reduction efficiency due to O_2-rich beam exposure underscores the ability of Pd surfaces to withstand the oxidizing regime and demonstrate the feasibility to manage NO-

reduction. It is to be noted that the maximum intensity observed with short pulses between t = 340-400 s matches to that of longer SS experiment given on extreme left in Figure 5.7.

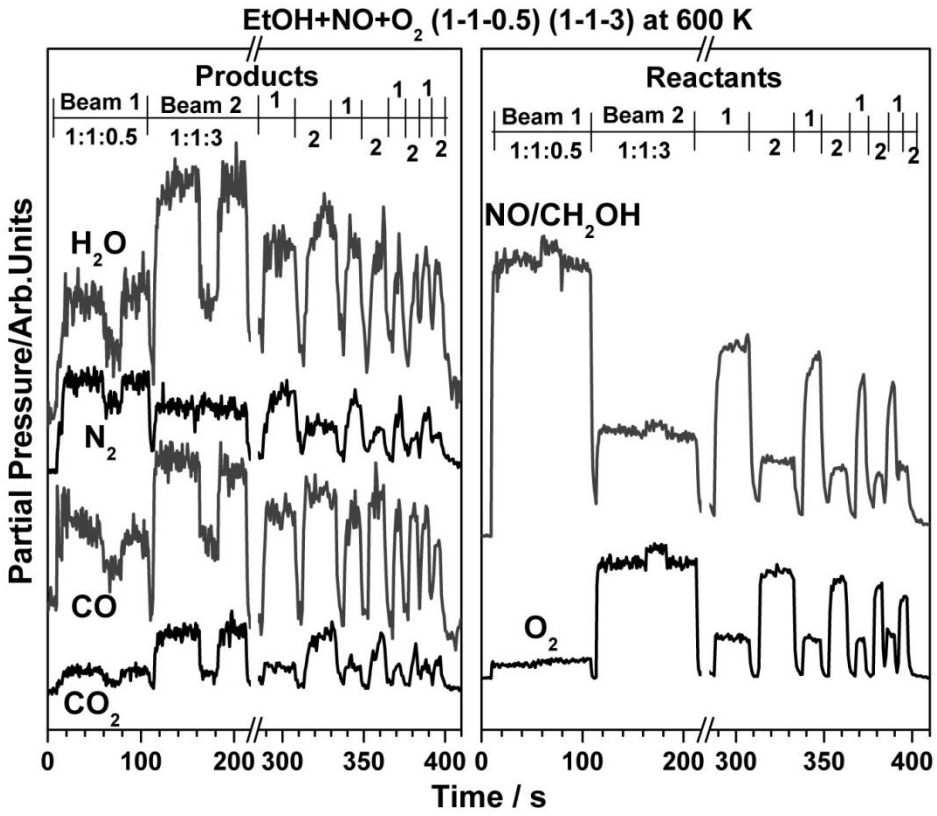

Figure 5.7 A typical raw kinetic data obtained in beam switching experiments. In this example, the traces for all (a) products observed, CO, CO_2, H_2O and N_2 and (b) reactants are shown as a function of time and the composition of the beam is switched between 1:1:0.5 (O_2-lean – beam **1**) and 1:1:3 (O_2-rich – beam **2**) ethanol + NO + O_2 compositions on Pd(111) surface at 600 K. Clearly, the rate for N_2 production is high with O_2-lean beam and oxidized products show high rates with O_2-rich beam. It is also to be noted that the changes in reactivity seen here are completely reversible. Most important to notice are the transient kinetics observed immediately after beam switching, especially with last three sets of beam switching between t = 335-400 s, where a comparable rate of product formation observed, irrespective of O_2-lean or rich beams. C and O along with solid and dotted arrow indicates the shutter closing and opening, respectively.

This particular observation confirms that the background contribution percentage remains the same with longer and shorter pulses. Even with H_2O (which exhibit high sticking on chamber walls), the intensity remains the same with short pulses demonstrating the

conclusions derived from our observations are correct. Indeed more water production from fuel-rich beam than in the SS (Fig 5.7 left) indicating the surface oxygen is preferentially removed by hydrogen to water formation.

The beam switching experiments has been carried out with ethanol + NO + O_2 (2:3:1) and (2:1:3) at 550 and 600 K on Pd(111) surfaces and the results are shown in Figure 5.8 Fast beam switching between both the above beams at t = 30 – 400 s shows the same nitrogen intensity, and supports the NO-reduction in net oxidizing environment. The above NO-reduction activity under net oxidizing conditions is attributed to the relatively strong chemisorption and dissociation of NO, in the presence of other reactants such as O_2 and ethanol, especially on clean-Pd surfaces in the TS [19]. However with the O_2-rich beams, eventually the surface will be O-covered and all oxidation reactions are favored. Nonetheless by fast beam switching, the surface is not allowed to reach the SS to build significant oxygen coverage, and hence the NO-reduction was managed by maintaining the catalyst in the transient state kinetic regime. In addition to the above, there is oxygen diffusion into the Pd sub-surfaces and that keeps the surface relatively oxygen free [13]. Due to the above two factors, NO-reduction under net oxidizing conditions is still manageable. More studies are in progress to understand the changes on the surface composition of adsorbates during the fast beam-switching kinetics. It is to be noted that a simple increase in NO-content does not seem to increase N_2 production, in spite of the presence of a smaller of amount of oxygen (while keeping ethanol content the same). Rather, the same amount of N_2 production was obtained with smaller amounts of NO and larger amounts of O_2, indicating that the NO-reduction in the TS may be at an optimum level. This also supports that NO-reduction management is possible in net-oxidizing conditions by suitable oscillation between fuel-rich and fuel-lean conditions.

The main reaction occurring in these experiments are as follows, reactions 5-10 having been described earlier for ethanol reaction on Pd [8, 10].

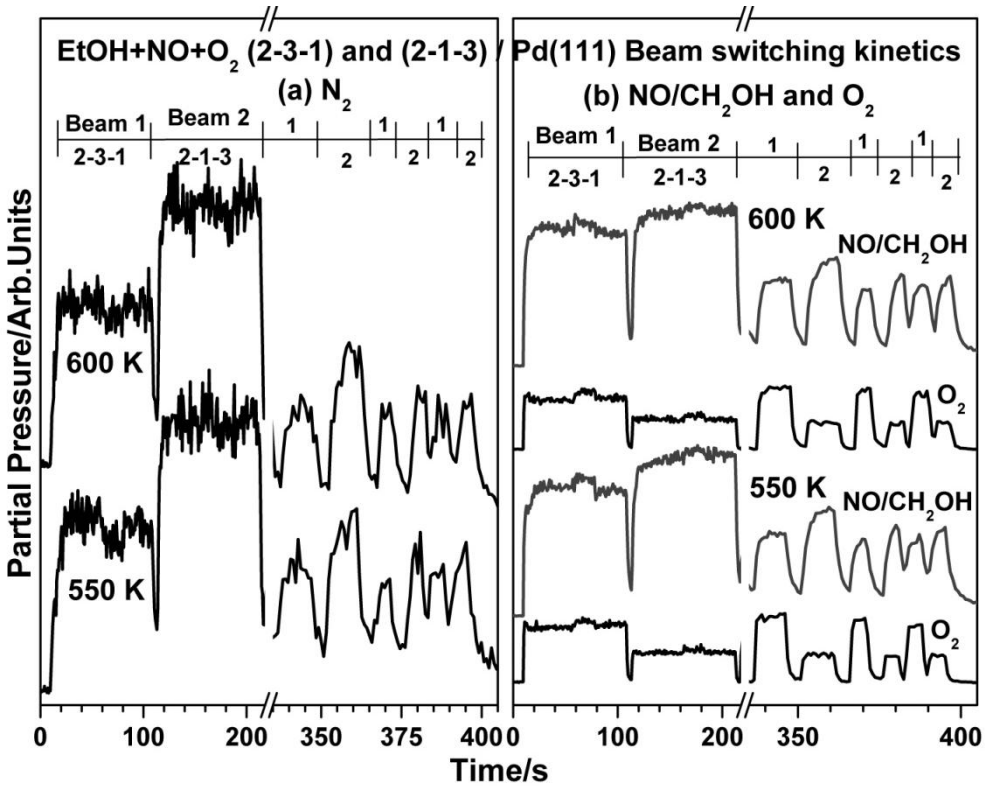

Figure 5.8 (a) N_2, and (b) reactants traces from beam switching experiments between ethanol + NO + O_2 (2:1:3 – beam **1**) and (2:3:1 – beam **2**) at 550 and 600 K on Pd(111) surfaces. The total flux remains the same in both oxygen rich and oxygen lean beams. Note a comparable production of nitrogen from oxygen-rich and oxygen-lean beams under fast-switching kinetics at t = 365-400 s.

$$O_2\,(g) \rightarrow 2O_a \quad (1)$$

$$NO\,(g) \rightarrow NO_a \quad (2)$$

$$NO_a \rightarrow N_a + O_a \quad (3)$$

$$2N_a \rightarrow N_2\,(g) \quad (4)$$

$$C_2H_5OH\,(g) \rightarrow CO_a + 6H_a + C_a \quad (5)$$

$$C_a + O_a \rightarrow CO_a \quad (6)$$

$$CO_a + O_a \rightarrow CO_2\,(g) \quad (7)$$

$$CO_a \rightarrow CO\,(g) \quad (8)$$

$$2H_a \rightarrow H_2\ (g) \quad (9)$$

$$2H_a + O_a \rightarrow H_2O\ (g) \quad (10)$$

Clearly the ability to dissociate NO depends on a number of factors, but mainly on the availability of free sites on the surface. In the presence of oxygen this availability is severely hampered due to the much higher efficiency of O_2 dissociation (498 kJ/mol) compared with NO dissociation energy (598.3 kJ/mol) (in turn related to the lower bond dissociation energy of O_2) [19-21]. If ethanol is added this reduces the surface coverage of oxygen by efficient reduction of the surface, thus enhancing the ability of NO to dissociate and react. However, if the ethanol partial pressure is too high then C poisoning (step 5) occurs due to limited supply of oxygen. Thus, with careful control of the reactant ratios, good NO conversion can be achieved. Figure 5.9 demonstrates a model for the interaction of Pd(111) surface with ethanol + NO + O_2 system under different conditions in TS as well as SS conditions.

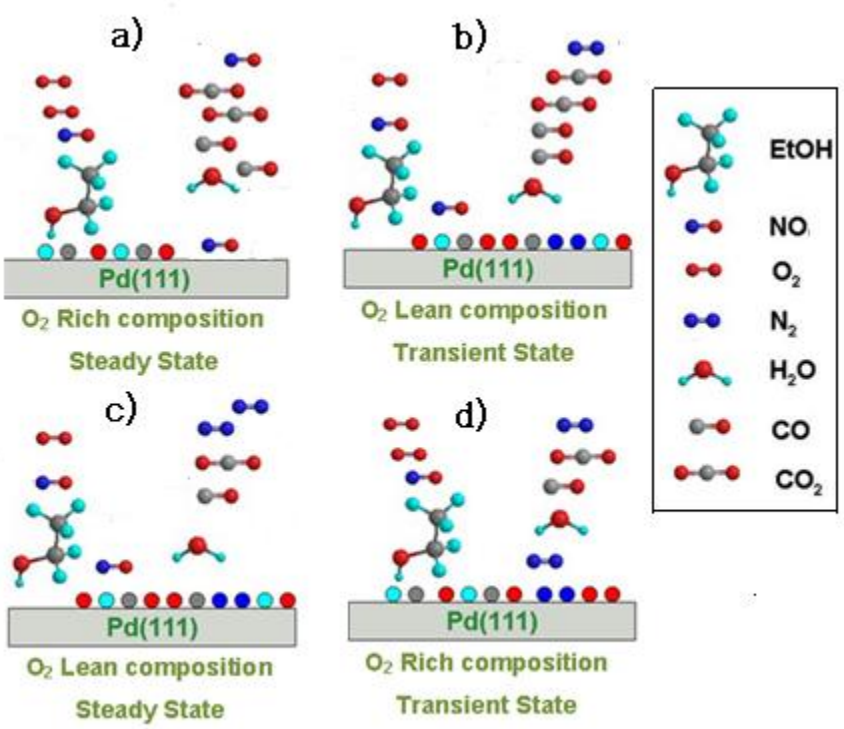

Figure 5.9 Model system of Pd(111) demonstrates the product formations in four different conditions (a) O_2-rich SS, (b) O_2-lean TS, (c) O_2-lean SS and (d) O_2-rich TS conditions.

When the condition is O_2-rich SS (Figure 5.9a), NO adsorption is poor, and hence no N_2 production was observed, as the surface Pd atoms are poisoned by chemisorbed oxygen. This is proved when the beam switched to O_2-lean TS (Figure 5.9b), little N_2 production was observed along with CO, CO_2 and H_2O. When the above is continued to O_2-lean SS (Figure 5.9c) it produces more N_2 as the composition contains less oxygen on Pd surfaces. Finally when the beam is turned to O_2-rich conditions, TS (Figure 5.9d) N_2 formation was observed for the few seconds as it initially contains less oxygen, and slowly when the chemisorbed oxygen concentration buildup on surfaces leads to poison the surfaces and N_2 was not observed further. The results suggests that, effective NO reduction is possible even under net-oxidizing condition in fast beam switching experiments.

5.4. Conclusions

Nitric oxide reduction with ethanol has been studied on Pd(111) surfaces under oxygen rich and lean conditions using a molecular beam approach. Significant nitrogen production and ethanol oxidation was observed with the ethanol + NO (and O_2) beams at temperatures above ~ 500 K, even though ethanol sticking coefficient was immeasurably low ≤400 K on clean and oxygen covered Pd(111) surfaces. Generally, oxygen favors the complete ethanol oxidation on Pd(111) surfaces, and CO_2 production increases with increasing oxygen content. Fast beam switching experiments were performed in order to show NO-reduction management under net oxidizing environments.

5.5. References

1. (a) Shelef, M., *Catal. Rev. Sci. Eng*. **1975**, *11*, 1; (b) Shelef, M., *Chem. Rev*. **1995**, *95*, 209. (c) Belton, D. N.; Taylor, K. C., *Curr. Opin. Solid State Mater Sci*. **1999**, *4*, 97.
2. (a) Miyadera, T., *Appl. Catal. B* **1997**, *13*, 157.
3. Dong, H.; Shuai, S.; Li, R.; Wang, J.; Shi, X.; He, H., *Chem. Engn. J*. **2008**, *135*, 195.
4. Dzwigaj, S.; Janas, J.; Machej, T.; Che, M., *Catal. Today* **2007**, *119*, 133.

5. (a) De Mello, L. F.; Auxiliadora, M.; Baldanza, S.; Noronha, F. B.; Schmal, M., *Catal. Today*, **2003**, *385*, 3. (b) De Mello, L.F.; Noronha, F.B.; Schmal, M., *J. Catal*. **2003**, *220*, 358.
6. (a) Velu, S.; Satoh, N.; Gopinath, C. S.; Suzuki, K., *Catal. Lett*. **2002**, *82*, 145. (b) Velu, S.; Suzuki, K.; Vijayaraj, M.; Barman, S.; Gopinath, C. S., *Appl. Catal. B*. **2005**, *55*, 287. (c) Velu, S.; Suzuki, K.; Gopinath, C. S.; Hattori, T.; Yoshida, H., *Phys. Chem. Chem. Phys.* **2002**, *4*, 1990.
7. (a) Gopinath, C. S.; Zaera, F., *J. Catal*. **1999,** *186*, 387; (b) Gopinath, C. S.; Zaera, F., *J. Catal*. **2001,** *200*, 270; (c) Zaera, F.; Gopinath, C. S., *J. Chem. Phys.* **1999**, *111*, 8088. (d) Bustos, V.; Gopinath, C.S.; Uñac, R.; Zaera, F.; Zgrablich, G., *J. Chem. Phys.* **2001**, *114*, 10927.
8. Bowker, M.; Holroyd, R.P.; Sharpe, R.G.; Corneille, J.S.; Francis, S.M., *Surf. Sci*. **1997**, *370*, 113.
9. (a) Bowker, M.; Morgan, C.; Couves, J., *Surf. Sci.* **2004**, *555*, 145. (b) Bowker, M.; Hollroyd, R.; Elliott, A.; Morrall, P.; Alouche, A.; Entwistle, C.; Toerncroma, A., *Catal. Lett*. **2002**, *83*, 165.
10. Holroyd, R. P.; Bennett, R. A.; Jones, I. Z. ; Bowker, M., *J. Chem. Phys*. **1999**, *110*, 8703.
11. King, D. A.; Wells, M. G., *Surf. Sci.* **1972**, *29*, 454
12. (a) Thirunavukkarasu, K.; Gopinath, C. S., *Catal. Lett.* **2007**, *119*, 50; (b) Thirunavukkarasu, K.; Thirumoorthy, K.; Libuda, J.; Gopinath, C. S. *J. Phys. Chem. B.* **2005**, *109*, 13283. (c) Thirunavukkarasu, K.; Thirumoorthy, K.; Libuda, J. ; Gopinath, C. S. , *J. Phys. Chem. B.* **2005**, *109*, 13272. (d) Thirunavukkarasu, K.; Gopinath, C. S., *Catal. Lett*. **2007**, *119*, 50.
13. (a) Nagarajan, S.; Thirunavukkarasu, K.; Gopinath, C. S.; *J. Phys. Chem. C.* **2009**, *113*, 7385. (b) Gopinath, C. S.; Thirunavukkarasu, K.; Nagarajan, S., *Chem. Asia. J*. **2009**, *4*, 74.
14. Jones, I. Z., *PhD Thesis*, Univ. Reading, **1999.**
15. Sharpe, R.; Bowker, M., *Surf. Sci*. **1996**, *360*, 21.

16. (a) Gopinath, C. S.; Zaera, F., *J. Phys. Chem. B* **2000**, *104,* 3194. (b) Zaera, F.; Gopinath, C. S., *Chem. Phys. Lett*. **2000**, *332*, 209.
17. Zaera, F., *J. Phys. Chem. B* **2002**, *106*, 4043.
18. Zaera, F., *Acc. Chem. Res*. **2003**, *35*, 129.
19. Schmick, H.-D.; Wassmuth, H.-W. *Surf. Sci.* **1982**, *123*, 471.
20. Blanksby, S. J.; Barney Ellison, G., *Acc. Chem. Res.* **2003**, *36*, 255.
21. IUPAC. Compendium of Chemical Terminology, 2nd ed. (the "Gold Book"), compiled by McNaught, A. D.; Wilkinson, A., Blackwell Scientific Publications, Oxford, **1997**.

Chapter 6

Conclusions and Future Scope of the Work

6.1. Conclusions

Chapter 1 the importance of environmental catalysis and the role of catalytic converters in automobile industries were emphasized. The role of PGMs towards the understanding of NO_x reduction using various reductants like ethanol and CO briefly described. The importance of Pd and its application towards three way catalytic converter reactions are mentioned. Finally, the surface science aspect and the importance of oxygen diffusion into the Pd surfaces and its impact on oxidation catalysis have been summarized. A molecular beam instrument was fabricated successfully at National Chemical Laboratory, Pune, India, and the importance and the functioning of MBI for the three way catalytic converter reactions have been mentioned in **Chapter 2**.

Chapter 3 Interaction between O_2 and Pd-surfaces is a complex phenomenon, mainly due to diffusion of oxygen atoms into the sub-surfaces layers. Above interaction also varies depending on the temperature and oxygen partial pressure conditions. This is likely the first detailed kinetic work addressing the above issue, especially towards the influence of subsurface oxygen for oxidation catalysis. The presence of oxygen in the subsurface layers of Pd(111) mildly oxidizes Pd, and the surface layers are decoupled from bulk. Mildly oxidized Pd facilitates low as well as high temperature CO oxidation capacity in CO + O_2 reactions. MBI was successfully utilized to probe CO + O_2 on Pd(111) surface through isothermal kinetic experiments between 273 and 900 K and the beam composition varied between CO-rich (7:1) to O_2-rich (1:11) conditions. Positive kinetic evidences for oxygen diffusion into Pd(111) subsurface layers, and its significant influence towards CO oxidation at ambient temperatures as well as above 600 K was observed. Interesting information derived from the above studies is the necessity to fill up the sub-surface layers with oxygen atoms to threshold coverage$\left(\theta_{O_{sub}}\right)$. Time delay in

CO-adsorption (and/or CO_2 production) and $\theta_{O_{sub}}$ increases with increasing temperature and with CO-rich compositions. Maximum $\theta_{O_{sub}}$ was observed to be 0.45 ML at 900 K with pure O_2-beam. The rate of CO_2 production in the SS is considerable, even at high temperatures (700-850 K). In another set of experiments O_2 has been dosed systematically from 5 to 110 minutes at 900 K to populate oxygen into the subsurfaces prior to $CO+O_2$ (7:1) to (1:11) carried out from 300 to 525 K. The presence of oxygen in the subsurface layers of Pd facilitates low temperature CO oxidation too. The above work demonstrates that, oxygen in the subsurfaces of Pd can facilitates low as well as high temperature CO oxidation reactions.

To understand the influence of oxygen towards NO + CO reactions on Pd(111) surfaces, NO + CO + O_2 reaction on Pd(111) surfaces was studied between 400 and 800 K under isothermal kinetic measurements and discussed in **Chapter 4**. Maximum reactivity was found in the temperature between 500 K and 600 K for variety of beam compositions. A detailed analysis of the kinetic data led to the conclusion that the main effect of the oxygen addition to the NO + CO mixture is to inhibit the NO-dissociation rates. Surface oxygen seems to decrease the extent of NO dissociation for the overall reaction above 550 K and enhances the CO-oxidation rates. The overall reaction was largely controlled by the N+N recombination below 525 K and NO-dissociation also increasingly contribute to the RDS with increasing temperature and oxygen content in the beam. The rate of formation of CO_2, and N_2 does not vary much with CO flux was observed. Pd(111) surface shows reversible nature with respect to oxygen-rich and oxygen-lean conditions. Beam switching experiments suggests a better way to manage NO-reduction by fast oscillation between oxygen-rich and oxygen-lean compositions. Large NO-dissociation occurs on relatively oxygen-free Pd-surfaces (oxygen lean) or only in TS on oxygen rich conditions, which is observed through fast beam switching for better de-NO_x management.

In order to understand the ethanol blended gasoline system, ethanol + NO + O_2 reactions has been carried out and the same is given in **Chapter 5**. Nitric oxide reduction with ethanol has been studied on Pd(111) surfaces under oxygen rich and lean conditions using a molecular beam approach. Significant nitrogen production along with ethanol

oxidation was observed with the EtOH + NO (and O_2) beams at temperatures above ~ 500 K, even though ethanol sticking coefficient was very poor ≤400 K on clean and oxygen covered Pd(111) surfaces. In general, oxygen favors a complete ethanol oxidation on Pd(111) surfaces, and CO_2 production increases with increasing oxygen content. Fast beam switching experiments were performed in order to show NO-reduction management under net oxidizing environments. Above studies clearly indicate that more studies, especially spectroscopic studies with in-situ conditions are required for the reactions discussed in this dissertation particularly on Pd supported on a metal oxide.

6.2. Future scope of the work

Based on the findings of the present studies, there exists several opportunities to explore the fundamental and applied catalysis area. Future study should also focus more on structural analysis and the identification of the role of oxygen in the subsurfaces of Pd systems. In this dissertation, oxygen subsurface diffusion and its catalysis application towards CO oxidation on Pd surfaces has been explored with kinetic information's like TS and SS rate of the reactions. The above concept is yet to explored through in-situ spectroscopy techniques for oxidation catalysis. As discussed in chapter 3, oxygen present in the subsurfaces alters the electronic nature of Pd and the subsurface oxygen was not consumed by reactions. Sustainable CO_2 production was observed even for an hour without decrease in the SS rate at 273 K for the beam composition of CO + O_2 (1:11) supports the above factor. Hence, it is worth to explore the same concept to study the NO_x, and olefin related reduction reactions also.

6.2.1. In-situ characterization of O_{sub} and its influence in oxidation catalysis

As we discussed much about oxygen interaction on Pd single crystal surfaces, the formation of metastable Pd_xO_y can be identified only by in-situ techniques like high pressure XPS. Formation of metastable bulk oxide and two surface oxide peaks has been observed, when O_2 interacts with Pd at 573 K. Using In-situ XPS, the linear correlation between catalytic activity and the presence of subsurface oxygen species, within few nanometers using photon-energy-dependent depth-profiling. Our detailed experiments and the above references show that the pure metal is less active than the surface modified

Pd for oxidation reaction, but that a certain amount of oxygen has to be present in the subsurface region to activate the catalytic reaction. The results demonstrated that for an understanding of heterogeneous catalysts a characterization of the surface alone may not be sufficient, and that subsurface characterization is essential. Attempts to mirror a real catalyst more closely would be of interest, perhaps by producing Pd nanoparticles on a support (as in the real system). Lastly, the results of this study could be supported by theoretical analysis, perhaps by computer modeling.

6.2.2. Industrially important reactions on O_{sub}/Pd systems

In **(Chapter 3)**, the presence of oxygen in the subsurface layers of Pd facilitates CO oxidation above 700 K and at ambient temperature. Industrially important reactions, such as VOC oxidation, partial oxidation of methane, CH_3OH oxidation, and ethanol to acetaldehyde reactions needs to be reevaluated in the presence of oxygen in the subsurface layers of palladium. Subsurface nature of palladium and its catalytic effect on CO, CH_4, CH_3OH, C_2H_5OH, oxidation reactions need to be studied in a wide range of temperature and pressure conditions. The concept of subsurface diffusion of oxygen on Pd system is very interesting and it changes the trend of catalytic activity. In-situ characterization of this modified Pd surfaces gives fundamental understanding of molecular level mechanism. In order to understand the real world Pd based catalysts, same can be extended to powder catalyst too. The catalytic activity is likely to improve better with modification of the subsurfaces.

Interesting results are expected in oxidation catalysis; especially methane and ethanol has a poor sticking coefficient on Pd single crystals; with the modification in the subsurface of a catalyst changes in adsorption properties could be expected due to electronic structure changes. Industrially important reactions such as, partial oxidation of methane to methanol is possible, which will be a breakthrough in C_1 activation.

6.2.3. Reactions on Pd systems with subsurface Hydrogen and Carbon atoms

Carbon dissolution has been above 450 K, upon ethene, acetaldehyde and acetic acid interaction on Pd(110) surfaces. It is also observed during ethene oxidation on Pd(111) surfaces above 480 K. Carbon dissolution leads to appearance of an electronically altered, dissolved carbon phase with a C1s BE of 284.45 eV at ~ 500 K. Above 660 K, the dissolved carbon species decomposes, and the reaction occurred on an adsorbate-depleted Pd metal surface, with CO as the main product. Another interesting aspect is carbon dissolution on Pd that can selectively hydrogenate alkynes to alkenes. In situ XPS measurements under reaction conditions indicated that much less carbon was dissolved in palladium during unselective, total hydrogenation. The main conclusion from the above studies shows that, the population of subsurface sites of palladium, by either carbon or hydrogen, governs the selective hydrogenation events on the surface.

Systematic dosing of ethylene or propylene can result in the carbon subsurface diffusion on Pd surfaces. It would be interesting to do NO_x reduction reactions with CO, H_2, or VOC, when either C or H is in the subsurface layers of Pd.

List of Publications

1. "Kinetic Evidence for the Influence of Subsurface Oxygen on Palladium Surfaces towards CO Oxidation at High Temperatures" C. S. Gopinath, K. Thirunavukkarasu, **S. Nagarajan**. ***Chem - Asia. J***, **2009**, *4*, 74-80. (Article)

2. "A Revisit to Carbon Monoxide Oxidation on Pd(111) Surfaces" **S. Nagarajan**, K. Thirunavukkarasu, C. S. Gopinath. ***J. Phys. Chem. C***, **2009**, *113*, 7385–7397. (Article)

3. "Nitric Oxide Reduction with Ethanol on Palladium Surfaces: A Molecular Beam Study" **S. Nagarajan**, K. Thirunavukkarasu, C. Gopinath, Jonathan Counsell, Lee Gilbert, Mike Bowker. ***J. Phys. Chem. C***, **2009**, *113*, 9814–9819. (Article)

4. "Electronic decoupling of surface layers from bulk and its influence in oxidation catalysis: A molecular beam study" K. Thirunavukkarasu, **S. Nagarajan**, C. S. Gopinath. ***Appl. Surf. Sci***, **2009**, 256, 443-448. (Article)

5. "Carbon Dissolution and Segregation in Pd(110)" M. Bowker, J. Counsell, K. El-Abiary, L. Gilbert, C. Morgan, **S. Nagarajan**, C. S. Gopinath. ***J. Phys. Chem. C***, **2010**, *114*, 5060-5067. (Article)

6. "Diffusion of Chemisorbed Oxygen into Pd-Surfaces and its Influence in Oxidation Catalysis" **S. Nagarajan**, C. S. Gopinath. ***J. Ind. Inst. Sci.***, **2010**, *90*, 245-260. (Review)

7. "Kinetics of NO Adsorption on Pd(111) through Molecular Beam Experiments: A Quantitative Study" **S. Nagarajan**, K. Thirunavukkarasu, C. S. Gopinath, S. D. Prasad .(Submitted to ***J. Phys. Chem. C***) (Article)

8. "Sustainable Room Temperature Catalytic CO Oxidation on Subsurface Modified Pd(111)" **S. Nagarajan**, Kanak Roy and C. S. Gopinath. (Communication - Submitted)

9. "$^{15}NO + CO + O_2$ reactions on Pd(111); A molecular beam Study" **S. Nagarajan**, K. Thirunavukkarasu, C. Gopinath, (submitted to ***J. Catal***.) (Article)

10. "Propylene Oxidation Reactions on Pd(111); A Molecular Beam Study" **S. Nagarajan**, C. S. Gopinath. (Will be submitted to ***Catal. Lett.***) (Article)

11. "Kinetics of CO Adsorption on Pd(111) through Molecular Beam Experiments: A Quantitative Study" **S. Nagarajan**, K. Thirunavukkarasu, C. S. Gopinath and S. D. Prasad (Manuscript under preparation) (Article)

Presentations in National/International Conferences/Symposia

1. **20th National Symposium on Catalysis**, NCCR, IITM, Chennai Dec 19-22, 2010 (Oral and Poster)
2. **DAE-BRNS 3rd International Symposium on Materials Chemistry (ISMC-2010)**, BARC, Mumbai Dec 07-11, 2010 (Poster)
3. **Recent trends in Chemistry -V**, The American College, Madurai, India Feb 16, 2010 (Oral - Invited)
4. **Dept of Chemistry (Sir David King's Group)**, University of Cambridge, UK July 24, 2009 (Oral)
5. **4th Taylor conference**, Cardiff University, UK, Between June 22- 25, 2009 (Oral)
6. **Recent trend in Chemistry-IV**, The American College, Madurai, India (Organized)
7. **19th National Symposium on Catalysis**, Jan 18-21, 2009 NCL, Pune, India (Poster)
8. **10th CRSI-NSC Symposium**, Feb. 1-3, 2008, IISc, Bangalore, India (Poster)
9. **Symposium on Vacuum Science and Technology**, Nov 28-30, 2007, TIFR, Mumbai (Oral)

Awards and Fellowships

1. **Best Research Fellow** (Keerti Sangoram Award) of the year 2010 (March-2011).
2. **Best poster award** in National Symposium on Catalysis ($^{20}NSC_{10}$) December 19-22, 2010
3. **Best poster award** in International Symposium on Materials Chemistry (ISMC-2010- December 7-11, 2010)
4. **Best bowler of the year 2010** in Research Scholar Meet (RSM) cricket
5. **Best poster award** in science day celebration, NCL, February 2010
6. Awarded **Research Fellowship** by Council of Scientific and Industrial Research (CSIR), India (July 2006 – June 2011)
7. **Flint Prize** for first rank during B.Sc Chemistry (2001-2004)